

FLEXURAL CHARACTERISTICS OF BIO-BASED SANDWICH BEAMS MADE  
OF PAPER HONEYCOMB CORES AND FLAX FRP SKINS

by

Yuchen Fu

Submitted in partial fulfilment of the requirements  
for the degree of Master of Applied Sciences

at

Dalhousie University  
Halifax, Nova Scotia  
July 2022

© Copyright by Yuchen Fu, 2022

## TABLE OF CONTENTS

LIST OF TABLES .....	v
LIST OF FIGURES .....	vi
ABSTRACT.....	x
LIST OF ABBREVIATIONS AND SYMBOLS USED.....	xi
ACKNOWLEDGMENTS .....	xiv
CHAPTER 1 INTRODUCTION .....	1
1.1. BACKGROUND .....	1
1.2 PROBLEM STATEMENT.....	3
1.3 OBJECTIVE .....	4
1.4 THESIS STRUCTURE.....	4
CHAPTER 2 LITERATURE REVIEW.....	7
2.1. INTRODUCTION TO BIO-BASED MATERIALS .....	7
2.1.1. General Information and History .....	7
2.1.2. Current Situation of Bio-based Materials Using in FRP .....	9
2.1.3. Advantages of Bio-based Material Application .....	14
2.2. INTRODUCTION TO HONEYCOMB .....	16
2.3. INTRODUCTION TO SANDWICH PANELS.....	17
2.3.1. Sandwich Beam Theory.....	18
2.3.2. Testing Methods of Sandwich beams.....	23
2.3.3. Sandwich Beam Failure Modes .....	27
2.3.4. History and Current Applications of Sandwich Structures .....	30
2.3.5. Sandwich Composites made of Bio-based Materials.....	32
CHAPTER 3 EXPERIMENTAL PROGRAM .....	34
3.1. GENERAL INFORMATION.....	34
3.2. TEST MATRIX.....	34
3.3. MATERIAL PROPERTIES .....	35
3.3.1. Facing Material Properties.....	35
3.3.2. Core material properties.....	40

3.4. FABRICATION OF SANDWICH PANELS .....	48
3.5. INSTRUMENTATION AND TEST-UP .....	50
3.6. DATA ANALYSIS AND TEST RESULTS .....	52
3.6.1. Failure Mode .....	53
3.6.2. Load-deflection Behavior .....	55
3.6.3. Moment-curvature Behavior .....	56
3.6.4. Effect of Honeycomb core types.....	57
3.6.5. Effect of Facing Thickness.....	59
CHAPTER 4 ANALYTICAL MODEL .....	61
4.1. SYNOPSIS.....	61
4.2. MODELLING LOAD-DEFLECTION BEHAVIOR.....	61
4.2.1. Linear Model.....	61
4.2.2. Non-Linear Model .....	62
4.2.3. Verification of Load-deflection Models.....	68
4.3. BREAKDOWN OF SHEAR AND BENDING DEFLECTIONS .....	69
4.4. PREDICTION OF FAILURE MODES .....	71
4.5. PARAMETRIC STUDY .....	74
4.5.1. Effect of Core Thickness (Hollow Paper Honeycomb Core and Foam-filled Paper Honeycomb Core) .....	78
4.5.2. Effect of Facing Thickness (Hollow Paper Honeycomb Core and Foam-filled Paper Honeycomb Core) .....	79
4.5.3. Effect of Span Length (Hollow Paper Honeycomb Core and Foam-filled Paper Honeycomb Core).....	80
CHAPTER 5 CONCLUSIONS AND RECOMMENDATIONS.....	82
5.1 CONCLUSIONS.....	82
5.2 RECOMMENDATIONS FOR FUTURE RESEARCH.....	85
BIBLIOGRAPHY .....	86
APPENDIX A Debonding Failure Mode .....	90
A1 Overview .....	90

A2 Analysis of Debonding Failure Mode .....	90
Appendix B Bilinear Model of Sandwich Beam .....	93
B1 Overview .....	93
B2 Bilinear Model.....	93

## LIST OF TABLES

Table 2-1 Average price of natural and synthetic fibers (Väisänen, 2017) .....	12
Table 3-1 Test matrix .....	35
Table 3-2 Core Shear Test Results .....	43
Table 3-3 Summary of test results.....	53
Table 4-1 Initial stiffness comparison between models and test data .....	69
Table 4-2 Shear Contribution to Total Deflection.....	71
Table 4-3 Data Comparison Test and Model.....	73
Table 4-4 Mechanical properties of sandwich beams with varying core thickness and core type ( $t = 3$ mm, $L = 1$ m) .....	76
Table 4-5 Mechanical properties of sandwich beams with varying facing thickness and core type ( $c = 150$ mm, $L = 1$ m) .....	76
Table 4-6 Mechanical properties of sandwich beams with varying core thickness and core type ( $t = 3$ mm, $c = 150$ mm).....	77
Table A-1 Calculation Results of Debonding Failure .....	92

## LIST OF FIGURES

Figure 1-1 Breakdown of research stages .....	6
Figure 2-1 French mirror made by bio-based plastics in nineteenth century (Sharma et al., 2011).....	8
Figure 2-2 Jewellery box made by kopal resin (Sharma et al., 2011).....	9
Figure 2-3 Citation trends of patents in recent years (Babu et al., 2013). .....	10
Figure 2-4 Basic material components that are combined to create an FRP composite. (Source: ISIS Canada Educational Module No.2: FRP Composites for Construction).....	11
Figure 2-5 Fiber cells under microscope: a) Sisal fiber; b) glass fiber (Zhu et al., 2013). .....	15
Figure 2-6 Hexagonal cell of honeycomb structure (Wang, 2019).....	16
Figure 2-7 Hexagonal structure of honeycomb material made by aluminum and paper (Aktay et al., 2008).....	17
Figure 2-8 Sandwich Panel (Source: ISIS Canada Educational Module No.2: FRP Composites for Construction). .....	18
Figure 2-9 Dimension of sandwich beam and cross-section (Allen, 1969).....	19
Figure 2-10 Normal and shear stresses for different levels of assumptions. ....	21
Figure 2-11 Deflection of sandwich beam (Allen, 1969). .....	22
Figure 2-12 Beam curvature (Source: <a href="http://www.ecourses.ou.edu">www.ecourses.ou.edu</a> ).....	22
Figure 2-13 Different shapes of tensile specimens: a) dumbbell shape; b) rectangular shape; c) rectangular shape with tabs; d) notched rectangular shape with tabs (Zenkert, 1997).....	23
Figure 2-14 Different shapes of compressive specimens: a) the specimen with a waist; b) the specimen with tabs; c) the notch specimen (Zenkert, 1997). ....	24
Figure 2-15 Schematic view of a honeycomb core shear test (Soltani et al., 2014). .....	25
Figure 2-16 Schematic view of flexural tests: a) three-point bending; b) four-point bending (Zenkert, 1997).....	26

Figure 2-17 Failure modes of sandwich beams: a) face yielding/rupture; b) core shear failure; c) and d) top face wrinkling (Zenkert, 1997).	27
Figure 2-18 Failure mode map of FFRP-foam sandwich panel (Betts, 2018).	30
Figure 2-19 The application of sandwich structures in A380 (Herrmann et al., 2005).	31
Figure 2-20 Sandwich structures application of civil engineering: a) Wind-mill housing structure in GFRP-sandwich; b) Large doors in sandwich construction (Zenkert, 1997).	32
Figure 3-1 Stress-strain curve of facing materials in tension and compression (Betts, 2018).	36
Figure 3-2 Parameters of bilinear model.	37
Figure 3-3 Nonlinear stress-strain curve with parameters.	38
Figure 3-4 Bilinear and parabolic model comparing to original test data	39
Figure 3-5 Core fabrication: a) unexpanded paper honeycomb; b) two wooden boards; c) applying epoxy resin to wood surfaces; d) curing with clips; e) stretching and setting; f) cutting	41
Figure 3-6 Foam filling: a) filling foam with dispensing gun; b) removal extra foam; c) finished foam-filled core.	42
Figure 3-7 Core shear testing setup: a) core specimen set on Instron machine for shear test; b) shear test apparatus.	43
Figure 3-8 Core shear test results: a) shear stress-strain curve of foam-filled paper honeycomb; b) shear stress-strain curve of hollow paper honeycomb.	44
Figure 3-9 Resin absorbed by paper.	46
Figure 3-10 Nonlinear shear stress-strain curve with parameters.	46
Figure 3-11 Parabolic model comparing to test results: a) Hollow honeycomb core; b) foam-filled honeycomb core.	48
Figure 3-12 Sandwich panel fabrication: a) cutting flax fabric; b) applying a layer of resin; c) placing a layer of flax fabric; d) saturating flax fabric; e) removal of extra resin and air bubbles; f) placing core and weighed wooden board.	50

Figure 3-13 Test setup and instrumentation: a) schematic drawing (dimensions in mm); b) test setup photo .....	52
Figure 3-14 Example of failure modes: a) core shear failure on foam-filled core; b) core shear failure on hollow core; c) debonding failure on foam-filled core	55
Figure 3-15 Load-deflection behavior of specimens: a) specimens with foam-filled paper honeycomb core; b) specimens with hollow paper honeycomb core. .	56
Figure 3-16 Moment-curvature behavior of specimens: a) specimens with foam-filled paper honeycomb core; b) specimens with hollow paper honeycomb core. ....	57
Figure 3-17 Effect of honeycomb core type on load-deflection and moment-curvature diagrams: a) load-deflection for 1-layer specimens; b) load-deflection for 2-layer specimens; c) load-deflection for 3-layer specimens; d) moment-curvature for 1-layer specimens; e) moment-curvature for 2-layer specimens; f) moment-curvature for 3-layer specimens .....	58
Figure 3-18 Effect of facing thickness on load-deflection and moment-curvature diagrams: a) load-deflection for foam-filled core; b) load-deflection for hollow core; c) moment-curvature for foam-filled core; d) moment-curvature for hollow core.....	60
Figure 4-1 Stress-strain curve with varying secant modulus .....	63
Figure 4-2 Flowchart of deflection model due to bending.....	64
Figure 4-3 Shear stress-strain curve with varying secant modulus.....	65
Figure 4-4 Relation between shear deflection and shear strain .....	65
Figure 4-5 Flowchart of deflection model due to shear .....	67
Figure 4-6 Load-deflection curve comparison between linear model, non-linear model, and test data: a) 1FL-H; b) 1FL-F; c) 2FL-H; d) 2FL-F; e) 3FL-H; f) 3FL-F.....	68
Figure 4-7 Breakdown of total deflection into shear and bending deflections: a) 1FL-H; b) 1FL-F; c) 2FL-H; d) 2FL-F; e) 3FL-H; f) 3FL-F. ....	70
Figure 4-8 Load-deflection curve with predicted peak loads as terminal points: a)	

1FL-H; b) 1FL-F; c) 2FL-H; d) 2FL-F; e) 3FL-H; f) 3FL-F. ....	72
Figure 4-9 Initial stiffness and ultimate stiffness. ....	75
Figure 4-10 Load-deflection and load-strain curves for sandwich beams with varying core thickness and core type: a-b) hollow paper honeycomb core; c-d) foam-filled paper honeycomb core. ....	78
Figure 4-11 Load-deflection and load-strain curves for sandwich beams with varying facing thickness and core type: a-b) hollow paper honeycomb core; c- d) foam-filled paper honeycomb core. ....	80
Figure 4-12 Load-deflection and load-strain curves for sandwich beams with varying unsupported span length and core type: a-b) hollow paper honeycomb core; c-d) foam-filled paper honeycomb core. ....	81
Figure A-1 a) Crack length greater than the depth of the core; b) Crack length less than the depth of the core; c) Double shear test setup (Triantafillou et al., 1989) .....	91
Figure B-1 Load-deflection curve comparison between linear model, Bilinear model, and test data: a) 1FL-H; b) 1FL-F; c) 2FL-H; d) 2FL-F; e) 3FL-H; f) 3FL-F. ....	94

## ABSTRACT

Sandwich structures have been used for building applications as building envelope and cladding systems. The sandwich structures used today are made of conventional synthetic Fiber Reinforced Polymer (FRP), such as glass fiber and carbon fiber, and synthetic foam core. With the increasing of environmental consciousness, it is important to develop sustainable building materials to replace conventional building materials. The use of bio-based materials for construction is a good way to improve the sustainability of buildings. However, bio-based sandwich structure has not been widely used today. Therefore, it is essential to investigate and understand the characteristics of structures made with bio-based materials. In this study, a total of 6 groups of large-scale bio-based sandwich beams made of flax FRP skins and two types of paper honeycomb core were studied. Three identical sandwich beams for each group were tested to obtain the experimental results. The parameters of the tests were skin thickness (1,2 and 3 layers of flax FRP) and core types (namely, hollow and foam-filled). Each specimen was 1200 mm long, 100 mm wide and approximately 80 mm thick and was tested by three-point bending. The failure modes were observed, and the test data were collected and processed. The test results were shown by load-deflection diagrams, and moment-curvature diagrams. Overall, the bio-based sandwich structures have potential to be used for building applications with much less environmental footprints in comparison with other synthetic counterparts.

## LIST OF ABBREVIATIONS AND SYMBOLS USED

### Abbreviations

ASTM	American Society for Testing Materials
CS	Core Shear
DB	Debonding
ECO	Epoxidized Canola Oil
FRP	Fiber Reinforced Polymer
FFRP	Flax Fiber Reinforced Polymer
FR	Facing Rupture
GFRP	Glass Fiber Reinforced Polymer
HSS	Hollow Structural Section
LP	Linear Potentiometer
MAESS	Methacrylated Epoxidized Sucrose Soyate
PA	Phthalic anhydride
VE	Vinyl Ester
WR	Wrinkling

### Symbols

AG	Shear stiffness
D	Flexural rigidity
$D_c$	Bending stiffness of the core
$D_f$	Bending stiffness of the faces
$D_o$	Bending stiffness of the faces about the middle axis
EI	Flexural rigidity

$E_c$	Elastic modulus of sandwich core component
$E_f$	Elastic modulus of sandwich facing component
$E_{sec}$	Secant elastic modulus
$E_1$	First modulus of elasticity
$E_p/E_2$	Plastic/secondary modulus of elasticity
$F_d$	Load of delamination
$G$	Shear modulus of core component
$G_{sec}$	Secant shear modulus
$I$	Second moment of inertia
$K$	Initial stiffness
$K_u$	Ultimate stiffness
$L$	Unsupported span length
$M$	Moment
$P_{cr}$	Peak load at failure
$P_{FR}$	Facing rupture failure load
$P_{CS}$	Core shear failure load
$P_{WR}$	Wrinkling failure load
$P_i$	Initial applied load
$P_f$	Final applied load
$P_u$	Ultimate applied load
$Q$	Shear force
$S$	First moment of area
$b$	Width of sandwich beam
$c$	Core thickness

$d$	Distance between centroids of facings
$f_0$	Stress at the intercept of second slope with stress axis
$h$	Height of sandwich beam
$n$	Shape parameter
$t$	Facing thickness
$z$	Distance from the neutral axis
$\psi$	Curvature
$\Delta P$	Loading increments
$\delta_b$	Bending deflection
$\delta_s$	Shear deflection
$\delta_t$	Total deflection
$\delta_u$	Total deflection at peak load
$\epsilon$	Strain
$\epsilon_b$	Bottom strain
$\epsilon_t$	Top strain
$\epsilon_u$	Ultimate strain
$\gamma$	Shear strain
$\gamma_u$	Ultimate shear strain
$\sigma_{cr}$	Stress at failure
$\sigma_{wr}$	Stress due to wrinkling
$\tau_c$	Shear stress in core component
$\tau_u$	Ultimate shear stress

## ACKNOWLEDGMENTS

Firstly, I would like to thank my supervisor, Dr. Pedram Sadeghian, for providing me with the excellent opportunity to be a part of his research team and to work with a group of the nicest people. He helped and encouraged me throughout my graduate study program and made the whole research process a pleasant learning experience.

Then, I would like to acknowledge Dalhousie's technicians, Jesse Keane, and Jordan Maerz, for their lab support, which allowed me working in a safe and comfortable environment. Also, thank you to my colleagues, Dillon Betts, and Raghad Kassab, for their helps on lab and modeling work.

Finally, thank you to my parents for their endless support on everything. They always give me the best motivation and suggestions in my life.

## CHAPTER 1 INTRODUCTION

### 1.1. BACKGROUND

With the development of industry and the growth of populations, the average of 13,000 buildings will be built daily from now to 2050 (Statista, 2018). With the growing understanding of the impact on the environment caused by human activity, people need to find the ways to make building construction more sustainable. Natural organic fibers have been used since the beginning of the life on Earth as lines and ropes. Over 100 years ago, natural fibers composites were used for airplane seats and fuel-tanks, tubes, and pipes for electronic purposes (Sparnins, 2009). There are mainly 5 types of natural fibers: bast fibers, leaf fibers, core fibers, grass, and reed fibers. Flax fiber is a bast fiber, and it is the most widely used in the composites field (Faruk et al., 2012). Chemical composition (by weight) of flax fibers are 71% cellulose, 18.6-20.6% hemicellulose, 2.2% lignin, and 1.5% waxes. The tensile strength and Young's modulus were reported as 345-1035 MPa and 27.6 GPa, respectively (Faruk et al., 2012). Compared to conventional synthetic fibers (E-glass and carbon), lower pollution is emitted, and lower energy is required during production. Also, Natural fibers are renewable and biodegradable. It is also less harmful for people's health due to its non-toxic properties. Moreover, it has the potential to be used together with bio-based matrix to make Fiber reinforced polymer (FRP), so the totally biodegradable composite materials are obtained (Faruk et al., 2012). In this study, flax FRP is used for facing material of sandwich panels to show it has potential to replace conventional fibers on structural purpose.

Sandwich structure is a composite material consisting of a thick core and two thin facing materials, and it is a very effective system with high performance and minimum weight. The core is normally lightweight and separates the strong skin materials apart to provide a higher moment of inertia under flexure, and it also provides shear resistance and insulation (water and sound) for the sandwich system. The two facings are very stiff and strong to resist tension and compression force that is resulting from the bending moment (Sadeghian, 2018). Nowadays, sandwich composites made by FRP facings and core have been practiced for a couple of decades. The conventional fibers used for FRP are synthetic, such as carbon and glass fibers (Florence et al., 2020; MacDonnell et al., 2020). The most popular core materials are used to be synthetic foam and plastic (Betts, 2018). Compared to the FRP made by synthetic fibers, the FRP made by bio-based fibers has lower strength. However, because of the relatively lower strength of core materials, the failure of sandwich structure is usually governed by the core, which means the FRP skin rarely reach their ultimate strength. Therefore, the high strength of synthetic fibers is not fully utilized in most cases (Betts, 2018). Therefore, a lower strength, but more environmentally friendly, natural fibers can be used to replace conventional synthetic fibers. In this study, flax is used for manufacturing the FRP skin. Based on the previous research, lots of natural fibers have been studied for manufacturing FRP. Flax is readily available and has relatively higher strength and stiffness (Ramesh et al., 2017). A bio-based epoxy resin was used for the matrix of FRP. Paper honeycomb (hollow and foam-filled) was selected to be the core material. In Canada, almost 100% of cardboard and paper are made from recycled material and they

are 100% biodegradable (McCracken et al.,2018). Overall, the whole sandwich panel can be considered as a bio-based composite.

Today, sandwich panels made by conventional synthetic materials are mainly used as a part of building envelopes and cladding walls. However, bio-based sandwich structure has not been widely used today. Therefore, it is essential to investigate and understand the characteristics of structures made with bio-based materials.

## **1.2 PROBLEM STATEMENT**

A lot of research has been done on sandwich panels in recent years. However, most of them focused on the sandwich panels made by synthetic materials. Some of them considered sandwich panels made by bio-based facings and synthetic core, or bio-based core and synthetic facings. There are very few literatures concerning the sandwich panels made by fully bio-based material. Besides, honeycomb shape structures provide minimal density and efficient resistance of compression and shear. Sandwich panels with plastic and aramid honeycomb core were relatively widely studied, but, currently, the literature regarding paper honeycomb core is very limited. The currently available research on sandwich structures made by flax FRP and paper honeycomb core has focused on small-scale specimens under four-point bending (Fu. et al., 2020). The research gap in the performance of large-scale sandwich beams made by flax FRP and paper honeycomb core needs to be filled. The tests of large-scale specimens will eliminate the potential results influence caused by size effects. The purpose of this study is to investigate the mechanical performance of sandwich panels made from flax FRP and paper honeycomb core through experimental tests and analytical models.

### 1.3 OBJECTIVE

The main goal of this research is to obtain a general concept of mechanical performance of sandwich structures with flax FRP and honeycomb. This goal will be achieved by completing the following objectives:

- Identify the mechanical properties of flax FRP and honeycomb core.
- Investigate the mechanical behavior of sandwich beams made of flax FRP facings and two types of honeycomb core (namely, hollow and foam-filled) under three-point bending.
- Develop a model to predict and verify the load-deflection behavior and failure criteria of tested sandwich beams.
- Provide a parametric study using this model to predict the load-deflection behavior and failure criteria of sandwich beams in different dimensions.

### 1.4 THESIS STRUCTURE

There are four main steps in this study, and Figure 1-1 summarizes each essential stage.

In this study, it is important to understand the basic knowledge of bio-based materials and the difference between bio-based materials and synthetic materials. Therefore, an introduction to bio-based materials will be provided in Chapter 2's literature review. This introduction to bio-based materials will explain the advantages of using bio-based materials compared to conventional synthetic materials, and the current bio-based applications will be introduced. Also, in Chapter 2, the FRP and sandwich structure will be introduced in detail.

Following the literature review, Chapter 3 will present a detailed procedure of specimen

fabrication, test method, and results. A total of 18 sandwich beam specimens (1200 mm long x 80 mm thick x 100 mm wide) were fabricated and tested under three-point bending. A total of 6 core specimens (240 mm long x 20 mm thick x 50 mm wide) were fabricated and tested under shear. The test setup will also be presented. The summary of test results will be shown in diagrams and table in this Chapter.

In Chapter 4, the test results will be analyzed through the load-deflection, load-strain, moment-curvature diagrams. Moreover, an analytical model will be developed to predict and verify the test results. A parametric study will be provided to predict the mechanical properties of sandwich beams in different dimensions.

Chapter 5 will summarize the findings of this study and present the conclusion of the research process. The conclusion will include the experience of working on these kinds of materials, and a future recommendation will be provided for future studies.

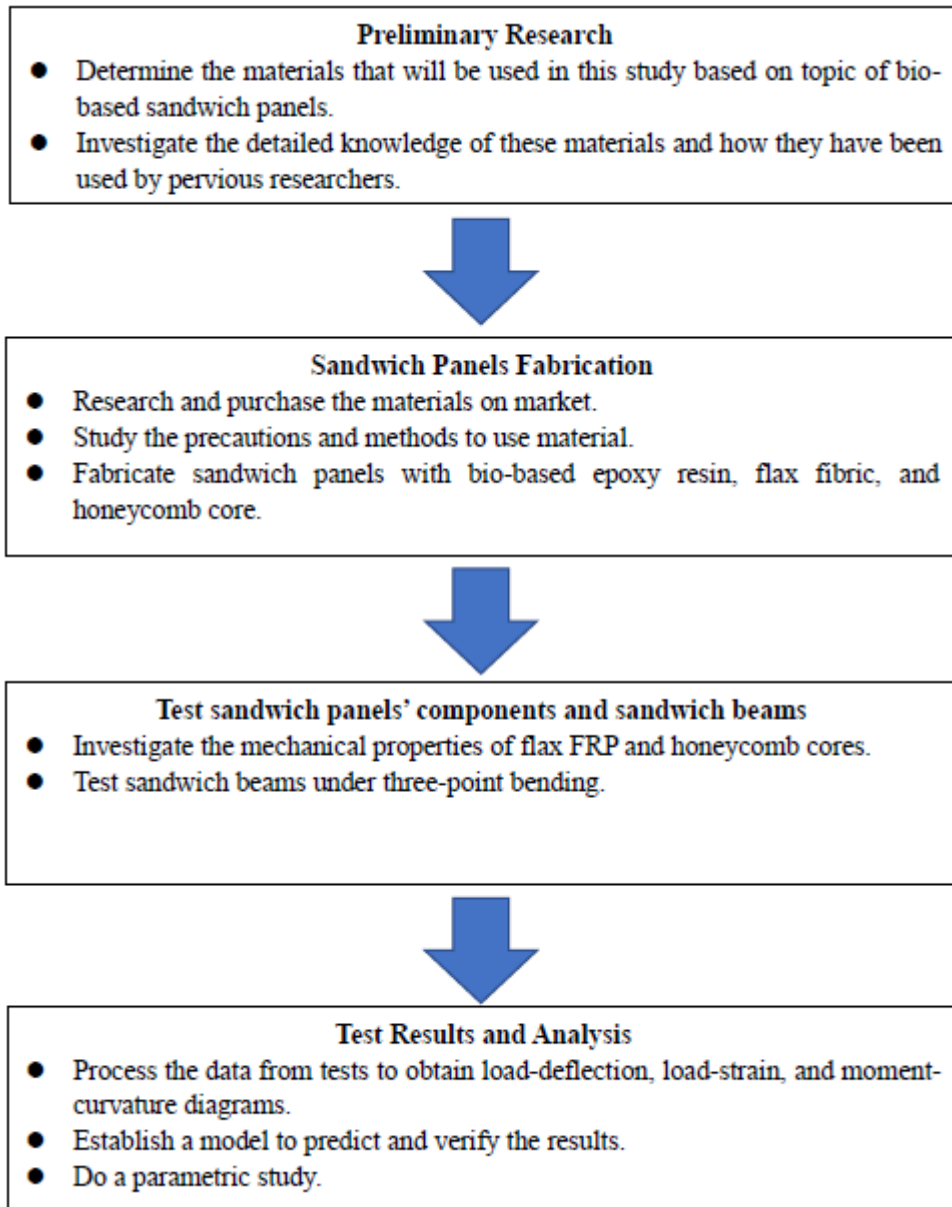


Figure 1-1 Breakdown of research stages

## CHAPTER 2 LITERATURE REVIEW

### 2.1. INTRODUCTION TO BIO-BASED MATERIALS

#### 2.1.1. General Information and History

According to Kabasci (2014), recently years, people have been increasingly aware of the fact that fossil raw material is not an infinite resource. In the past decade, over 7 billion tons of carbon were derived annually from fossil raw materials, such as coal, fuel, and natural gas. It affected the world's climate. Moreover, fossil raw material would be depleted soon. Bio-based raw material is a renewable alternative to replace fossil raw materials.

Bio-based material is any product that made by materials that come from plants or animals. There are couple of definitions for bio-based materials. The US Department of Agriculture defines bio-based material as “commercial or industrial goods, (other than feed or food), composed in whole or in a significant part of biological products, forestry material, or renewable domestic agriculture materials, including plants, animal, or marine materials” (Edwards et al., 2012). ASTM defines bio-based materials as “an organic material in which carbon is derived from a renewable resource via biological processes” (Edwards et al., 2012). Compared to conventional materials, natural materials are more eco-friendly as they are renewable, recycled, reused, and biodegradable. Because of its lightweight, lower energy is required during the transportation and installation. Moreover, it is good for people's health by using bio-based material because it is nontoxic property (Rajesh et al., 2016; URBANE, 2019).

According to the German Plastic Museum, the first product made by bio-based material

was found in the year 1530. The artificial horn was made from casein which is a milk protein (Kabasci, 2014). The recipe of this product is kept until today. In the eighteenth and early nineteenth centuries, bio-based materials were developed as natural rubber and used in different applications, such as erasers and masticators (Kabasci, 2014). In the late nineteenth century, a French mirror made by bio-based plastic was found, as shown in Figure 2-1. The main raw material was sawdust mixed with vegetable oils and mineral (Sharma et al., 2011).



Figure 2-1 French mirror made by bio-based plastics in nineteenth century (Sharma et al., 2011).

In the twentieth century, people started to use a mixture of wood fiber, tree resin, and pigments to fabricate some of bowls, containers, boxes, lamps, radios, and clocks (Sharma et al., 2011). A jewellery box made by kopal resin is shown in Figure 2-2.



Figure 2-2 Jewellery box made by kopal resin (Sharma et al., 2011).

#### 2.1.2. Current Situation of Bio-based Materials Using in FRP

Currently, although people started to use bio-based plastics over a couple of hundreds year ago, they still hold a little fraction (around 1%) of the total global plastic market in 2015. However, in recent years, people desire to find a renewable material to replace fossil raw materials. The number of publications of bio-based plastics and applications is sharply increased (Babu et al., 2013), as shown in Figure 2-3.

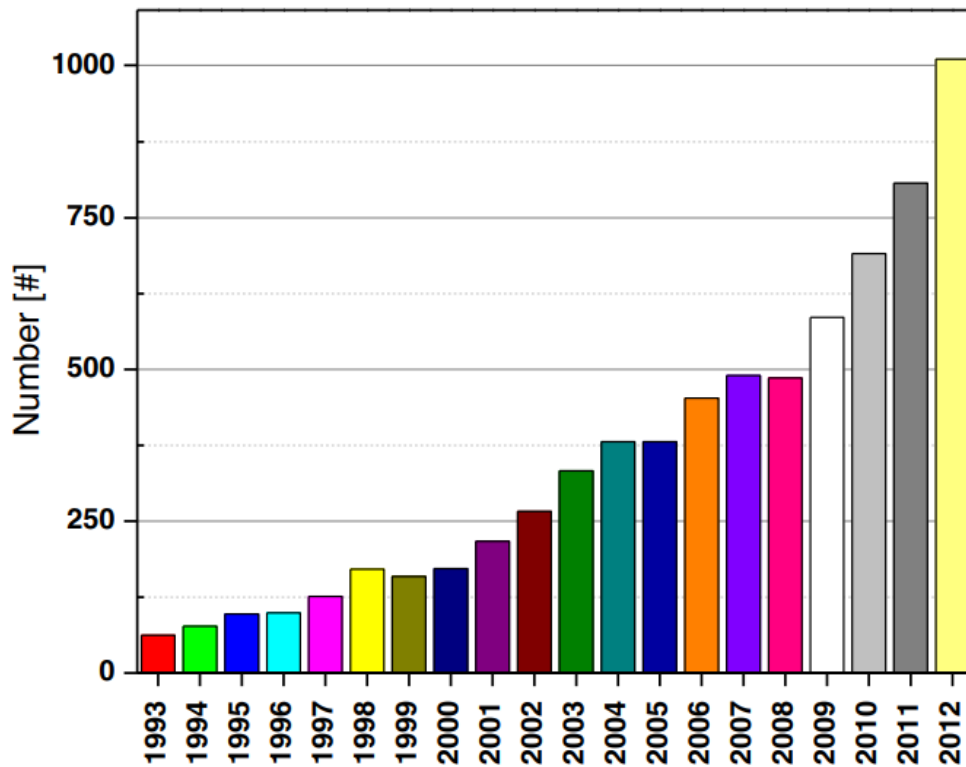


Figure 2-3 Citation trends of patents in recent years (Babu et al., 2013).

### Bio-based FRP

Nowadays, bio-based fibers and bio-based resins are widely used for fiber reinforced polymers (FRP). FRP is subgroup of the class of composites materials. Composites are defined as “materials created by the combination of two or more materials, on a macroscopic scale, to form a new and useful material with enhanced properties that are superior to those of the individual constituents alone” (ISIS Canada, 2006). FRP is a composite combining high strength fibers and matrix shown in Figure 2-4. It has been used in the automotive and aerospace industries for more than 50 years. The fibers in FRP are used to be glass fibers, carbon fibers, and aramid fibers, and they have properties of high stiffness and high ultimate strength. The matrix in FRP is used to be polyesters, vinylesters, and epoxies, and they provide bonds, protection, and force

transferring of fibers. Comparing to conventional construction materials (concrete and steel), the main advantages of FRP are high strength-to-weight ratios, high durability under complex environment, high speed of transportation and installation because of its lightweight (ISIS Canada, 2006). As a high-efficient composite, many potential applications and developments are under researching.

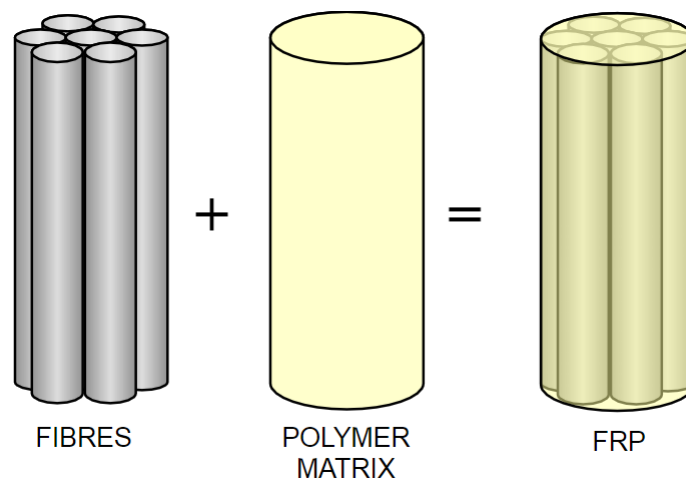


Figure 2-4 Basic material components that are combined to create an FRP composite. (Source: ISIS Canada Educational Module No.2: FRP Composites for Construction)

To apply bio-based material to FRP, the speciality of high-efficient of FRP will be remained while less environment damage will be achieved. Instead of using conventional fibers (glass fiber, carbon fiber, and aramid fiber), the natural fibers are used, such as flax, hemp, and jute. The conventional matrix is replaced by bio-based resins derived from natural oils (Wool et al., 2005). The natural fibers have lower costs (as shown in table 2-1), densities, and weights than synthetic fiber. At the same time, they minimize the health hazard for human, and less environment footprint are obtained.

Table 2-1 Average price of natural and synthetic fibers (Väisänen, 2017)

Fiber	Price (US\$/kg)
Wood	0.3–0.6
Flax	2.1–4.2
Hemp	1.0–2.1
Jute	0.4–1.5
Coir	0.3–0.5
Cotton	2.1–4.2
Sisal	0.6–0.7
Kenaf	0.3–0.5
Bamboo	0.5
Wool	1.6–2.4
Feather	1.1–2.0
Silk	2.6–40.0
Glass	2.0
Carbon	22.0–27.0

### **Bio-based matrix**

Epoxy resin can be used as matrix in FRP. According to Omonov (2014), an epoxy resin can be successfully derived from canola oil. By changing the ratio of Epoxidized Canola Oil (ECO) and Phthalic anhydride (PA) and curing temperature, the preferred thermomechanical properties could be obtained.

At the same time, in Adekunle’s paper (2012), bio-based thermoset resins from soybean oil (methacrylated soybean oil, and methacrylic anhydride modified soybean oil) were used as matrix. Two different types of flax fibers (non-woven flax mat and woven flax mat) and a glass (woven) fiber mat were used as reinforcements. The specimens were cut into dumbbell shape with an overall length of 150 mm (length of narrow, 20 mm width at end, 10 mm width at narrow part, 50 mm gauge length). The results show that, the resins from soybean oil works very well with bio-based fibers, and it can substitute for conventional thermoset resins.

Also, based on Hosseini's tests (2016) of bio-based resin, Epoxidized Sucrose Soyate (ESS) resin was synthesized from fully esterified sucrose soyate, and reacted with methacrylic acid to produce methacrylated epoxidized sucrose soyate (MAESS). MAESS resin (bio-based) reinforced with glass-fiber and vinyl ester (VE) reinforced with glass-fiber were fabricated and mechanical properties were tested. To compare the mechanical properties, the tensile strength, and modules of MAESS and VE resins reinforced with E-glass fiber are 532 MPa, 36.79 GPa and 536 MPa, 36.4 GPa, respectively. The flexural strength and modules of MAESS and VE resins reinforced with E-glass fibers are 459 MPa, 34 GPa, and 432 MPa, 37 GPa, respectively. In other words, the composite with MAESS obtained the comparable strength in tensile and flexural to the composite with traditional resin (VE). Also, the interlaminar shear strength test shows that stronger adhesion between fiber and matrix and greater interfacial bonding were obtained by MAESS resin reinforced with glass-fiber. Overall, these bio-based resin has potential to be used in composites.

### **Bio-based fiber**

Comparing to synthetic fibers, bio-based fibers have lower strength. However, despite of the mechanical properties of FFR composites made by bio-based materials, the effect of deterioration of bio-based material would be considered. According to Hristozov et al. (2016), a total of 490 (245 FFRP and 245 GFRP) were manufactured and tested under uniaxial tensile loading. A vinyl ester resin (petroleum-based resin) was used, and the specimens were fabricated by wet-layup method. The parameter of tests is fiber type (flax vs. glass), environmental aging condition (dry heat and immersion in water, salt

water, and alkaline solutions), exposure duration (21, 42, 83, and 125 days), and temperature during exposure (20, 50, and 60 °C). The results show that, the flax FRP gain more moisture than glass during exposure. However, the tests on the 125 days of condition at 20, 50 and 60 °C show that FFRP specimen had strength retentions of 88, 71, and 68% in water; 81, 69, and 65% in salt water; and 74, 59, and 49% in alkaline, respectively. On the other hand, GFRP specimens had strength retentions of 89, 58 and 45% in water; 88, 60, and 54% in salt water; and 68, 43, and 30% in alkaline, respectively. Therefore, the strength retention of flax FRP is slightly higher than that of glass FRP. To conclude, the long-term mechanical behavior of composites made of flax fibers is not worse or is better than composites made of glass fiber.

### 2.1.3. Advantages of Bio-based Material Application

#### 2.1.3.1. Sound Insulation

Noise has negative effects on people's psychological health. Sound insulation properties must be considered for building construction material. Natural fibers are more efficient on sound absorption than synthetic fibers. As shown in Figure 2-5, comparing sisal fiber to glass fiber, sisal fiber consists of a group of hollow tubules. On the other hand, glass fiber has solid circular shape. Therefore, because of the unique porous structural characteristics of natural fibers, they have more air cavities, which play the major role of sound energy absorption, than synthetic fibers (Zhu et al., 2013).

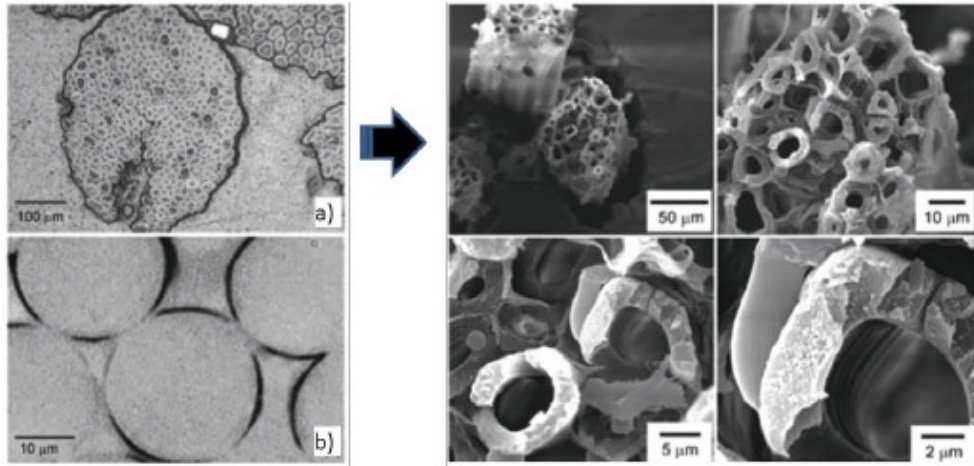


Figure 2-5 Fiber cells under microscope: a) Sisal fiber; b) glass fiber (Zhu et al., 2013).

### 2.1.3.2. Environmentally Friendly and Sustainability

Comparing to fossil-based materials, the most of bio-based materials are renewable, reusable, and biodegradable. “40% of global raw material is expended by the building industry. 50% of carbon dioxide releases into the atmosphere come from the construction sector” (Yadav, et al., 2021). Conventional building materials have an impact on the environment not only caused by their production but also from their disposal. In the other words, today’s building materials are rarely recyclable, and they are also harmful to the environment in disposal process. The way to solve this problem is to use bio-based materials. To take hemp as an example (Yadav, et al., 2021), hemp is common natural fiber used in composite. It can be grown fast, and carbon dioxide can be absorbed when it grows. Also, it provides good air exchange and humidity resistance to building, so the total power usage can be saved. Moreover, the most bio-based materials are renewable and recyclable after their life span, so bio-based building materials will play an important role in the future to reduce the carbon footprint of building construction and demolition.

Bio-based materials are also widely used in packaging. A study shows that, because of its non-toxic properties, plant-based material is a better container to package liquid comparing to plastic and glass packages (Johansson et al., 2012). In addition, bio-based material packaging has the lower weight, so the transportation energy can be saved.

## 2.2. INTRODUCTION TO HONEYCOMB

Honeycomb structure is a gift from nature. Scientists found it from bee's honeycomb that was showing a huge mechanical potential. The hexagonal cell (as shown in Figure 2-6) structure contains large useable space, and it provides high density efficient performance. The first artificial honeycomb structure was made by paper in China 2000 years ago, and the first modern honeycomb structure was made by aluminum around 1945 (Wang, 2019). Then, honeycomb structure rapid grew in couple decades until now. Nowadays, honeycomb materials are commonly made by aluminum, steel, titanium, and non-metallic materials (Wang, 2019).

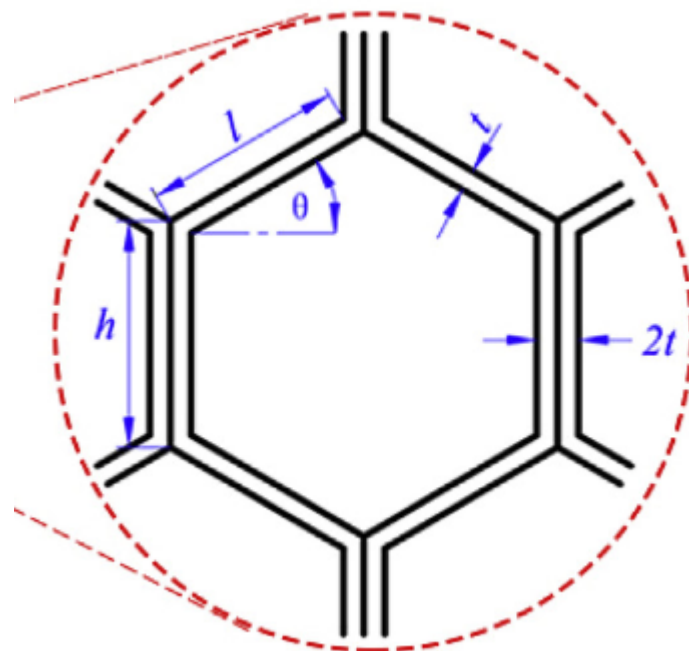


Figure 2-6 Hexagonal cell of honeycomb structure (Wang, 2019).

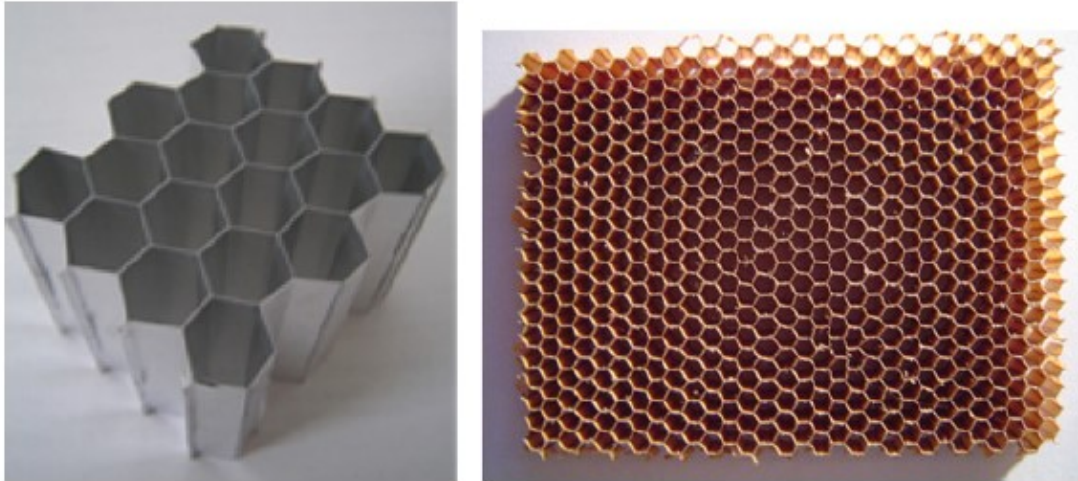


Figure 2-7 Hexagonal structure of honeycomb material made by aluminum and paper (Aktay et al., 2008).

Honeycomb structures have been widely used in engineering field. Honeycomb structure provides a material with minimal density, lightweight, and cost saving. At the same time, it provides outstanding through-thickness compression resistance. Honeycomb structure also has good energy absorption performance. Energy can be absorbed by plastic deformation of the cell (Asprone et al., 2013). For the currently application of honeycomb structure, it is not only used for furniture and racing boats but also used for aerospace and automotives (Wang, 2019).

### **2.3. INTRODUCTION TO SANDWICH PANELS**

Sandwich structure, shown in Figure 2-8, is a special class of composite material consisting of two thin skins, which are very stiff and strong to resist tension and compression stress on the two faces, and a thick and light weight core to separate the skins; at the same time, the core provides water resistance and noise resistance. Compared to traditional construction materials, sandwich structure are lightweight, higher stiffness and low cost. Sandwich panels have been used in construction as bridge

deck for several decades. Besides, another advantage of sandwich structure is flexibility, so it can be designed by different materials and sizes to obtain desire resistance based on the requirements. It allows engineers to use materials wisely and high effectively. It is considered as an efficient structural system and growing in civil engineering.

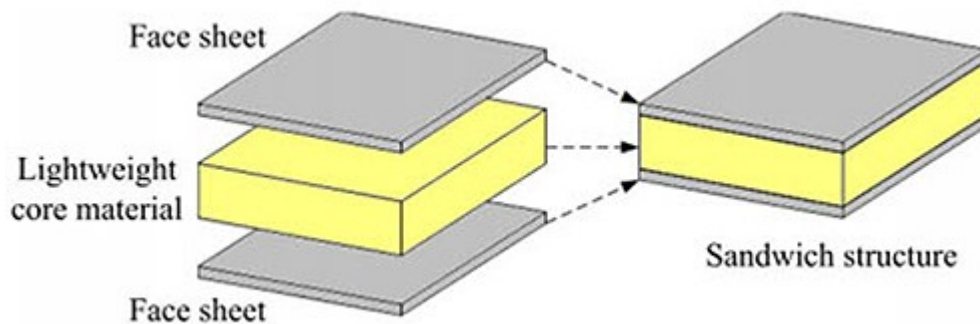


Figure 2-8 Sandwich Panel (Source: ISIS Canada Educational Module No.2: FRP Composites for Construction).

### 2.3.1. Sandwich Beam Theory

#### 2.3.1.1. Flexural Rigidity

As shown in Figure 2-9, a sandwich beam consists of two facings with each thin thickness “ $t$ ” and a thick core with thickness “ $c$ ” under three-point bending. The total height of the beam is “ $h$ ”, and the width is “ $b$ ”. To model the flexural rigidity,  $D$ , of the sandwich beam, the following assumptions are made:

- The facing material is much stiffer than core material.
- The facing material is well-bonded with core material.
- Both facing material and core material are isotropic.
- The cross-section is perpendicular to the longitudinal axis of the unloading beam when bending happens.

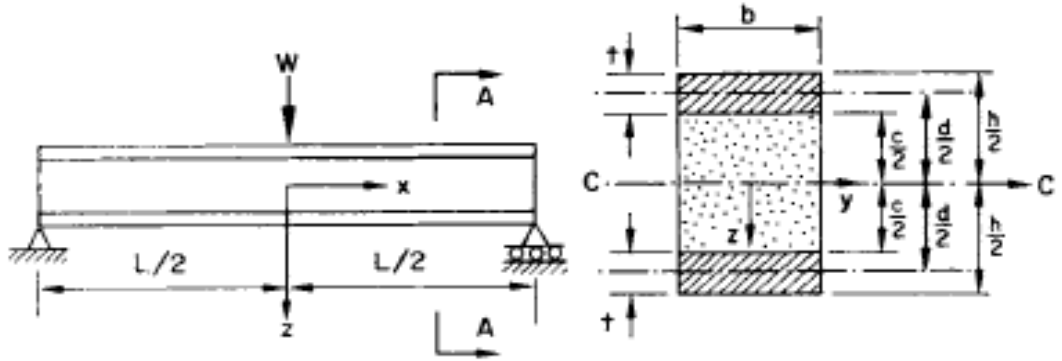


Figure 2-9 Dimension of sandwich beam and cross-section (Allen, 1969).

The flexural rigidity can be modeled by equation 2-1 (Allen, 1969; Zenkert, 1997):

$$D = 2D_f + D_o + D_c = E_f \frac{bt^3}{6} + E_f \frac{btd^2}{2} + E_c \frac{bc^3}{12} \quad \text{Eq. 2-1}$$

Where “ $D_f$ ” is the bending stiffness of the faces about their individual neutral axis, “ $D_o$ ” is the bending stiffness of the faces about the middle axis, “ $D_c$ ” is the bending stiffness of the core, “ $E_f$ ” and “ $E_c$ ” are the moduli of elasticity of the faces and core respectively, “ $d$ ” is the distance between the central lines of the faces and can be calculated by equation 2-2.

$$d = \frac{h + c}{2} \quad \text{Eq. 2-2}$$

### 2.3.1.2. Stress

Based on the same assumptions that were presented in the previous section, the stress in the facings and core can be demonstrated in equation 2-3 and 2-4 (Allen, 1969):

$$\sigma_f = \frac{Mz}{D} E_f \quad \text{Eq. 2-3}$$

$$\sigma_c = \frac{Mz}{D} E_c \quad \text{Eq. 2-4}$$

Where “ $\sigma_f$ ” is stress in the facings, “ $\sigma_c$ ” is stress in the core, “ $z$ ” is the distance from the neutral axis.

The maximum facing stress is obtained with  $z = \pm h/2$ , and the maximum core stress is

obtained with  $z = \pm c/2$ . Therefore, the maximum facings and core stress can be presented as (Allen, 1969):

$$\sigma_f = \pm \frac{ME_f}{D} \times \frac{h}{2} \quad \text{Eq. 2-5}$$

$$\sigma_c = \pm \frac{ME_c}{D} \times \frac{c}{2} \quad \text{Eq. 2-6}$$

The shear stress,  $\tau$ , of the sandwich beams can be demonstrated as equation 2-7 by assuming the beam is homogeneous (Allen, 1969).

$$\tau = \frac{QS}{Ib} \quad \text{Eq. 2-7}$$

Where “Q” is the shear force, “b” is the width at the level  $z_1$ , “I” is the second moment of area of the entire section about the neutral axis, “S” is the first moment of area of the part of the section that  $z$  is greater than  $z_1$ .

However, the difference between moduli of elasticity of facings and core needs to be considered. The equation is improved in 2-8 (Allen, 1969).

$$\tau = \frac{Q}{D} \left[ E_f \frac{td}{2} + \frac{E_c}{2} \left( \frac{c^2}{4} - z^2 \right) \right] \quad \text{Eq. 2-8}$$

To simplify the shear stress equation,  $E_c$  can be considered as 0 since the core is much weaker than facing material. Then, the equation is written as (Allen, 1969):

$$\tau = \frac{Q E_f td}{D \cdot 2} \quad \text{Eq. 2-9}$$

Then, assuming the thickness of facing is much smaller than the thickness of core, the bending stiffness of the facings about their individual neutral axis is neglectable.

Therefore, flexural rigidity here can be written as (Allen, 1969):

$$D = E_f \frac{btd^2}{2} \quad \text{Eq. 2-10}$$

Finally, equation 2-8 can be simplify to (Allen, 1969):

$$\tau = \frac{Q}{bd} \quad \text{Eq. 2-11}$$

Figure 2-10 (Zenkert, 1997) shows how the normal stresses and shear stresses profiles change after the corresponding assumptions were made.

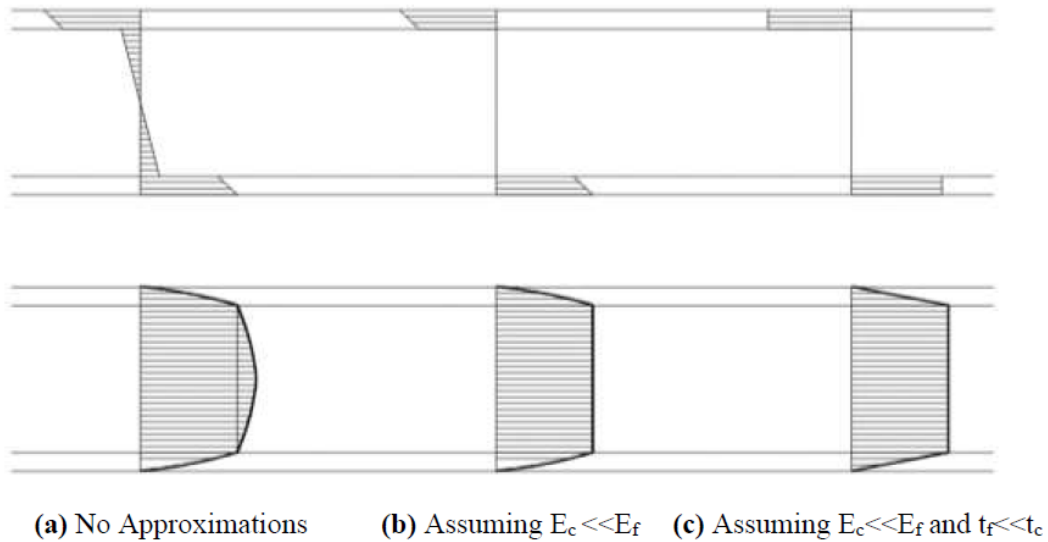


Figure 2-10 Normal and shear stresses for different levels of assumptions.

### 2.3.1.3. Mid-span Deflection (Based on Simply supported Sandwich Beam Under Three-point Bending)

The total mid-span deflection of a sandwich beam is the sum of the deflection due to bending of facing component and the deflection due to shear of core component, as shown in Figure 2-11 (Allen, 1969). The concept will be used for sandwich beam modeling in CHAPTER 4.

The total mid-span deflection is written as (Allen, 1969):

$$\Delta = \Delta_1 + \Delta_2 = \frac{WL^3}{48D} + \frac{WL}{4AG} \quad \text{Eq. 2-12}$$

$$AG = \frac{Gbd^2}{c} \quad \text{Eq. 2-13}$$

Where “ $\Delta$ ” is total mid-span deflection, “ $\Delta_1$ ” is deflection due to bending, “ $\Delta_2$ ” deflection due to shear, “ $W$ ” is the point force applying on the mid-span, “ $L$ ” is the

length of beam, “AG” is shear stiffness of the sandwich beam, “G” is the shear modulus of the core.

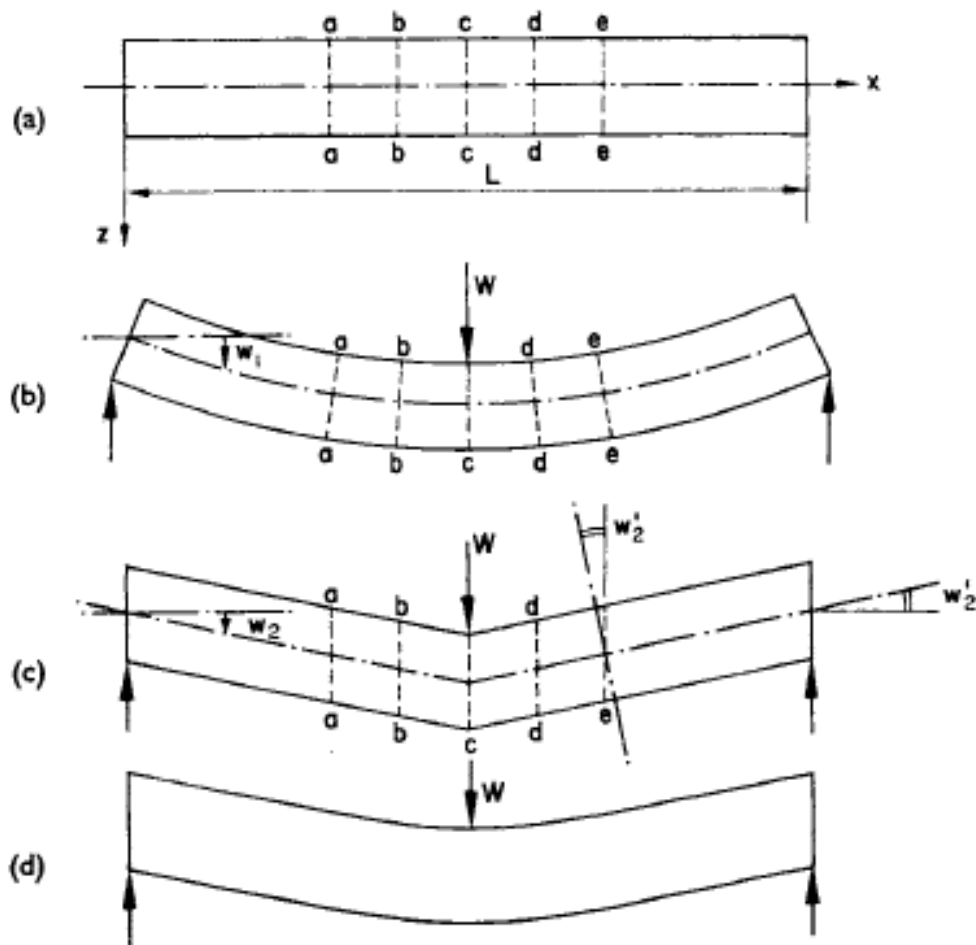


Figure 2-11 Deflection of sandwich beam (Allen, 1969).

#### 2.3.1.4. Curvature

Curvature is also an important property for beam analysis, as shown in Figure 2-12.

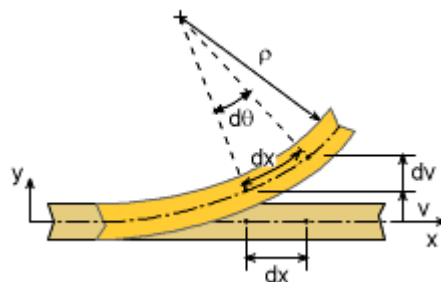


Figure 2-12 Beam curvature (Source: [www.ecourses.ou.edu](http://www.ecourses.ou.edu))

The curvature,  $\psi$ , is calculated by top strain of the sandwich beam,  $\epsilon_t$ , bottom strain of the sandwich beam,  $\epsilon_b$ , and total height of the sandwich beam,  $h$ , by equation 2-14.

$$\psi = \frac{\epsilon_t - \epsilon_b}{h} \quad \text{Eq. 2-14}$$

### 2.3.2. Testing Methods of Sandwich beams

#### 2.3.2.1. Tensile and Compressive Tests on Facing Component

The aim of tensile tests is to obtain the tensile data of the materials to research and to use for the beam analysis. The specimens need to be fabricated in the geometries that showing in Figure 2-13 (Zenkert, 1997).

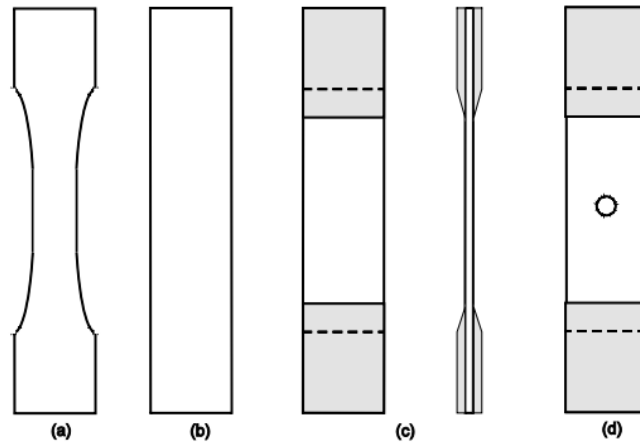


Figure 2-13 Different shapes of tensile specimens: a) dumbbell shape; b) rectangular shape; c) rectangular shape with tabs; d) notched rectangular shape with tabs (Zenkert, 1997).

The dimensions of specimens are measured before testing. The specimens must be placed properly on the testing machine. The longitudinal axis must be aligned with the test direction. Then, the load is applied on the specimens at the specified rate, which is based on different materials, until the failure happens. The ultimate strength can be determined by equation 2-15 (Zenkert, 1997):

$$\sigma_{cr} = \frac{P_{cr}}{tw} \quad \text{Eq. 2-15}$$

Where “ $\sigma_{cr}$ ” is the tensile stress at the failure load, “ $P_{cr}$ ” is load at the failure, “ $w$ ” is the width of material at testing section, “ $t$ ” is the thickness of specimen.

Similarly, the aim of compressive tests is to obtain the compressive data of materials. However, the geometries of compressive tests specimens are used to prevent buckling, as shown in Figure 2-14 (Zenkert, 1997).

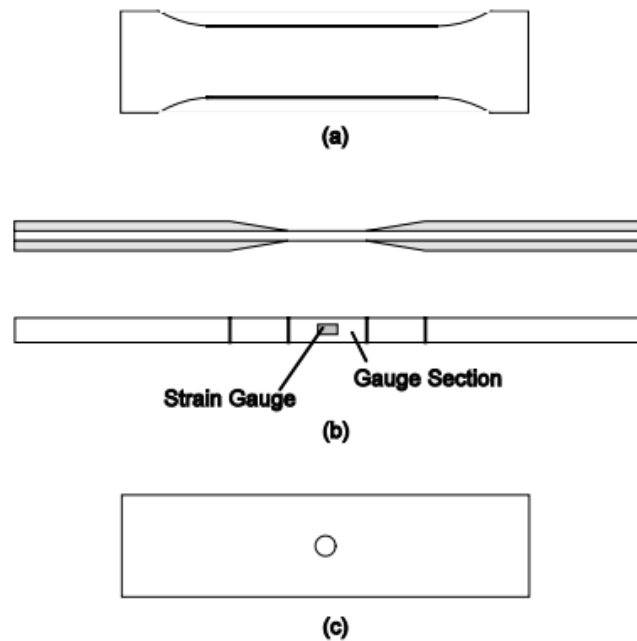


Figure 2-14 Different shapes of compressive specimens: a) the specimen with a waist; b) the specimen with tabs; c) the notch specimen (Zenkert, 1997).

The compressive strength is also calculated as equation 2-15.

### 2.3.2.2. Shear Test on Core Component

Shear test provides information of load-deflection behavior of the core material, and shear modulus is obtained based on the load-deflection curve. There are some dimension requirements of a shear test specimen (Zenkert, 1997):

- The thickness of specimen shall be equal to the thickness of the sandwich.
- The width of specimen shall not be less than twice of the thickness.

- The length of specimen shall be greater than twelve time of thickness.

An example of schematic view of testing honeycomb core is showing in Figure 2-15 (Soltani et al., 2014).

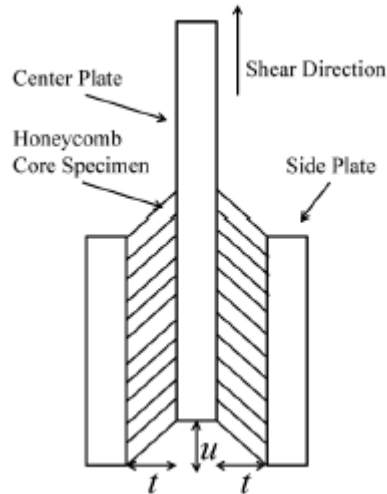


Figure 2-15 Schematic view of a honeycomb core shear test (Soltani et al., 2014).

Based on this test schematic, the shear stress,  $\tau$ , is calculated as follows (Soltani et al., 2014).

$$\tau = \frac{P}{2Lb} \quad \text{Eq. 2-16}$$

Where “P” is the load at the failure, “L” is the length of specimen, “b” is width of specimen.

Then, shear strain,  $\gamma$ , and shear stress,  $G_c$ , are calculated as follows (Soltani et al., 2014; Zenkert, 1997).

$$\gamma = \frac{u}{t} \quad \text{Eq. 2-17}$$

$$G_c = \frac{\tau}{\gamma} = \frac{Pt}{2uLb} \quad \text{Eq. 2-18}$$

### 2.3.2.3. Flexural Test on Sandwich Beams

The main flexural test methods are three-point bending and four-point bending. The behaviors of load-deflection and moment-curvature are achieved by flexural test for further beam analysis. The schematic views of three-point bending, and four-point bending are showing in Figure 2-16 (Zenkert, 1997).

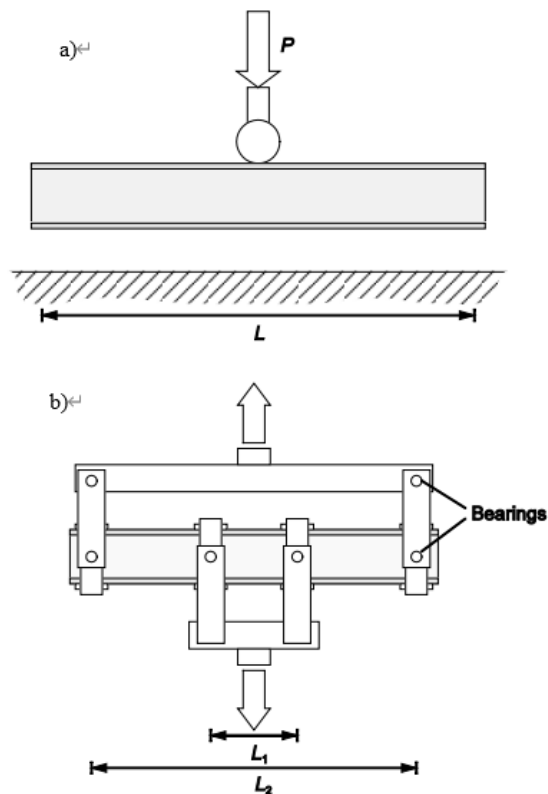


Figure 2-16 Schematic view of flexural tests: a) three-point bending; b) four-point bending (Zenkert, 1997).

There are some requirements must be met for specimens (Zenkert, 1997):

- Core shall be thick materials (e.g., foam, honeycomb), facing shall be thin.
- Width of the specimen shall not be less than the thickness of the sandwich beam.
- The ratio of  $(t_c + t_f)$  to  $t_f$  shall be greater or equal to 5.7.
- The facings and core must be well-bonded to prevent premature failure.

The load is applied on specimens at the rate of 1-10 mm/s based on different materials.

The maximum bending moment,  $M_{max}$ , and transverse force,  $T_{max}$ , are calculated for three-point bending test as follow (Zenkert, 1997).

$$M_{max} = \frac{PL}{4} \quad \text{Eq. 2-19}$$

$$T_{max} = \frac{P}{2} \quad \text{Eq. 2-20}$$

### 2.3.3. Sandwich Beam Failure Modes

Sandwich beams can fail in several modes, and each failure mode indicates a constrain in design process. Failure modes are important for the design of conventional materials, such as steel reinforced concrete, because the failure of steel or concrete indicates the failure is ductile or brittle. Similarly, it is also important to understand the failure criteria of sandwich beam. Different failure modes determine the limits of performance of whole sandwich system. Sandwich beams can be failed by facing or core materials, and there several failure modes for each component. The most common failure modes of sandwich beams are face yielding/rupture, core shear failure, and top face wrinkling, as shown in Figure 2-17 (Zenkert, 1997).

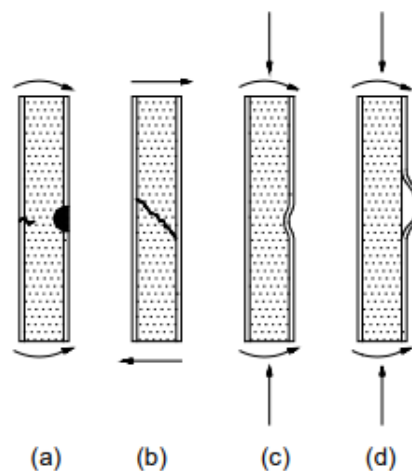


Figure 2-17 Failure modes of sandwich beams: a) face yielding/rupture; b) core shear failure; c) and d) top face wrinkling (Zenkert, 1997).

### 2.3.3.1. Facing Yielding/rupture

When the failure mode of face yielding/rupture happens, the facing material is failed earlier than core material caused by compressive stress on the top face or tensile stress on the bottom face. Although facing material is stronger than core material in sandwich beams, the face yielding/rupture is a common failure mode because the facing material resists almost all the stresses caused by flexural. The peak load of a sandwich beam that is failed by face yielding/rupture,  $P_{FR}$ , under three-point bending can be predicted by the equation 2-21 (Triantafillou et al., 1987).

$$P_{FR} = \frac{4\sigma_f bct}{L} \quad \text{Eq. 2-21}$$

### 2.3.3.2. Core Shear Failure

The core of sandwich beam is mainly failed by shear force since it carries almost all transverse force for the system. In addition, the facing materials, such as metal and FRP, are much stiffer and stronger than core materials, such as foam and honeycomb. Therefore, the failure mode of core shear is the most common failure in sandwich beam tests. The failure loads the core shear,  $P_{CS}$ , under three-point bending is presented in equation 2-22 (Triantafillou et al., 1987).

$$P_{CS} = \frac{2\tau_c bc}{\sqrt{\left(\frac{LE_c}{4tE_f}\right)^2 + 1}} \quad \text{Eq. 2-22}$$

### 2.3.3.3. Top Face Wrinkling

Face wrinkling can occur in the situations of in-plane compression, in the compressive face during bending, or shearing if the core is too soft (Zenkert, 1997; Su et al., 2021). Wrinkling is a local buckling phenomenon that sometimes governing the failure instead of other global buckling failure modes. Therefore, face wrinkling failure modes have

been studied by a lot of researchers for a long time. Yusuff (1955) determined the wrinkling stress,  $\sigma_{wr}$ , as follows.

$$\sigma_{wr} = k_1 \sqrt[3]{E_f E_c G_c} \quad \text{Eq. 2-23}$$

Where “ $k_1$ ” should be set to be different value in different models.

Allen (1969) presented the wrinkling stress as follows.

$$\sigma_{wr} = \frac{3}{\sqrt[3]{12(3 - \nu_c)^2(1 + \nu_c)^2}} \sqrt[3]{E_f E_c^2} \quad \text{Eq. 2-24}$$

Where “ $\nu_c$ ” is the Poisson’s ratio of the core material.

Carlsson and Kardomateas (2011) presented the wrinkling stress as follows.

$$\sigma_{wr} = 2 \sqrt{\frac{E_f E_c f}{12c}} \quad \text{Eq. 2-25}$$

#### 2.3.3.4. Failure Mode Maps

A failure mode map can be obtained by rearranging and developing the face yielding/rupture, core shear failure, and face wrinkling equations in mathematical programming software (e.g., MATLAB). The failure mode maps will be helpful for the designers to ensure the failure modes and failure loads of the sandwich beams by providing minimum design parameters (Betts et al., 2018). Betts et al. (2018) also used a failure mode map that developed by Triantafillou and Gibson (1987) to verify the failure modes of the sandwich beam, as shown in Figure 2-18.

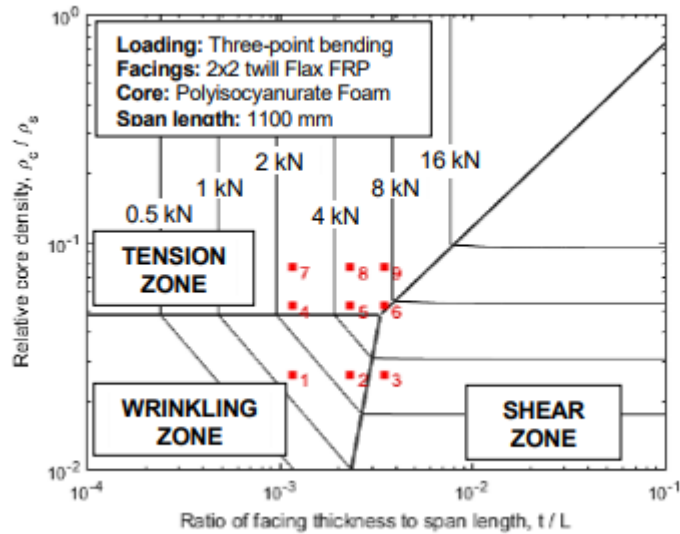


Figure 2-18 Failure mode map of FFRP-foam sandwich panel (Betts et al., 2018)

#### 2.3.4. History and Current Applications of Sandwich Structures

The concept of sandwich structures is a common principle in nature, which means the sandwich structures appeared earlier than mankind on this world. For example, the branches of trees are very similar to foam core sandwich structures. Also, the bones of human and animals are sandwich structure. The creatures on the world shows Nature selection of minimum use of material for maximum performance (Herrmann et al., 2005). The sandwich structure was firstly introduced by Fairbairn in 1849 for a bridge construction in England. Until around a hundred years later, sandwich structures started to be widely used for air force in World War II. At the same time, the first research paper about testing of sandwich structure was published by Marguerre in Germany in 1944, and the first paper of modeling sandwich structures was published by Hoff in 1948 (Vinson, 2005). In 1968, sandwich structure was successfully used in the Apollo project helping people to land on the moon (Herrmann et al., 2005). After that, sandwich structures started to be developed rapidly in field of aircraft and aerospace.

Today, 46% of the wetted surface of Boeing 757/767 is honeycomb sandwich (Vinson., 2005). Also, the use of sandwich structure is common in Airbus aircraft, as shown in Figure 2-19 (Herrmann et al., 2005).

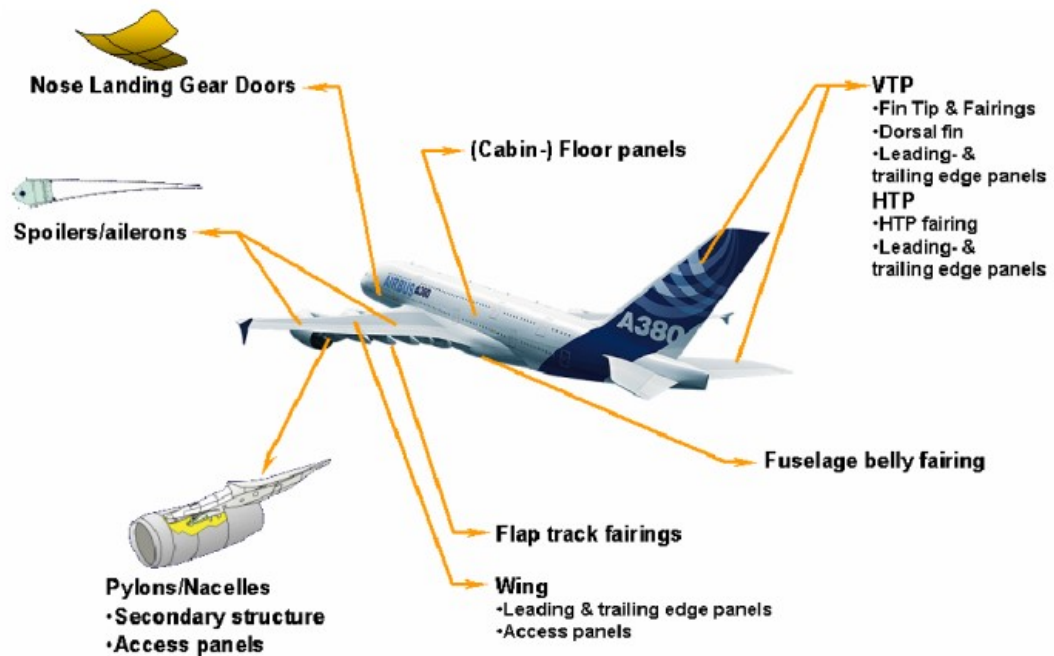


Figure 2-19 The application of sandwich structures in A380 (Herrmann et al., 2005).

For the application in civil engineering, sandwich structure has been used for a long time since its properties of lightweight and thermal insulation, as shown in Figure 2-20. It also has been used for building envelopes and roof panels. In the future, it will be commonly used for bridge deck (Vinson, 2005).

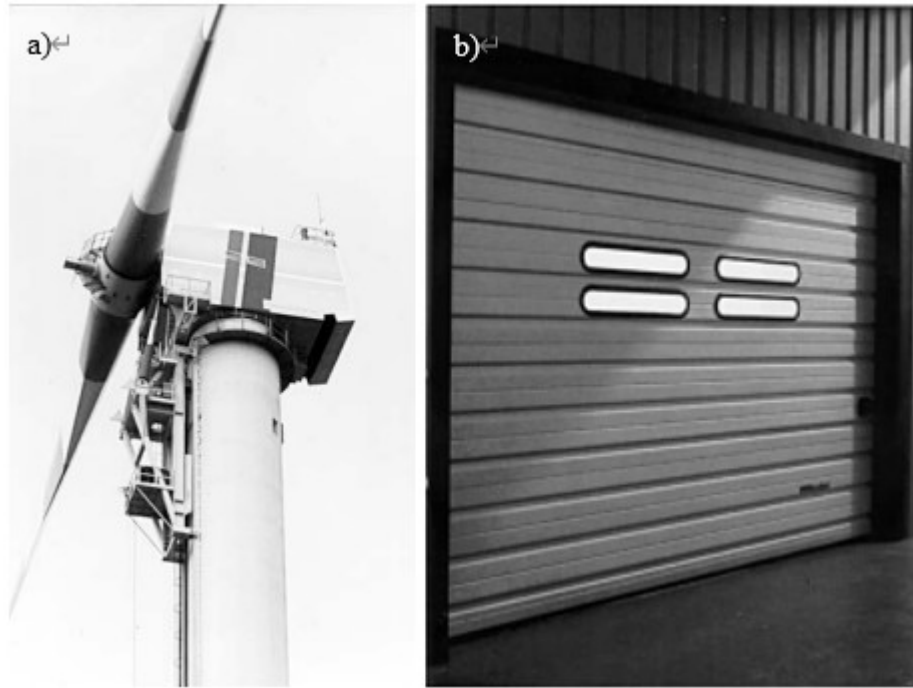


Figure 2-20 Sandwich structures application of civil engineering: a) Wind-mill housing structure in GFRP-sandwich; b) Large doors in sandwich construction (Zenkert, 1997).

### 2.3.5. Sandwich Composites made of Bio-based Materials

Currently, sandwich composites made of bio-based materials have been widely studied by researchers. Most of them were made of bio-based facing materials and synthetic cores. For example, the sandwich beams made by bio-based FRP facing and foam core were studied by Betts et al. (2018). The FRP facings were made of plant-based bidirectional flax fiber and a bio-based epoxy resin with 30% bio-content after mixing. The specimens were tested under three-point bending (Betts et al., 2018) and impacted load (Betts et al., 2021). Also, the post-impact residual flexural performance was evaluated (Betts et al., 2021). Furthermore, a sandwich beam and a stub column were fabricated by flax FRP and foam core and tested under four-point bending and axial compression, respectively, by CoDyre (2018). In this study, the capacities of the

specimens with flax FRP facing were compared to the specimens with glass FRP. The results were found that a three-layer flax FRP had a comparable thickness to a single-layer glass FRP, and they still had equivalent flexural and axial strengths.

In recent year, the sandwich beams made by fully bio-based materials were also appeared in research topics, a fully bio-based sandwich beam with flax FRP facing and cardboard core was studied, and the small-scale specimens were tested under four-point bending by McCracken et al. (2020). Then, Betts et al. (2021) tested this fully bio-based sandwich beam in large-scale under three-point bending and drop weight impact. Besides, another fully bio-based sandwich beam with flax FRP facing and paper honeycomb core was studied, and the small-scale specimens were tested under four-point bending by Fu et al. (2020). Moreover, a fully bio-based sandwich beam made of flax FRP facing and balsa wood core was fabricated and tested under damping by Monti et al. (2017). The vibration tests were carried out on flax FRP facing and balsa wood core separately to evaluate the damping behaviors of each component. Also, the damping properties of sandwich beam were studied, and a finite elements model was established.

## **CHAPTER 3 EXPERIMENTAL PROGRAM**

### **3.1. GENERAL INFORMATION**

In this study, sandwich beams with flax FRP and paper honeycomb (hollow and foam-filled) were tested under three-point bending. This chapter will present the details of test matrix, material properties, specimen fabrication, and test setup and instrumentation. Also, the test results will be reported and analysed. The models of facing and core component will be included.

### **3.2. TEST MATRIX**

A total of 18 flax FRP and paper honeycomb core sandwich beams which were 1200 mm long, 100 mm width, and 80 mm thickness, were tested. The dimensions were selected based on the literature. These are the most common dimensions for the large-scale sandwich beam tests. Therefore, the test results from this study will be easier to be compared to the results from the literature. The main parameters were the facing thickness and the type of paper honeycomb core (namely, hollow and foam-filled). Three facing thickness were studied experimentally: one layer, two layers, and three layers of flax FRP on each side. The thickness of each layer was measured to be approximately 1.5 mm. Two configurations of paper honeycomb core were studied experimentally: hollow and foam-filled cores. As shown in Table 3-1, a total of 6 sets were considered, and three identical specimens per set were manufactured and tested. A specimen identification with format of XFL-Y is used to identify each specimen. X is the number of flax FRP layers in each face, and FL represents “Flax Layers”. Y indicates the core type, where F is foam-filled, and H is hollow.

Table 3-1 Test matrix

No.	Specimen I.D.	Number of FFRP layers in each facing	Core types	Number of Specimens
1	1FL-H	1	Hollow	3
2	1FL-F	1	Foam Filled	3
3	2FL-H	2	Hollow	3
4	2FL-F	2	Foam Filled	3
5	3FL-H	3	Hollow	3
6	3FL-F	3	Foam Filled	3
			Total	18

Note: H =Hollow; F = Foam-filled

### 3.3. MATERIAL PROPERTIES

Prior to fabrication and testing sandwich beams, the materials properties of facing and core components were studied based on the data from supplier and tests. The flax FRP was fabricated by the same materials in Betts's (2018) previous research, so the mechanical properties of facing component were analysed and modeled based on Betts's test data. The core specimens were fabricated and tested under shear to obtain its material properties.

#### 3.3.1. Facing Material Properties

##### 3.3.1.1. General Information and Test Results from Betts et. al. (2018)

All the sandwich panels were fabricated by flax FRP as facing component. The flax FRP was fabricated by a bidirectional flax fabric (Biotex Flax, Composites Evolution, Chesterfield, UK) with a density of 410 g/m<sup>2</sup> and a bio-based epoxy resin with a bio-content of 21% after mixing (SuperSap, Entropy Resins, Hayward, CA, US). The flax FRP was fabricated by the same materials that were tested by Betts (2018) in previous research. According to Betts' tests on flax FRP coupons, the specimens were 250 mm

long and 25 mm wide. A uniaxial tension force was applied on five identical flax FRP specimens at the rate of 2 mm/min. The tensile modulus, strength, and ultimate strain of this flax FRP were tested to be  $7.51 \pm 0.69$  GPa,  $45.4 \pm 1.8$  MPa and  $0.0083 \pm 0.0009$  mm/mm, respectively. Also, five compression coupons were fabricated and tested in uniaxial compression at rate of 0.5 mm/min by Betts. The specimens were 70 mm long, 25 mm wide, and 25 mm thick. The compressive modulus, strength, and corresponding strain were tested to be  $6.73 \pm 1.59$  GPa,  $86.4 \pm 2.2$  MPa and  $0.0327 \pm 0.0010$  mm/mm, respectively. The stress-strain curve is shown in Figure 3-1. The tensile modulus and strength were used in the model since the tension face rupture is more possible to happen than compression face failure.

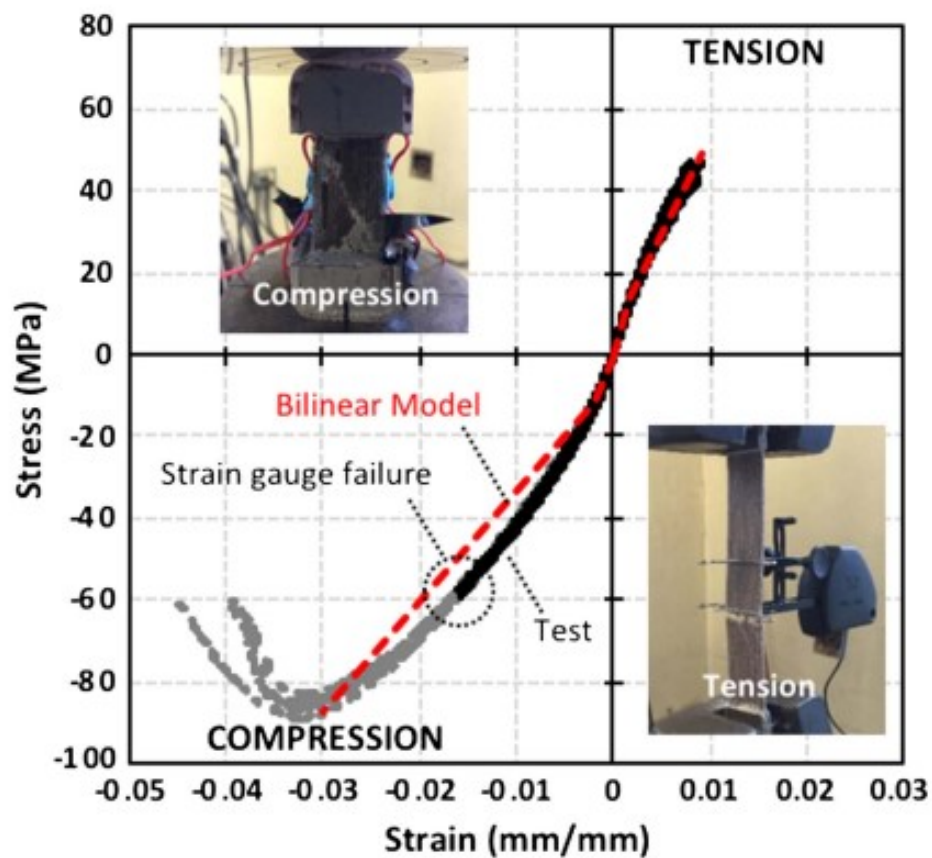


Figure 3-1 Stress-strain curve of facing materials in tension and compression (Betts, 2018).

### 3.3.1.2. Bilinear Stress-Strain Model of Flax FRP

The stress-strain curve of flax FRP can be modeled by a bilinear curve using Richard and Abbott equation showing below.

$$f = \frac{(E_1 - E_p)\varepsilon}{\left(1 + \left|\frac{(E_1 - E_p)\varepsilon}{f_0}\right|^n\right)^{1/n}} + E_p\varepsilon \quad \text{Eq. 3-1}$$

Where, as shown in Figure 3-2,  $\varepsilon$  and  $f$  are axial strain and stress of flax FRP, respectively;  $E_1$  and  $E_p$  are first and second modulus of flax FRP, and  $f_0$  is the stress at the intercept of second slope with stress axis;  $n$  is curve-shaped parameter that controls the curvature of the connection between two linear stress-strain relations.

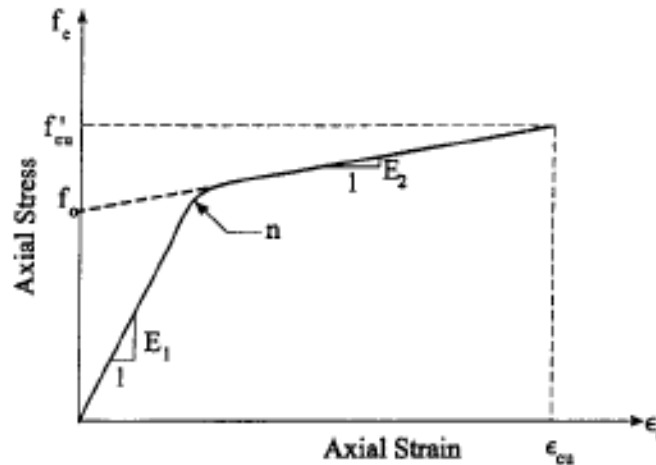


Figure 3-2 Parameters of bilinear model

The model can be divided into 3 parts. The first and third parts of model are two linear stress-strain relations with slopes of  $E_1$  and  $E_2$  ( $E_p$ ), which are 7.51 GPa and 4.59 GPa reported by Betts (2018). The point of transition was assumed to be at the strain of 0.0018 mm/mm (Betts, 2018), so  $f_0$  can be simply calculated to be 5.3 MPa. Then,  $n$  was assumed to be 3. The bilinear model function was plotted and compared to original test data shown in Figure 3-4.

### 3.3.1.3. Parabolic Stress-Strain Model of Flax FRP

The stress-strain curve of flax FRP can also be modeled using parabolic equation showing below and Figure 3-3 shows the parameters in stress-strain curve.

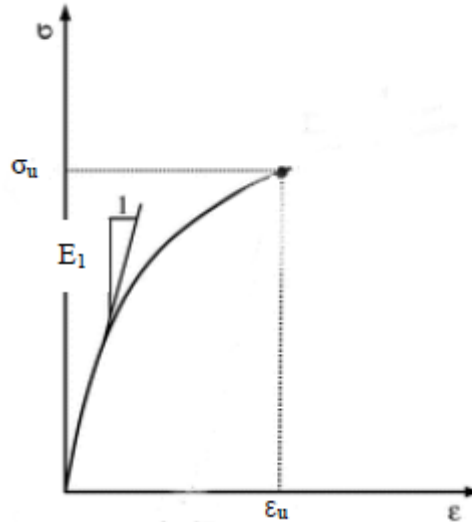


Figure 3-3 Nonlinear stress-strain curve with parameters.

$$y = Ax^2 + Bx + C \quad \text{Eq. 3-2}$$

Where “y” is the stress at the point that has the strain “x”. Since the stress-strain relation begins at the point (0, 0), the term “C” is zero. Then, the equation is rewritten as:

$$\sigma = A\varepsilon^2 + B\varepsilon \quad \text{Eq. 3-3}$$

To take the first derivative of stress,  $\sigma$ ,

$$\sigma' = \frac{\partial \sigma}{\partial \varepsilon} = 2A\varepsilon + B \quad \text{Eq. 3-4}$$

Which demonstrates the slope of stress-strain curve, and it is also known as modulus of the material. To apply the initial value of the strain ( $\varepsilon = 0$ ),

$$\sigma' = \frac{\partial \sigma}{\partial \varepsilon} = B = E_1 \quad \text{Eq. 3-5}$$

Then, applying the stress at the end point,  $\sigma_u$ , and the strain at the end point,  $\varepsilon_u$ , to Eq.

3-3, “A” is obtained.

$$A = \frac{\sigma_u - E_1 \varepsilon_u}{\varepsilon_u^2} \quad \text{Eq. 3-6}$$

Inputting “A” and “B” back to Eq. 3-3, the stress equation becomes:

$$\sigma = \frac{\sigma_u - E_1 \varepsilon_u}{\varepsilon_u^2} \varepsilon^2 + E_1 \varepsilon \quad \text{Eq. 3-7}$$

In this equation, there are totally three parameters ( $\sigma_u$ ,  $E_1$ ,  $\varepsilon_u$ ), and they were reported by Betts in the uniaxial tension test results. The parabolic model function was plotted and compared to original test data shown in Figure 3-4.

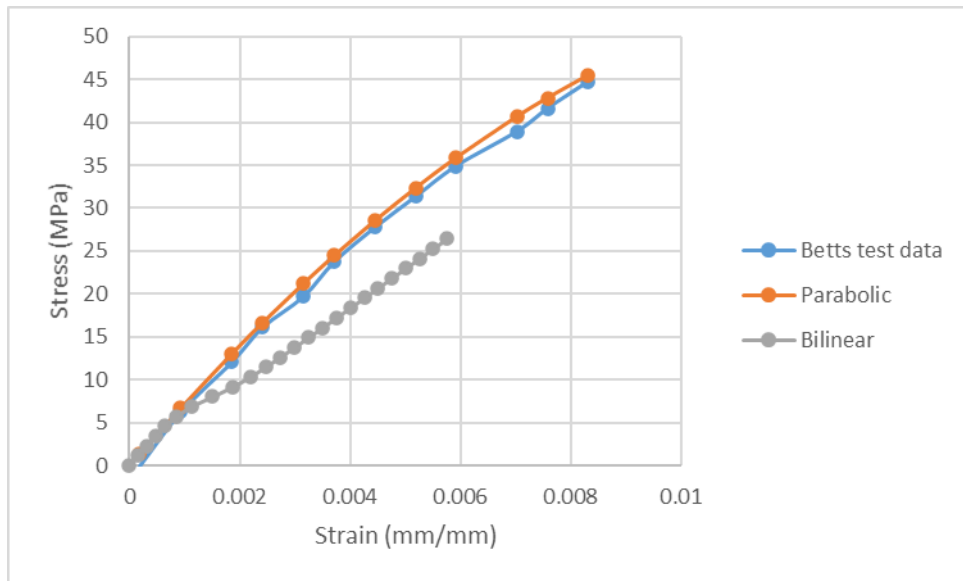


Figure 3-4 Bilinear and parabolic model comparing to original test data

#### 3.3.1.4. Discussion on Flax FRP Facing Modeling

Based on Figure 3-4, parabolic model fits better with original test data than bilinear model. Unlike other materials with nonlinear stress-strain behavior, such as steel, aluminum, or plastic fiber, the initial slope ( $E_1$ ) of stress-strain curve of flax FRP starts to decrease gradually from the beginning until it reaches its second slope ( $E_p$ ). For example, the stress-strain curve of the steel remains linear until it reaches the transition point at strain of 0.002 mm/mm. However, there is no transition point can be found in flax FRP stress-strain curve because the slope is always changing before it reaches to

the second slope. Therefore, parabolic model is better than bilinear model in this study for natural fiber FRP modeling, and it will be used for analytical study in Chapter 4.

### 3.3.2. Core material properties

All the sandwich panels were fabricated by hollow and foam-filled paper honeycomb cores. The density of fully stretched hollow core were measured to be  $19.12 \text{ kg/m}^3$  (JOY BUSINESS CO.,LTD., Jiashan, Zhejiang, China). The density of the spray foam that used to fill the hollow core was measured to be  $27.8 \text{ kg/m}^3$  (Quad Max Foam, LePage, Mississauga, ON, CA). The density of the foam-filled paper honeycomb core was measured to be  $43.87 \text{ kg/m}^3$ . To determine the mechanical properties of these two types of cores (hollow paper honeycomb, and foam-filled paper honeycomb), 3 specimens for each type of core were fabricated and tested under shear.

#### 3.3.2.1. Core Fabrication

Firstly, each honeycomb core panel is 1200 mm wide, 2400 mm long, and 76 mm thick; however, they were shipped in unexpanded form shown in Figure 3-5a). Therefore, the honeycomb core needs to be stretched before fabrication of core specimens or sandwich panels. Two wooden boards shown in Figure 3-5b) were used to fix both end of core, and epoxy resin was used as glue here. After one-day curing, the core was stretched, and the two wooden boards were braced by other two 2400 mm long wooden board shown in Figure 3-5e). The bracing wooden boards can be removed after 3 days set, and only the honeycomb core material from middle of the stretched paper honeycomb can be cut off and used for sandwich panel or core specimens' fabrication because the material near the edges was damaged during stretching, as shown in Figure 3-5f).



Figure 3-5 Core fabrication: a) unexpanded paper honeycomb; b) two wooden boards; c) applying epoxy resin to wood surfaces; d) curing with clips; e) stretching and setting; f) cutting

For the foam-filled honeycomb cores, the spray foam was filled into hollow paper honeycomb core by foam dispensing gun shown in Figure 3-6a). After 6 hours curing, a Surform Plane was used to remove extra foam on both sides, as shown in Figure 3-6b) and c).

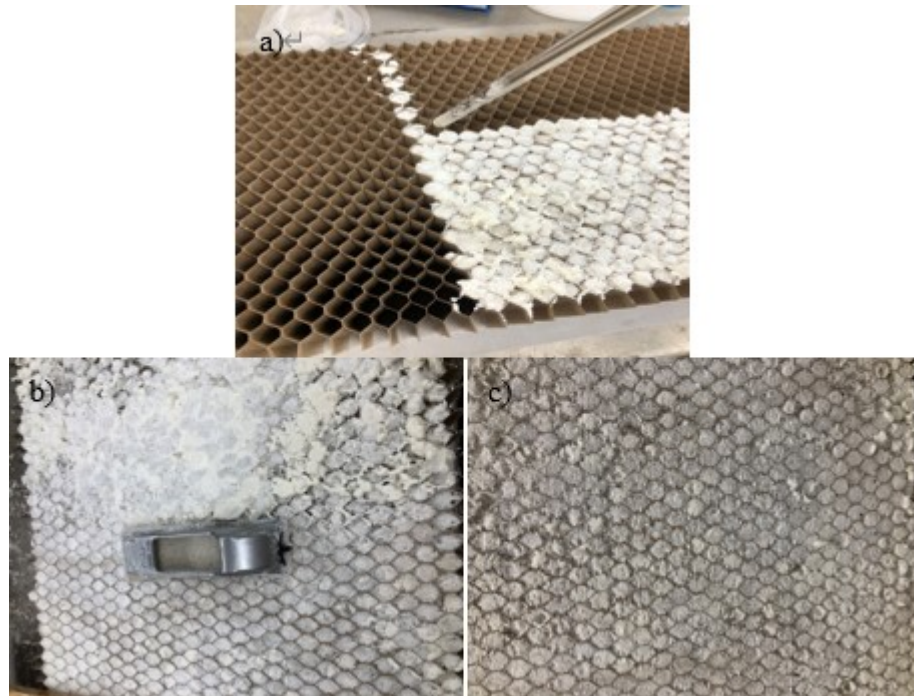


Figure 3-6 Foam filling: a) filling foam with dispensing gun; b) removal extra foam; c) finished foam-filled core

#### 3.3.2.2. Core Shear Test

In the sandwich structures, the shear force is mainly resisted by core material, so it is important to understand the shear properties of the core. The core specimens with 240 mm long, 50 mm wide, and 20 mm thick were cut from fabricated hollow and foam-filled paper honeycomb core panels. According to American Society for Testing Materials (ASTM) C273-94, both sides of specimens were fixed on steel plates by using epoxy resin as glue. The load was applied to the ends of the plates in compression through spherical bearing blocks, so the load was uniformly distributed to the width of the specimens. The constant movement rate of load was set to be 0.5 mm/min. The load resisted by the core specimen was recorded by Instron machine every 0.1s. The relative displacement between two steel plates was recorded by a linear potentiometer (LP), which was placed parallel to the longitudinal direction of the core specimen. As shown

in Figure3-7, the specimens were tested under shear.

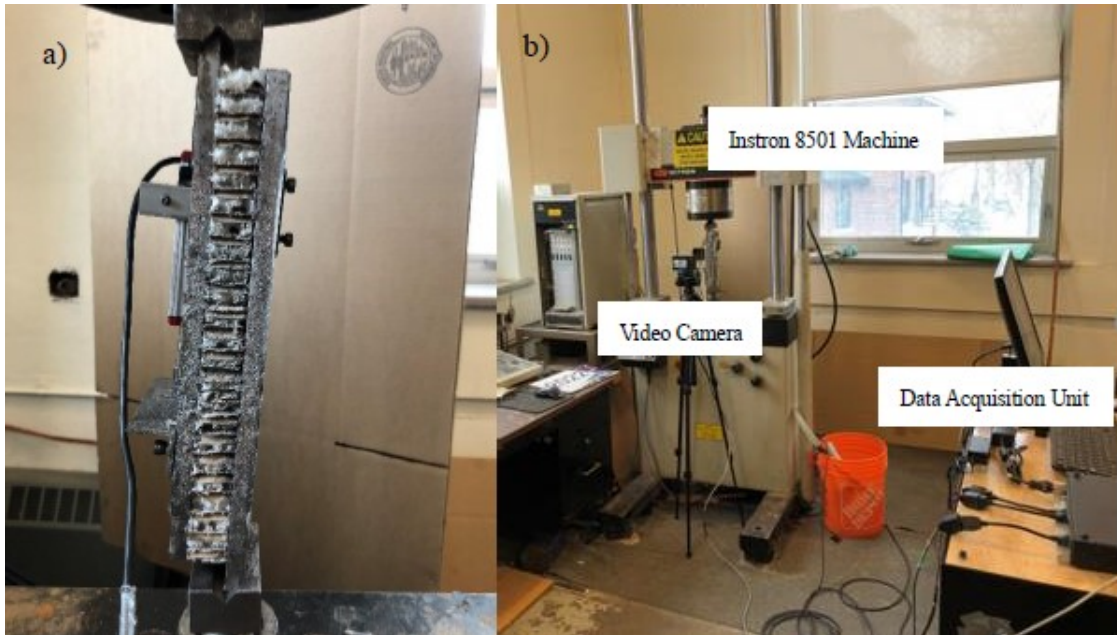


Figure 3-7 Core shear testing setup: a) core specimen set on Instron machine for shear test; b) shear test apparatus.

After finishing the tests, the data was processed by using Eq. 2-17 and Eq. 2-16 to obtain shear strain and corresponding shear stress. The test results are shown in Figure 3-8 and Table 3-2.

Table 3-2 Core Shear Test Results

Specimen Group ID	Shear Modulus, G (Mpa)				Shear Strength, $\tau_u$ (Mpa)				Shear strain at peak stress (mm)			
	Test	SD	COV (%)	Ave.	Test	SD	COV (%)	Ave.	Test	SD	COV (%)	Ave.
Hollow-1	11.110				0.1578				0.0367			
Hollow-2	9.778	0.757	7.394	10.236	0.1585	0.019	12.608	0.147	0.0412	0.004	10.725	0.0371
Hollow-3	9.821				0.1260				0.0333			
Foam-filled-1	17.870				0.2336				0.0261			
Foam-filled-2	12.169	4.823	37.763	12.773	0.2422	0.005	2.184	0.236	0.0407	0.012	31.582	0.039
Foam-filled-3	8.280				0.2329				0.0508			

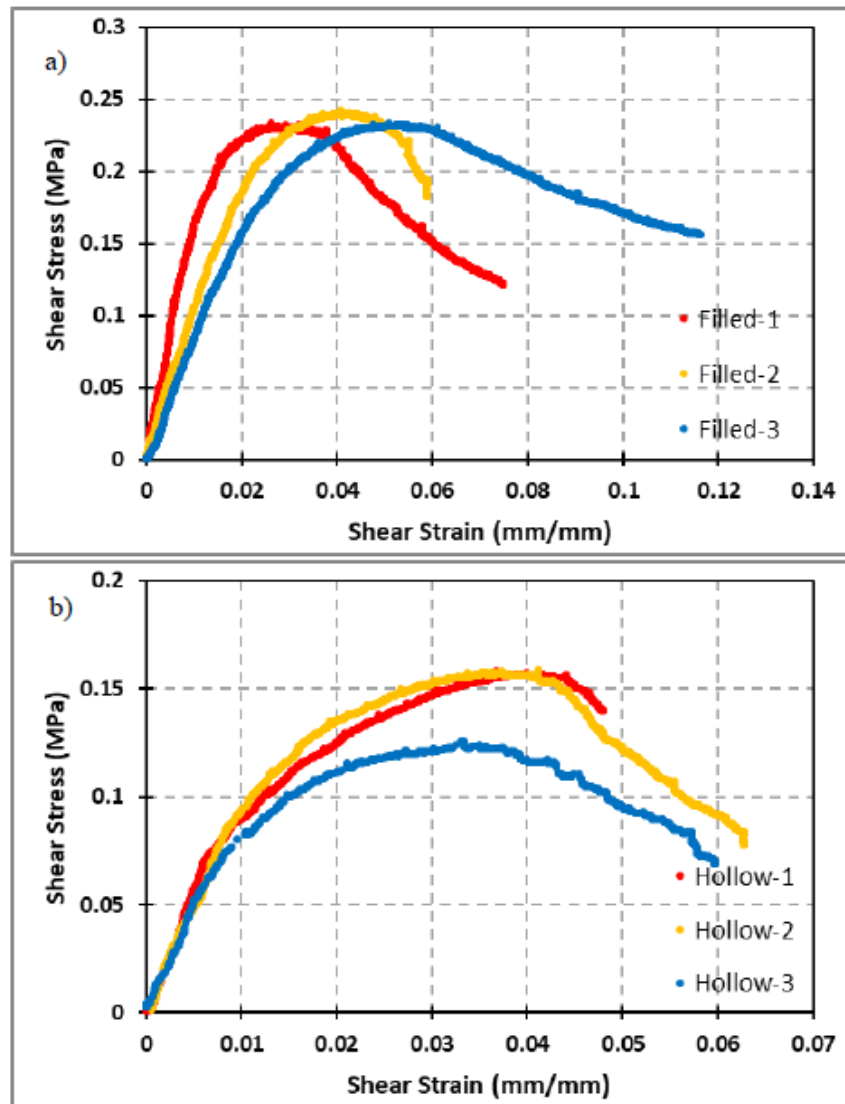


Figure 3-8 Core shear test results: a) shear stress-strain curve of foam-filled paper honeycomb; b) shear stress-strain curve of hollow paper honeycomb.

Looking at the shear stress-strain curves for both hollow and foam-filled paper honeycomb, a non-linear behavior of the curves was observed from beginning until the materials reach their ultimate shear strengths. After the materials yielded, instead of sudden rupture, there is no obvious failure path observed on the specimen, but the shear stress drops down gradually. The tests were stopped until the load drop by approximately 30% of the peak load. Looking at the shear stress-strain curves for hollow paper honeycomb, all the three first slopes, which indicates the initial shear

modulus (G), of the curves are identical, but the specimens failed at different peak shear stress. Looking at the shear stress-strain curves for the foam-filled paper honeycomb, the initial shear moduli are diverse, but they were failed at a constant stress. For example, the initial shear modulus of Foam-filled-3 was even lower than the hollow specimens, but it still failed at the same shear stress as other foam-filled specimens with higher shear strain at failure. This phenomenon was caused by the uncertainty of the filled foam. The foam was filled in the hollow paper honeycomb manually. Therefore, the errors were not possible to be avoided, such as the amount of foam in each cell was not exactly constant, the density of the foam may vary in different parts of honeycomb, the gaps between foam and cell wall were inevitable. The mechanical properties of foam-filled paper honeycomb core were obtained by averaging the test results of three specimens. For the hollow paper honeycomb core, the shear modulus, ultimate shear strength, and corresponding strain were tested to be 10.236 MPa, 0.147 MPa, and 0.037 mm/mm respectively. For the foam-filled paper honeycomb core, the shear modulus, ultimate shear strength, and corresponding strain were evaluated as 12.733 MPa, 0.236 MPa, and 0.039 mm/mm, respectively.

In addition, by the observation during the specimen fabrication, the shear test results may overestimate the strength of the core. The epoxy resin was used as glue to connect the specimens to the steel plates. The paper absorbed too much resin, and resin went through the whole thickness of the core specimens, as shown in Figure 3-9.



Figure 3-9 Resin absorbed by paper.

Therefore, the core material was reinforced by resin, it may show a higher strength in shear test than itself alone. This problem will be investigated more in Chapter 4.

### 3.3.2.3. Parabolic Shear Stress-Strain Model of Core

Like the parabolic model of flax FRP, core shear stress-strain curve can also be modeled by using parabolic equation showing below and Figure 3-10 shows the parameters in shear stress-strain curve.

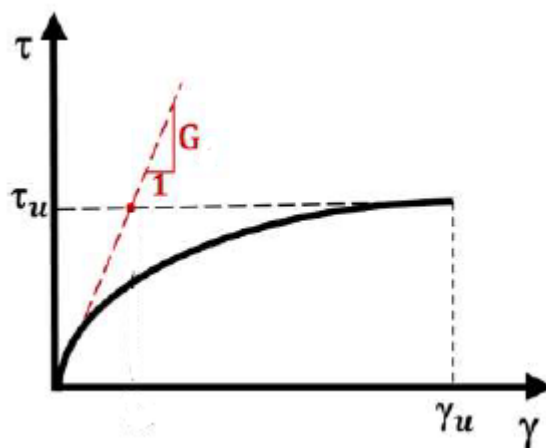


Figure 3-10 Nonlinear shear stress-strain curve with parameters.

$$y = Ax^2 + Bx + C \quad \text{Eq. 3-8}$$

Where “y” is the shear stress at the point that has the shear strain “x”. Since the shear

stress-strain relation also begins at the point (0, 0), the term “C” is zero. Then, the equation is rewritten as:

$$\tau = A\gamma^2 + B\gamma \quad \text{Eq. 3-9}$$

To take the first derivative of shear stress,  $\tau$ ,

$$\tau' = \frac{\partial \tau}{\partial \gamma} = 2A\gamma + B \quad \text{Eq. 3-10}$$

Which demonstrates the slope of shear stress-strain curve, and it is also known as shear modulus of the material. To apply the initial value of the shear strain ( $\gamma = 0$ ),

$$\tau' = \frac{\partial \tau}{\partial \gamma} = B = G \quad \text{Eq. 3-11}$$

Then, applying the ultimate shear stress,  $\tau_u$ , and the corresponding strain at the ultimate point,  $\gamma_u$ , to Eq. 3-9, “A” is obtained.

$$A = \frac{\tau_u - G\gamma_u}{\gamma_u^2} \quad \text{Eq. 3-12}$$

Inputting “A” and “B” back to Eq. 3-9, the shear stress equation becomes:

$$\tau = \frac{\tau_u - G\gamma_u}{\gamma_u^2} \gamma^2 + G\gamma \quad \text{Eq. 3-13}$$

Inputting the parameters to the Eq. 3-13, the models of hollow and foam-filled honeycomb core were plotted, as shown in Figure 3-11.

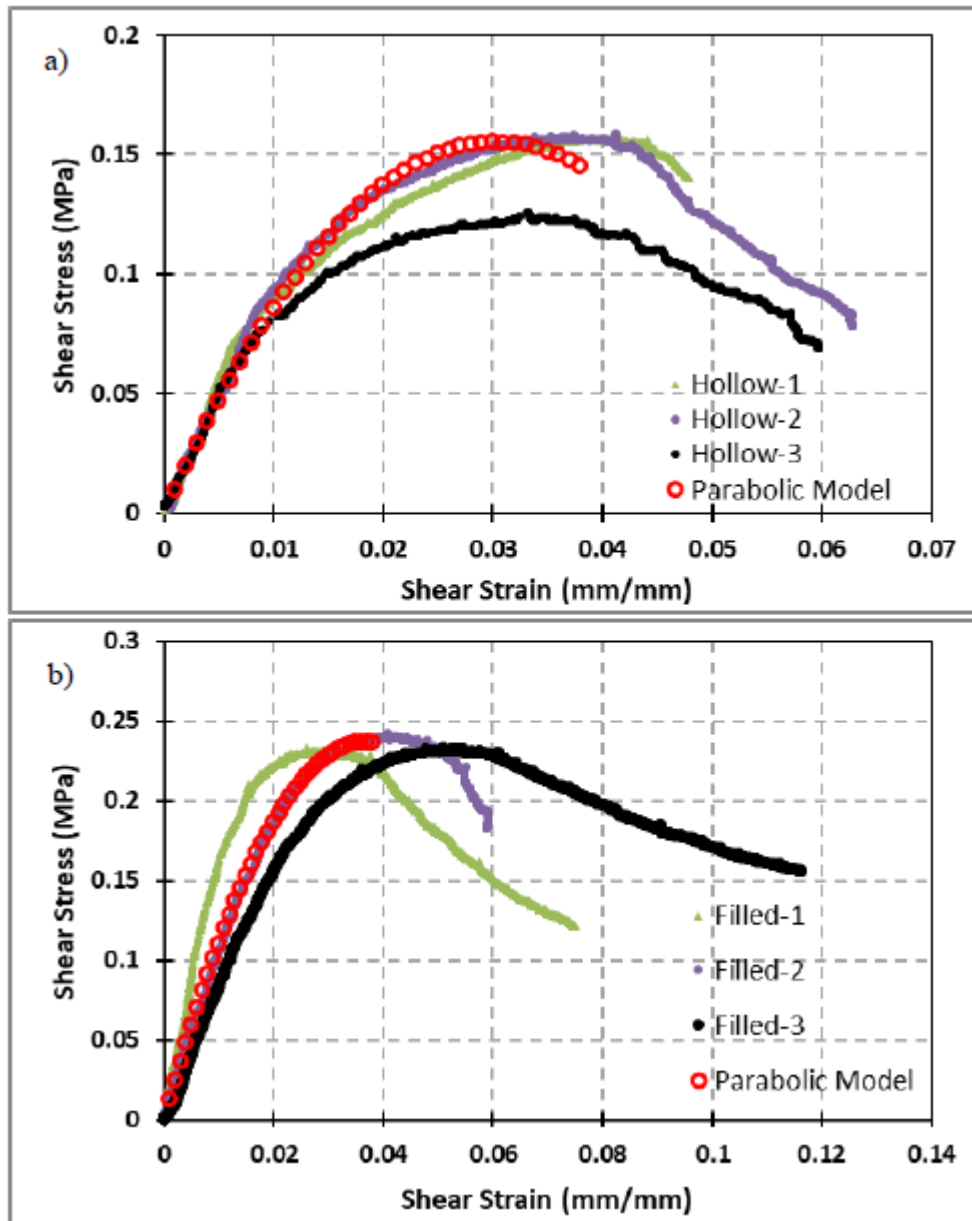


Figure 3-11 Parabolic model comparing to test results: a) Hollow honeycomb core; b) foam-filled honeycomb core.

### 3.4. FABRICATION OF SANDWICH PANELS

All the sandwich panels followed the same fabrication procedure, as shown in Figure 3-12. Firstly, the flax was cut to the proper dimensions by scissors, as shown in Figure 3-12a). Parchment paper was taped on a clean table surface to make sure the facings of final products are flat and easy to separate from table after resin is fully cured. Once a

layer of parchment paper was applied on a flat surface, the bio-based epoxy resin was mixed with hardener at a ratio of 100:43 by weight and applied to the parchment paper, as shown in Figure 3-12b). The brushes were used to evenly spread the mixed resin on the parchment paper. Then, the first layer of flax fabric was applied to the wetted parchment paper with the warp direction of the fabric parallel to the longitudinal direction of the specimen, as shown in Figure 3-12c). Then, another layer of bio-based epoxy resin was applied to the flax fabric to make the fabric fully saturated, as shown in Figure 3-12d). Based on the desired flax FRP layers, more flax fabric layers were applied in the same process. After the desired number of flax fabric layers had been applied (1, 2, or 3), another parchment paper was placed on the top surface of saturated flax fabric. A scraper was used to remove extra resin and air bubble, as shown in Figure 3-12e). Finally, the top face parchment paper was removed, and the correct paper honeycomb core (hollow or foam-filled) was placed on the flax fabric. A weighted wooden board also placed on the top of paper honeycomb core to squeeze the extra resin outflow from the sides and make sure the close contact between facing and core, as shown in Figure 3f). After one day curing, this entire procedure was repeated for the fabrication of the other face. Seven days were needed to make the specimen fully cure before cutting. A band saw was used to cut the sandwich panel into individual specimens with desired size of 1200 mm long and 100 mm wide.



Figure 3-12 Sandwich panel fabrication: a) cutting flax fabric; b) applying a layer of resin; c) placing a layer of flax fabric; d) saturating flax fabric; e) removal of extra resin and air bubbles; f) placing core and weighed wooden board

### 3.5. INSTRUMENTATION AND TEST-UP

Each specimen was tested under three-point bending. The load was applied to the specimen at a rate of 2 mm/min through a 150x150x275 mm Hollow Structure Section (HSS). The HSS was used to distribute the load evenly at the middle of the specimen to avoid the premature local failure. The weight of the HSS is 62.4 N, which will be accounted for data process of the test. Two strain gauge were installed at the center of compression and tension face to measure the change of longitudinal strain during the

test. To ensure that the strain gauge would not be damaged by HSS, a 35 mm diameter hole was cut at the middle of the bottom face of the HSS. A string potentiometer was applied at the center bottom of the specimen to measure mid-span deflection of the specimens. One support was a roller, and the other one was hinge. A data acquisition system was used to record the applied force, mid-span deflection, and changes of strains on both of compression and tension faces at a rate of 10 samples per second. The test setup is shown in Figure 3-13.

The tests were terminated when either sandwich beam specimens were crushed, or the load dropped by 30% from the peak load. The pictures of each failed specimen were taken by camera to identify the failure modes.

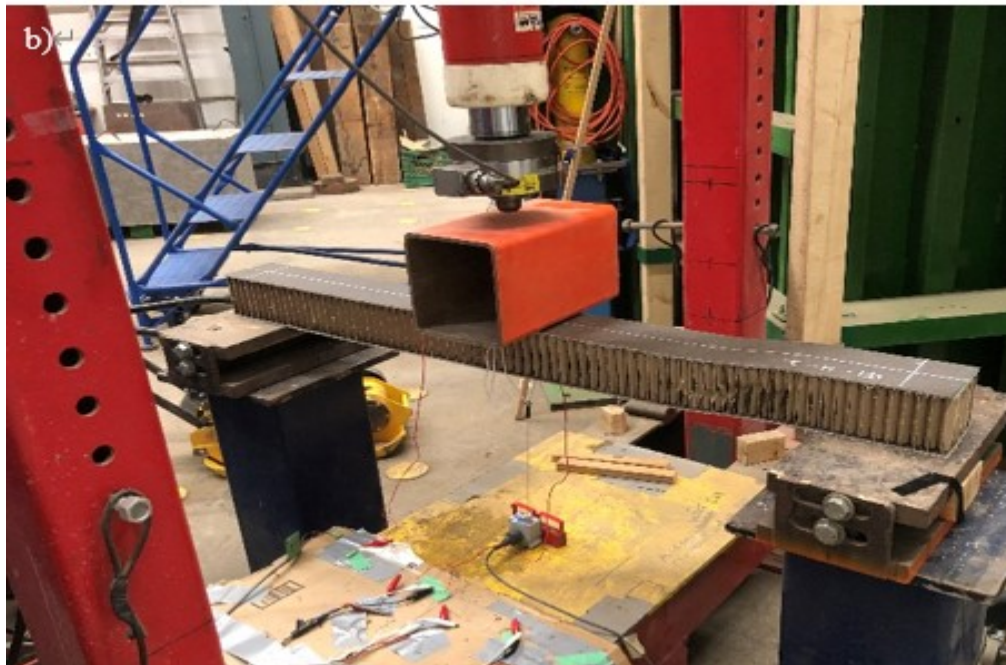
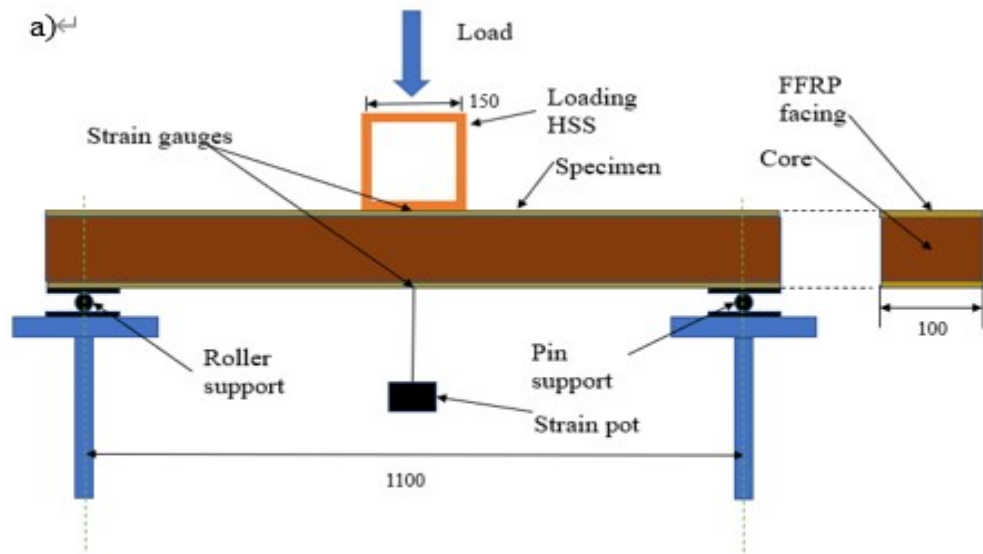


Figure 3-13 Test setup and instrumentation: a) schematic drawing (dimensions in mm); b) test setup photo

### 3.6. DATA ANALYSIS AND TEST RESULTS

The main test results are load-deflection, load-strain, and moment-curvature responses of the sandwich beam specimens. Table 3-3 shows the test results of each group of specimens, including: the peak load, initial stiffness, initial flexural rigidity, failure modes, and deflection at peak load. This section will present failure mode, load-

deflection diagrams, and moment-curvature diagrams. Also, the effect of facing thickness and honeycomb core types will be discussed. The initial stiffness and initial flexural rigidity were taken as the first linear slope of load-deflection and moment-curvature diagrams, respectively.

Table 3-3 Summary of test results.

Case #	Specimen Group ID	Peak load		Stiffness		Flexural Rigidity		Failure Modes	Deflection at Peak load (mm)	
		(N)		(kN/m)		(kN-m <sup>2</sup> )			(mm)	
		AVG	COV (%)	AVG	COV (%)	AVG	COV (%)		AVG	COV (%)
1	1FL-F	1039.6 (1358.2)	39.8	94.8	4.7	2.5	16.0	CS/Debonding	12.45	36.9
2	1FL-H	898	19.8	86.3	6.6	2.6	6.7	CS	12.76	21.6
3	2FL-F	2392	19.7	167.8	4.5	6.5	10.3	CS	16.74	6.5
4	2FL-H	926.3	26.6	146.1	6.9	5.5	5.8	CS	11.55	30.3
5	3FL-F	2377.9 (3068.3)	50.3	216.2	4.7	8.4	21.9	CS/Debonding	12.65	48.0
6	3FL-H	990.0	14.6	176.1	6.8	5.7	6.3	CS	7.33	10.2

Note: the number in the brackets is the average peak load ignoring the specimens with debonding failure.

### 3.6.1. Failure Mode

There are couple failure modes of sandwich beams. However, in this study, only two failure modes were obtained: core shear and debonding. The failure modes of each group of specimens are shown in Table 3-3. Figure 3-14 shows the examples of each failure modes on two core types. Specimen 1FL-F and 1FL-H with one layer flax FRP were failed by core shear. No surprisingly, when the thickness of facing is increasing, the failure mode of rest specimens would also be governed by core shear strength. On the other hand, looking at specimens with debonding failure mode, all of them were specimens with foam-filled honeycomb core. Debonding failure was possibly caused by an interfacial crack propagation between facing and core, and, in this study, it leaded

to premature failure of specimens. For example, when the specimens of 3FL-F-1 and 3FL-F-2 were failed by core shear with peak load of 3036.4 N and 3100.1 N, the specimen of 3FL-F-3 was failed by debonding with peak load of 997.1 N. The debonding was caused by the pre-existing crack between the facing and core. The reason why it always happened on the specimens with foam-filled core is fabrication method. All the foam-filled honeycomb cores were manually filled with foam in the lab, as mentioned in section 3.3.2.2. Even the extra foam on the surface was removed by Surfoam Plane and sandpaper carefully, it was still impossible to ensure that the surfaces of each specimen were perfectly flat. Another possible reason was that, in the procedure of fabricating sandwich panels, too much resin was removed before the foam-filled core was placed on the saturated flax fabric, which may result in the imperfect bond between core and facings. Therefore, there were some tiny gaps in the connection of facing and core after resin was applied, and they were difficult to be observed. The crack began at these tiny gaps and propagated to the whole interface, and they result in the premature debonding failure.

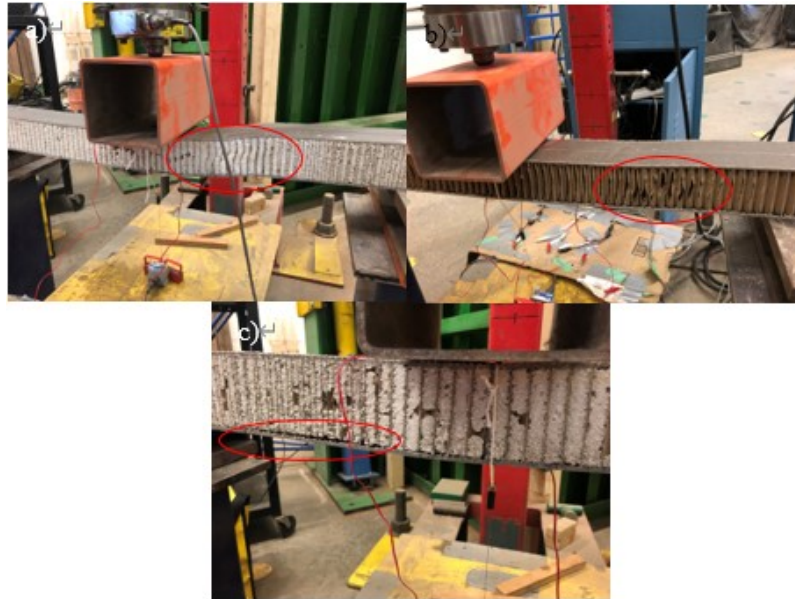


Figure 3-14 Example of failure modes: a) core shear failure on foam-filled core; b) core shear failure on hollow core; c) debonding failure on foam-filled core

In addition, when the specimens were failed by core shear, they were not crushed in sudden; at the same time, the specimens were still remaining a part of capacity to resist load. The resisting load was going down gradually along with the deforming of honeycomb core. This phenomenon was especially observed for the specimens with hollow paper honeycomb core.

### 3.6.2. Load-deflection Behavior

Deflection of beams under applied loads is an important factor to consider in beam design. It could be a governed criterion to meet serviceability limit state requirement. The changes of deflection were captured by a string potentiometer that was placed at the mid-span of each specimen. The load-deflection behaviors of each specimen are shown in Figure 3-15.

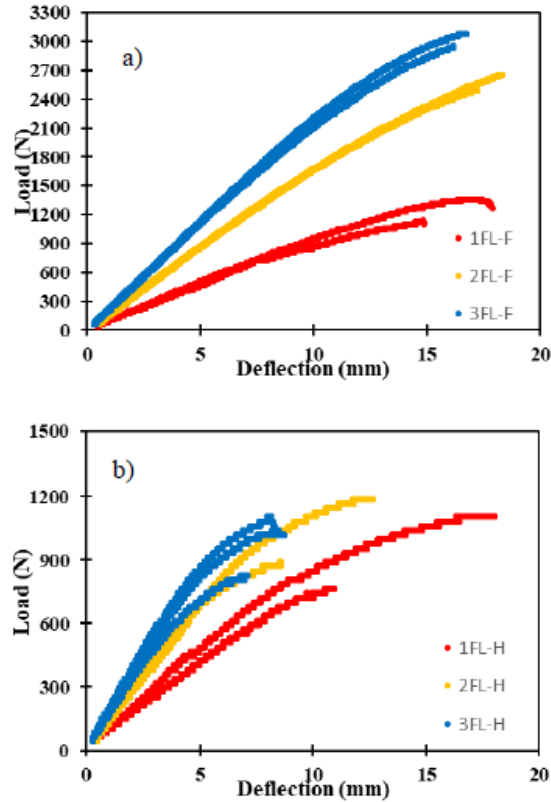


Figure 3-15 Load-deflection behavior of specimens: a) specimens with foam-filled paper honeycomb core; b) specimens with hollow paper honeycomb core.

The initial stiffness of each specimen was calculated based the initial slope of load-deflection curve. Because of the non-linear behavior of the specimens, the initial stiffness was calculated by truncating the non-linear tail of the curve until the diagram was close to a line representing the initial stiffness of the specimen. The peak loads and initial stiffness are shown in Table 3-3 and will be used in the analytical study in Chapter 4. Each value presented in the table is the average of three identical specimens. The standard deviation of each parameter is also provided in the table.

### 3.6.3. Moment-curvature Behavior

The moment was calculated for mid-span of the specimens and the curvature was calculated based on the values of strain from two strain gauges applied on the center of

each side of the specimens. The curvature,  $\varphi$ , was calculated by Eq.3-14 based on top face strain,  $\epsilon_t$ , bot face strain,  $\epsilon_b$ , and the height of specimen,  $h$ .

$$\varphi = \frac{\epsilon_t - \epsilon_b}{h} \quad \text{Eq. 3-14}$$

As shown in Figure 3-16, the slope of the moment-curvature represents the flexural stiffness,  $D$ , of each specimen and is presented in Table 3-3.

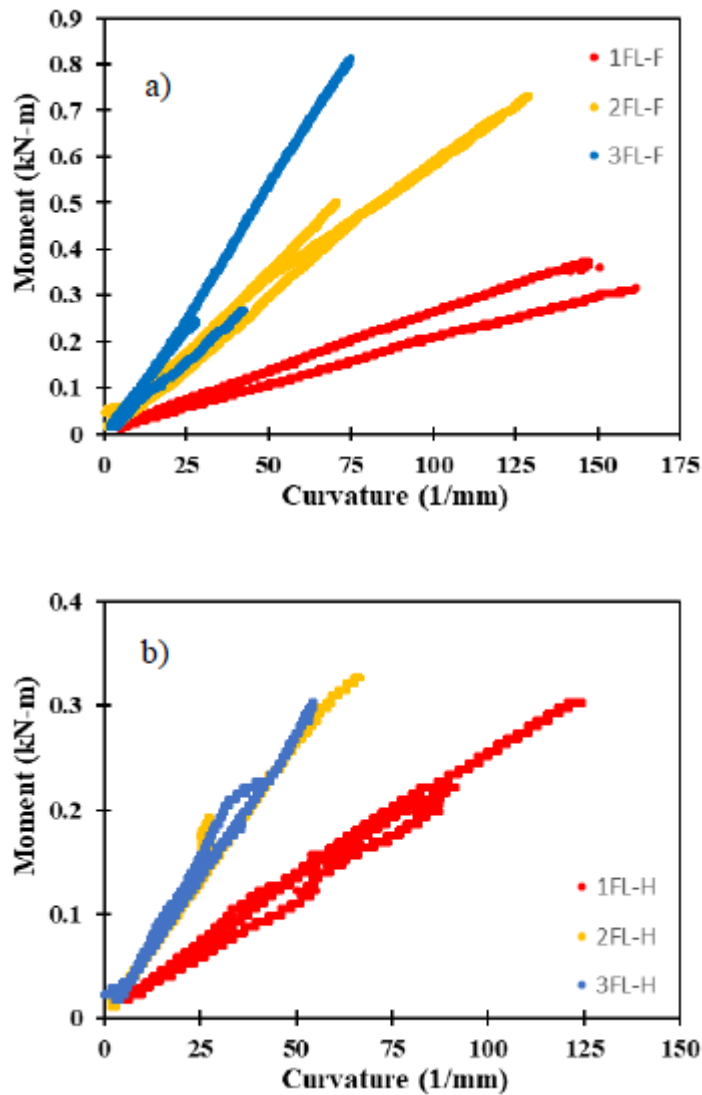


Figure 3-16 Moment-curvature behavior of specimens: a) specimens with foam-filled paper honeycomb core; b) specimens with hollow paper honeycomb core.

#### 3.6.4. Effect of Honeycomb core types

Honeycomb core configuration is one of main parameters in this study. As shown in

Figure 3-17, the honeycomb core type has relatively smaller effect on the initial stiffness and initial flexural rigidity. For example, looking at the difference between 1FL-F and 1FL-H, 2FL-F and 2FL-H, and 3FL-F and 3FL-H, the initial stiffness was increased by 9.8%, 14.9%, and 22.8%, and the initial flexural rigidity almost remained constant. However, looking at the specimen 3FL-F and 3FL-H, the specimen with hollow core had a lower initial flexural rigidity than the expectation, which may be caused by the failure of the strain gauges during the test.

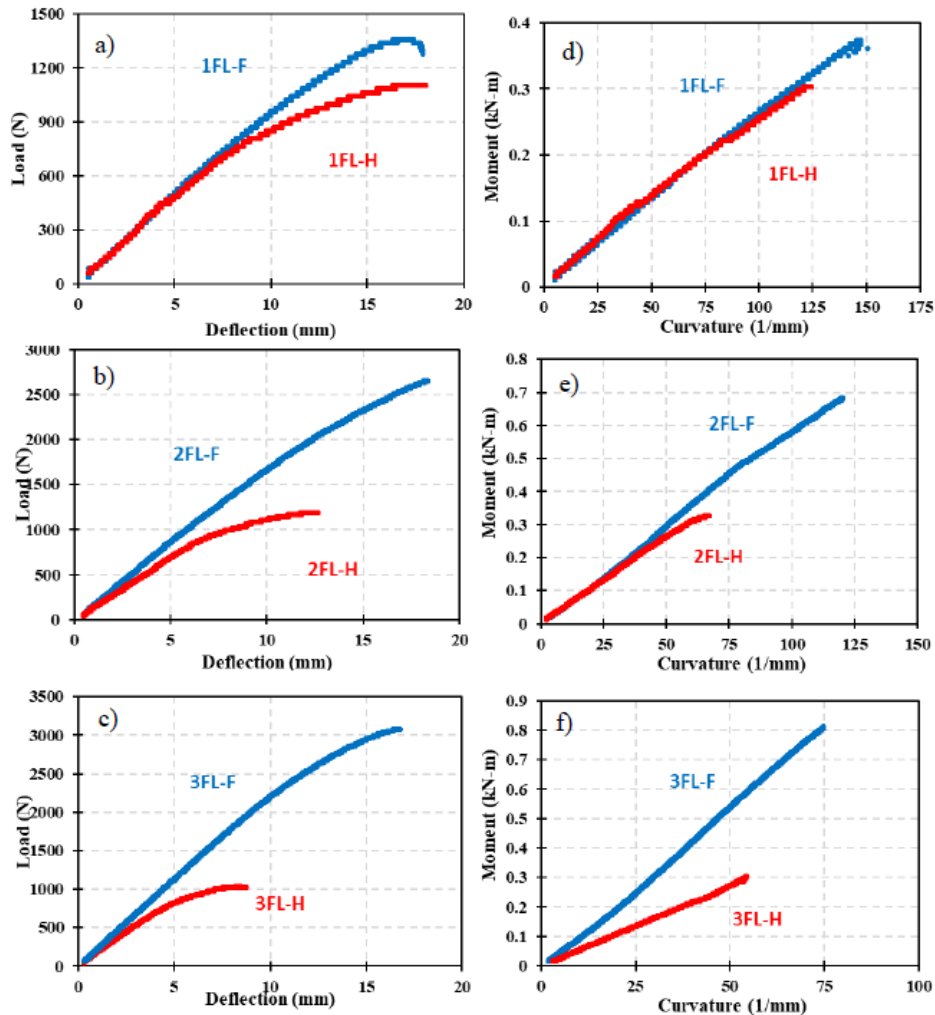


Figure 3-17 Effect of honeycomb core type on load-deflection and moment-curvature diagrams: a) load-deflection for 1-layer specimens; b) load-deflection for 2-layer specimens; c) load-deflection for 3-layer specimens; d) moment-curvature for 1-layer specimens; e) moment-curvature for 2-layer specimens; f) moment-curvature for 3-layer specimens

Moreover, in this study, the change in core type also had a major impact on the peak load and ultimate moment at the peak load. For example, looking at the different between 1FL-F and 1FL-H, 2FL-F and 2FL-H, and 3FL-F and 3FL-H, the peak loads were increased by 51.2%, 158.2%, and 209.9% (ignoring specimen with premature debonding failure). The reason of that is that all the failure modes of specimens were governed by core strength. Therefore, when core was getting stronger, the peak load was higher.

#### 3.6.5. Effect of Facing Thickness

Facing thickness is another main parameter in this study. The thickness of each layer of flax FRP is around 1.5 mm. As shown in Figure 3-18, the change of facing thickness had a major impact on initial stiffness and initial flexural rigidity for each honeycomb core type. For example, by changing the facing thickness from one to two layers (1FL-F to 2FL-F), the initial stiffness and initial flexural rigidity were increased by 77% and 160%, respectively. However, the specimen 3FL-H did not follow the trend, its initial flexural rigidity did not change when a thicker facing applied. The failure mode was not changed because the core is always critical, even in the 1-layer specimens. For the specimens with foam-filled core, their peak load and corresponding ultimate moment were increased by adding more flax FRP layers. For example, the peak load and corresponding ultimate moment were increased by 130% and 105%, respectively, from 1FL-F to 2FL-F. On the other hand, for the specimens with hollow core, the increasing of facing thickness did not affect their peak load and ultimate moment. To conclude, compared to the facing material, the core material was too weak. The strengths of the

sandwich beams were not effectively improved by applying more facing layers. Even for the specimen with 1-layer flax FRP facing, the failure was still governed by core strength, so the facing material would not be fully utilized when thicker facing was applied.

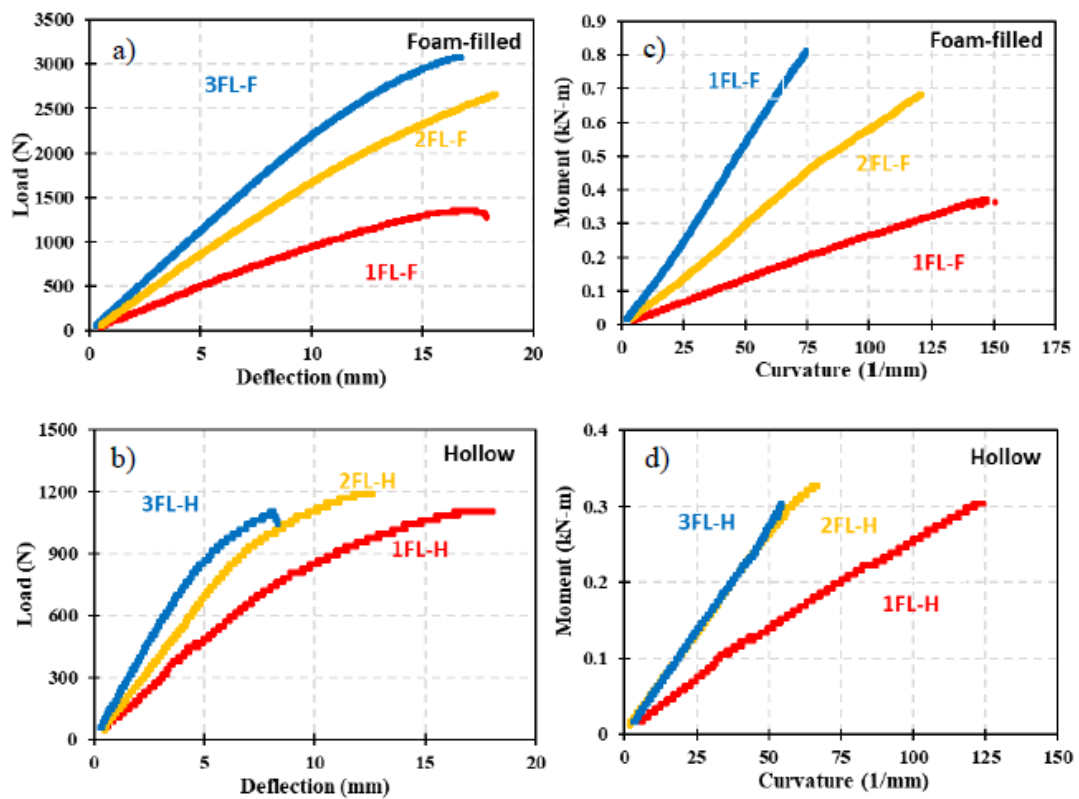


Figure 3-18 Effect of facing thickness on load-deflection and moment-curvature diagrams: a) load-deflection for foam-filled core; b) load-deflection for hollow core; c) moment-curvature for foam-filled core; d) moment-curvature for hollow core

## **CHAPTER 4 ANALYTICAL MODEL**

### **4.1. SYNOPSIS**

A numerical model of the sandwich structure was established by using the mechanical properties of each component (facing and core) of sandwich beams. The model provides the prediction of load-deflection behavior of each sandwich specimen. With the changes of parameters of facing thickness and core types, the model results in different load-deflection curves. The model was used to verify the testing results obtained by experimental program, and a parametric study will be included in this section based on the model to predict the mechanical properties of the specimens with different dimensions which were not tested in this study.. In this section, the procedure of establishing model will be presented, and the results of model will be analysed.

### **4.2. MODELLING LOAD-DEFLECTION BEHAVIOR**

As mentioned in Chapter 2, the total deflection of a sandwich beam is the sum of the deflection due to bending of facing component and the deflection due to shear of core component. The total deflection equation is shown in Chapter 2, and all the parameters of material properties were obtained directly from facing component and core component tests. For linear model, the initial moduli were inputted into the equation to obtain a linear load-deflection model. For non-linear model, it was developed by using the secant elastic and shear moduli that varied along with the different load stage, and the non-linearity of facing and core components were considered together in this model.

#### **4.2.1. Linear Model**

The linear model was developed by assuming that elastic modulus of flax FRP and shear

modulus of paper honeycomb cores were constant values. The total deflection was calculated by inputting initial moduli of flax FRP and paper honeycomb cores to Equation 2-12. Based on the tests of flax FRP coupons and paper honeycomb cores specimens that shown in Section 3.3, the stress-strain curves of facing and core components were non-linear. Therefore, the assumption was invalidated, and a non-linear model need to be developed. However, the initial stiffness of the beam can be obtained from the linear model.

#### 4.2.2. Non-Linear Model

The non-linear model was developed by considering the non-linear stress-strain behaviors of facing and core components. Therefore, the elastic modulus and facing and shear modulus of core were not inputted as constant values in total deflection equation. Instead, the secant elastic modulus of flax FRP was used to calculate the deflection due to bending, and the secant shear modulus of core shear was used to calculate the deflection due to shear.

##### 4.2.2.1. Deflection Due to Bending

To develop the non-linear load-deflection curve due to bending, the maximum moment,  $M$ , was calculated based on the applied concentric load,  $P$ , and length of the beam,  $L$ , by Eq. 4-1 for three-point bending.

$$M = \frac{PL}{4} \quad \text{Eq. 4-1}$$

Then, the stress,  $\sigma$ , resisted by facings was calculated by Eq. 4-2.

$$\sigma = \frac{M}{bdt} \quad \text{Eq. 4-2}$$

Then, by using the stress-strain curve of flax FRP that was modeled in Chapter 3, the

stress values were plugged into Eq. 3-7 to obtain the strain values for each load stage.

Once the stress and strain values were obtained for each load stage, the secant elastic modulus,  $E_{sec}$ , was calculated by Eq. 4-3.

$$E_{sec} = \sigma / \varepsilon \quad \text{Eq. 4-3}$$

The secant elastic modulus, shown in Figure 4-1, was used to calculate deflection due to bending by Eq. 4-4. The flowchart in Figure 4-2 demonstrates the steps of modelling bending deflection.

$$\delta_b = \frac{P_i L^3}{48 E_{sec} I} \quad \text{Eq. 4-4}$$

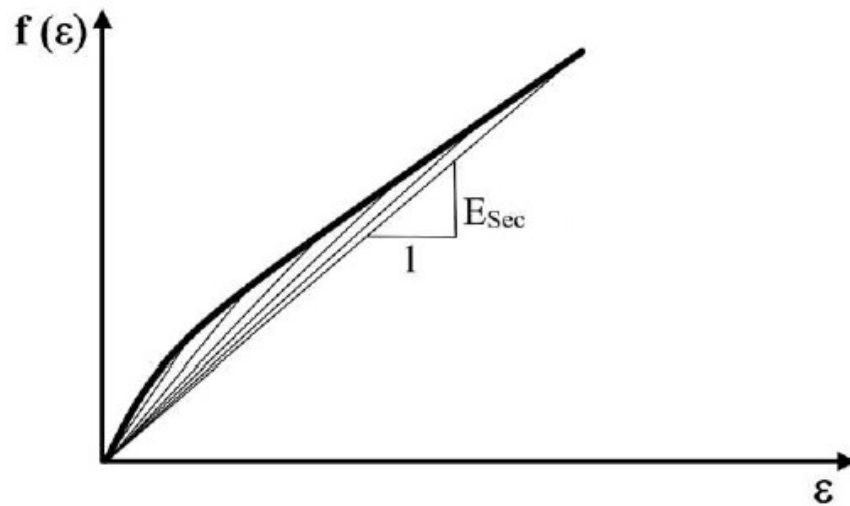


Figure 4-1 Stress-strain curve with varying secant modulus

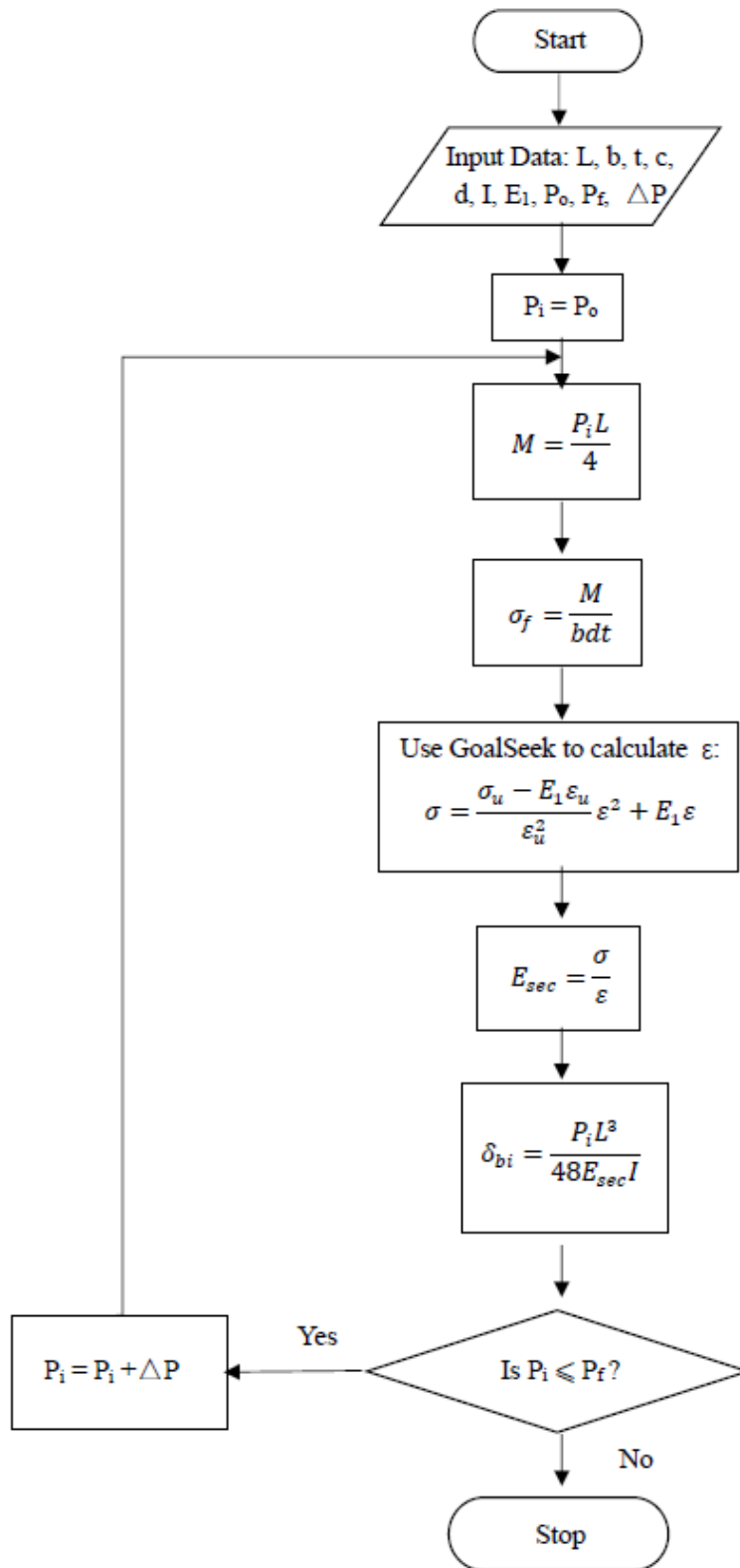


Figure 4-2 Flowchart of deflection model due to bending

#### 4.2.2.2. Deflection Due to Shear

To develop the non-linear load-deflection curve due to shear, the core shear model that presented in Eq. 3-13 was used to derive secant shear modulus,  $G_{sec}$ . The secant shear modulus, shown in Figure 4-3, was obtained by dividing shear stress by shear strain.

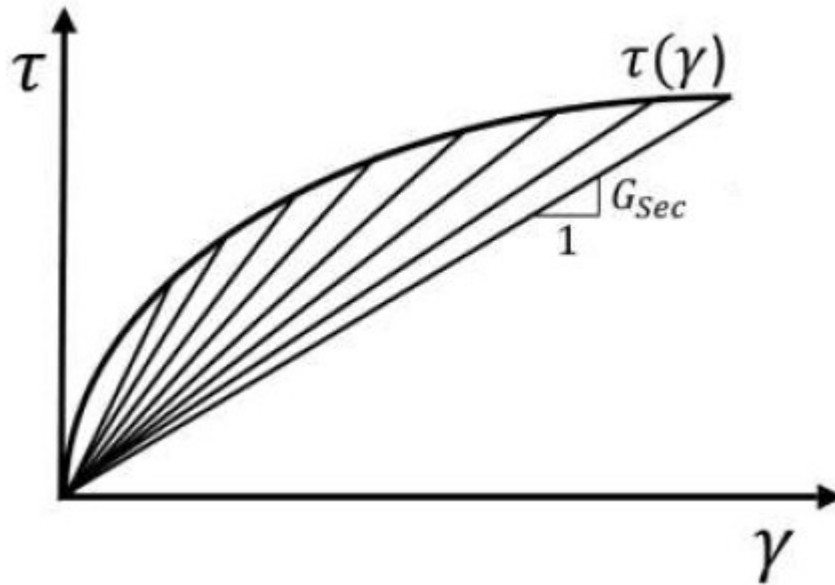


Figure 4-3 Shear stress-strain curve with varying secant modulus

$$G_{sec} = \frac{\tau}{\gamma} = \frac{\tau_u - G\gamma_u}{\gamma_u^2} \gamma + G \quad \text{Eq. 4-5}$$

Then, the relation between shear strain and shear deflection can be found by Figure 4-4 and Eq. 4-6.

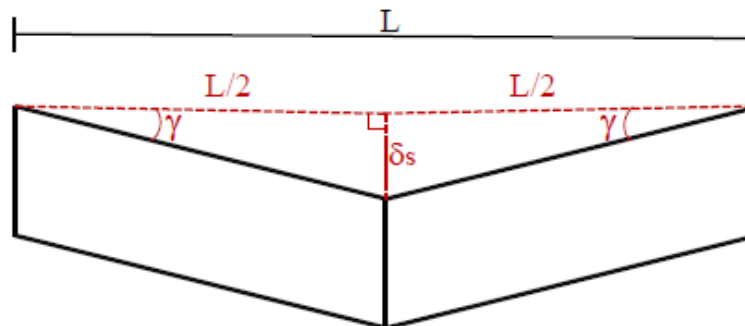


Figure 4-4 Relation between shear deflection and shear strain

$$\tan(\gamma) = \frac{\delta_s}{L/2} = \gamma \quad \text{Eq. 4-6}$$

When the value of shear strain,  $\gamma$ , is small, the value of  $\tan(\gamma)$  is close to value of  $\gamma$ .

Then, plugging Eq. 4-6 to Eq. 4-5, the secant shear modulus can be presented as:

$$G_{sec} = \frac{\tau_u - G\gamma_u}{\gamma_u^2} \frac{\delta_s}{L/2} + G \quad \text{Eq. 4-7}$$

Then, the shear deflection of each load stage was calculated by Eq. 4-6.

$$\delta_s = \frac{P_i L}{4bdG_{sec}} \quad \text{Eq. 4-8}$$

In Eq.4-7, the only variable is shear deflection. The beginning of the model is from the load of “0”, so the initial shear modulus was used to calculate the first deflection. Then, the secant modulus in next load stage can be calculated by using the load deflection from the previous load stage. The procedure of modelling the shear deflection is shown in Figure 4-5.

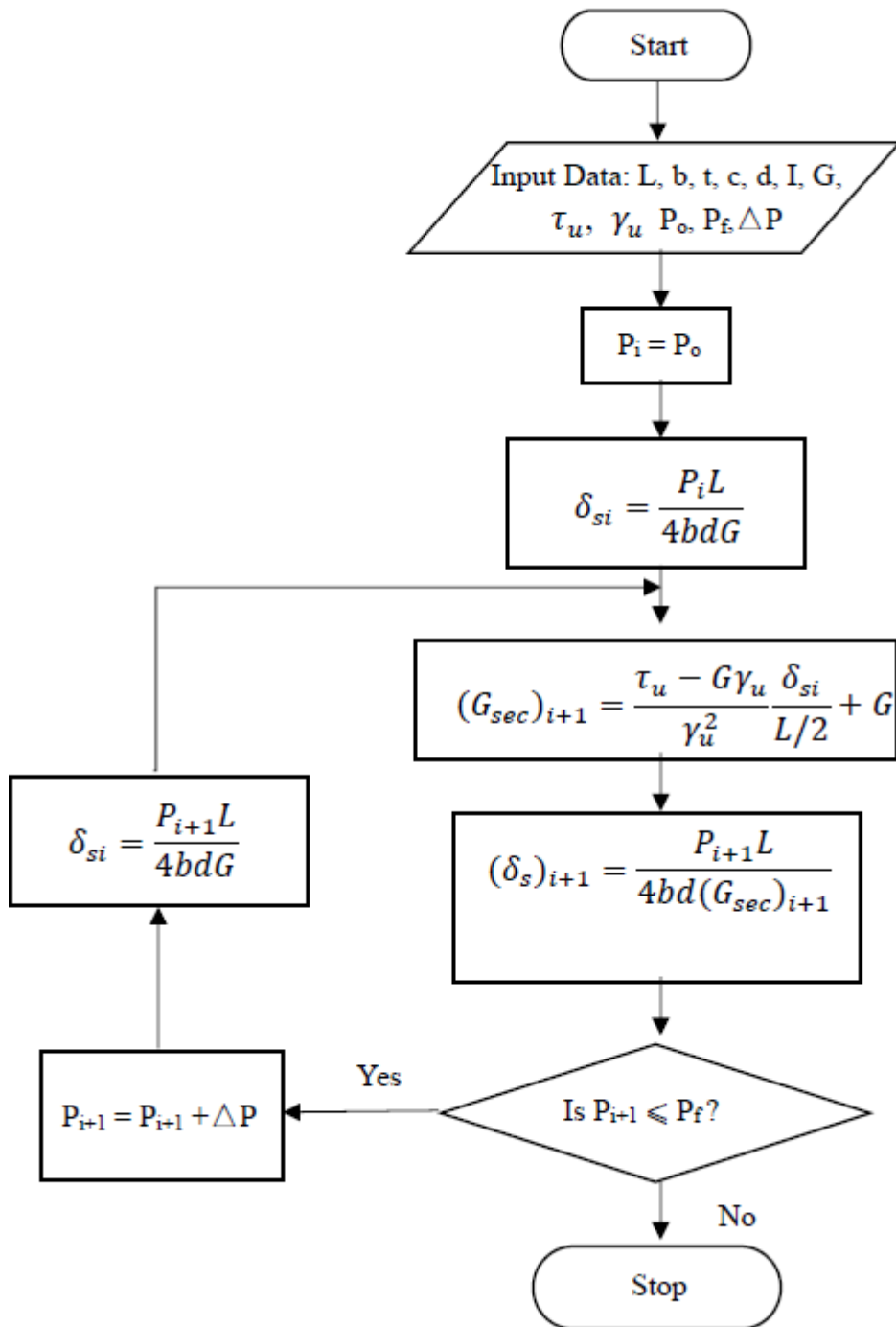


Figure 4-5 Flowchart of deflection model due to shear

#### 4.2.3. Verification of Load-deflection Models

The linear and non-linear numerical models developed in the previous section were compared to the testing data this section. The non-linear model is sum of bending and shear load-deflection models that were developed in the previous section. The peak loads at failure in the tests were used as the end point of model in this section. The diagrams are shown in Figure 4-6, and the values of initial stiffness were obtained from linear model and compared to test data in Table 4-1.

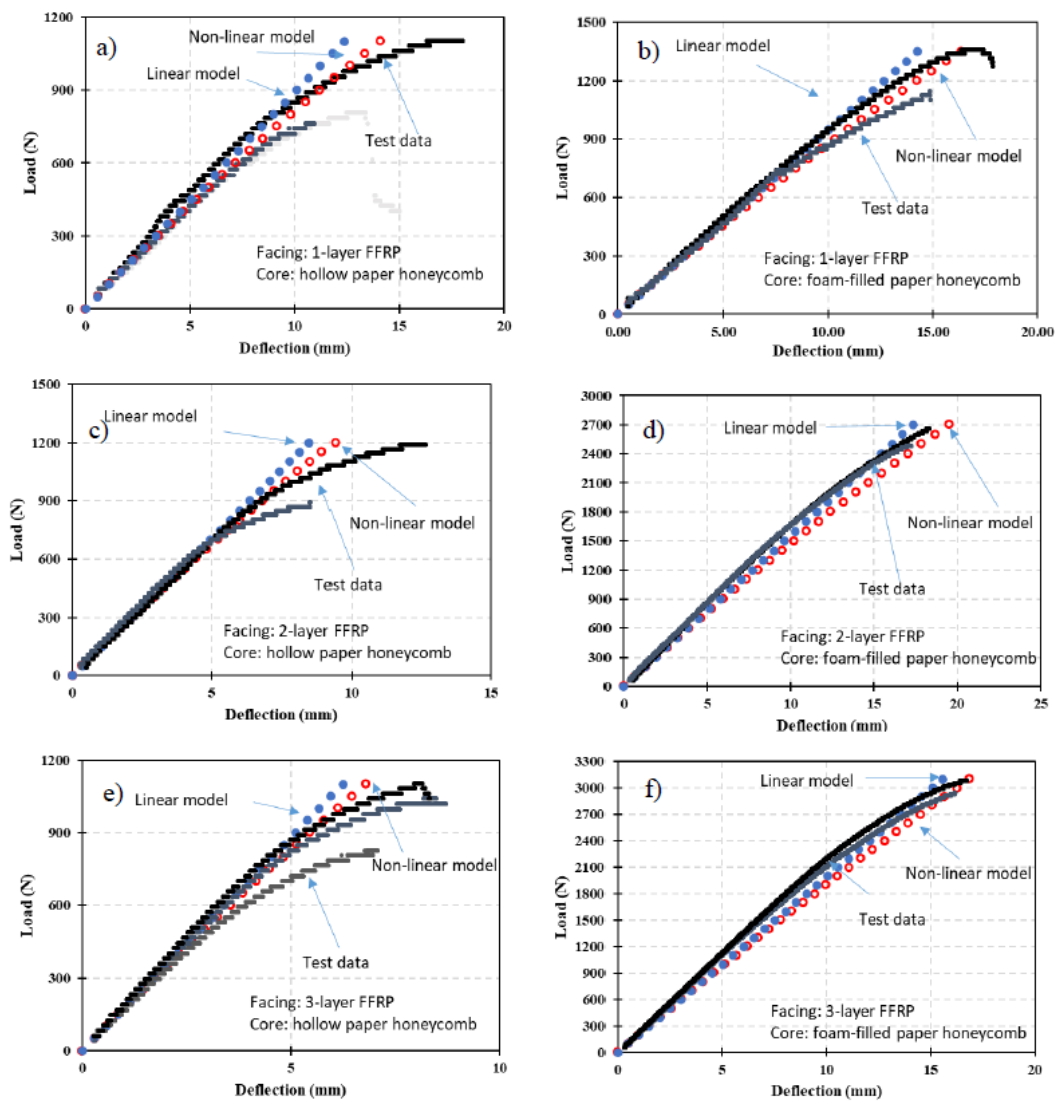


Figure 4-6 Load-deflection curve comparison between linear model, non-linear model, and test data: a) 1FL-H; b) 1FL-F; c) 2FL-H; d) 2FL-F; e) 3FL-H; f) 3FL-F.

Table 4-1 Initial stiffness comparison between models and test data

Case #	Specimen Group ID	Stiffness (kN/m)				
		Test			Model	Test to Model ratio
		AVG	SD	COV (%)		
1	1FL-F	94.8	4.5	4.7	94.676	1.00
2	1FL-H	86.3	5.7	6.6	89.042	0.97
3	2FL-F	167.8	7.5	4.5	155.44	1.08
4	2FL-H	146.1	10.1	6.9	141.06	1.04
5	3FL-F	216.2	10.2	4.7	198.81	1.09
6	3FL-H	176.1	12.0	6.8	176.25	1.00

As shown in the figure and table, both linear and non-linear model are accurate at the initial part of load-deflection curve. However, along with more load applied on the specimens, the load-deflection relations of the specimens become more parabolic, and the linear model gradually become less accurate than non-linear model. Therefore, non-linear model is more accurate than linear model at the terminal point. To conclude, both linear and non-linear model were used to verify the load-deflection behavior of the tested specimens. Non-linear model is more accurate than linear model throughout the whole test data, but linear model is a good tool to estimate the initial stiffness of the specimens.

#### 4.3. BREAKDOWN OF SHEAR AND BENDING DEFLECTIONS

Since the deflection due shear and the deflection due to bending were modeled separated in previous section, the contribution of each deflection is study in this section. Both changes of core type and facing thickness resulted in the changes of deflection contributions of shear and bending. As shown in Figure 4-7 and table 4-2, by filling the hollow paper honeycomb core with foam, the density of the core was increased, and the

shear contributions to total deflection were decreased by 7%, 10%, and 9%, respectively, for 1-layer, 2-layer, and 3-layer specimens. Also, by applying thicker facing from 1 to 3 layers of flax FRP, the shear contribution to total deflection were increased by 27% and 29%, respectively, for foam-filled and hollow paper honeycomb cores. Overall, the shear deflection contribution was decreased by increasing the core density, and it was increased by applying thicker facing component.

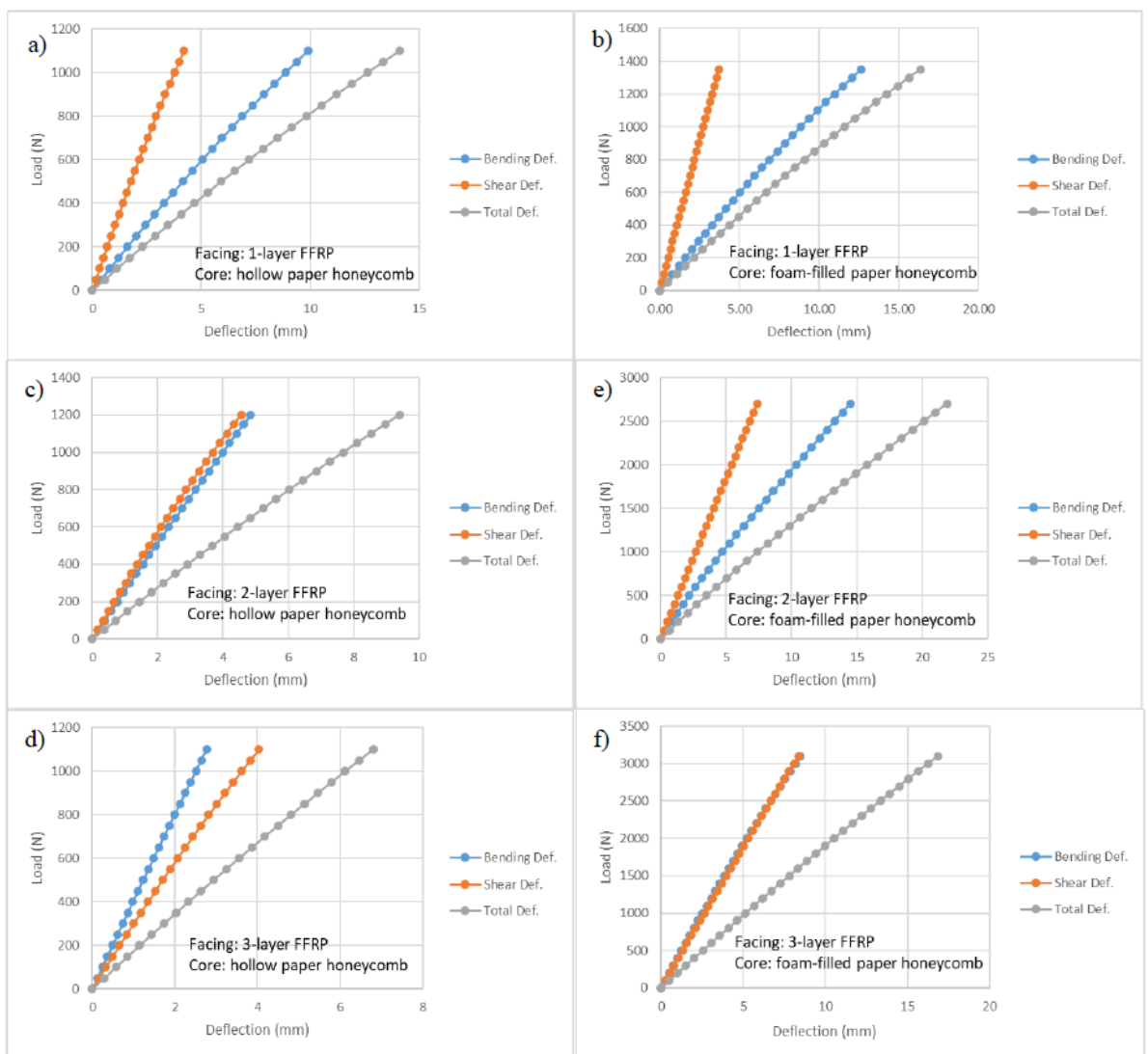


Figure 4-7 Breakdown of total deflection into shear and bending deflections: a) 1FL-H; b) 1FL-F; c) 2FL-H; d) 2FL-F; e) 3FL-H; f) 3FL-F.

Table 4-2 Shear Contribution to Total Deflection

Case #	Specimen Group ID	Ultimate mid span shear def. (mm)	Ultimate mid span bending def. (mm)	Total def. (mm)	Shear contribution to total def. (%)
1	1FL-F	3.70	12.65	16.36	23%
2	1FL-H	4.21	9.90	14.11	30%
3	2FL-F	7.39	12.13	19.51	38%
4	2FL-H	4.56	4.85	9.40	48%
5	3FL-F	8.36	8.48	16.85	50%
6	3FL-H	4.03	2.77	6.80	59%

#### 4.4. PREDICTION OF FAILURE MODES

The failure mode and peak load at failure of each specimen were predicted based on the equations from the literature in this section. In this study, three main failure modes were considered: facing rupture, core shear failure, and top face wrinkling. By plugging in the parameters of specimen dimension and material properties from facing and core components tests, the peak load at failure of each failure criteria was calculated by Eq. 2-21, Eq. 2-22, and Eq. 2-23 from literature, respectively. By comparing the values of peak loads that are calculated by these equations, the failure criteria with minimum peak load at failure is considered as critical failure modes. The predicted peak loads can be used as the terminal points of load-deflection behavior to finalize the model, and the predicted critical failure modes were compared to the failure modes in test, as shown in Figure 4-8 and Table 4-3.

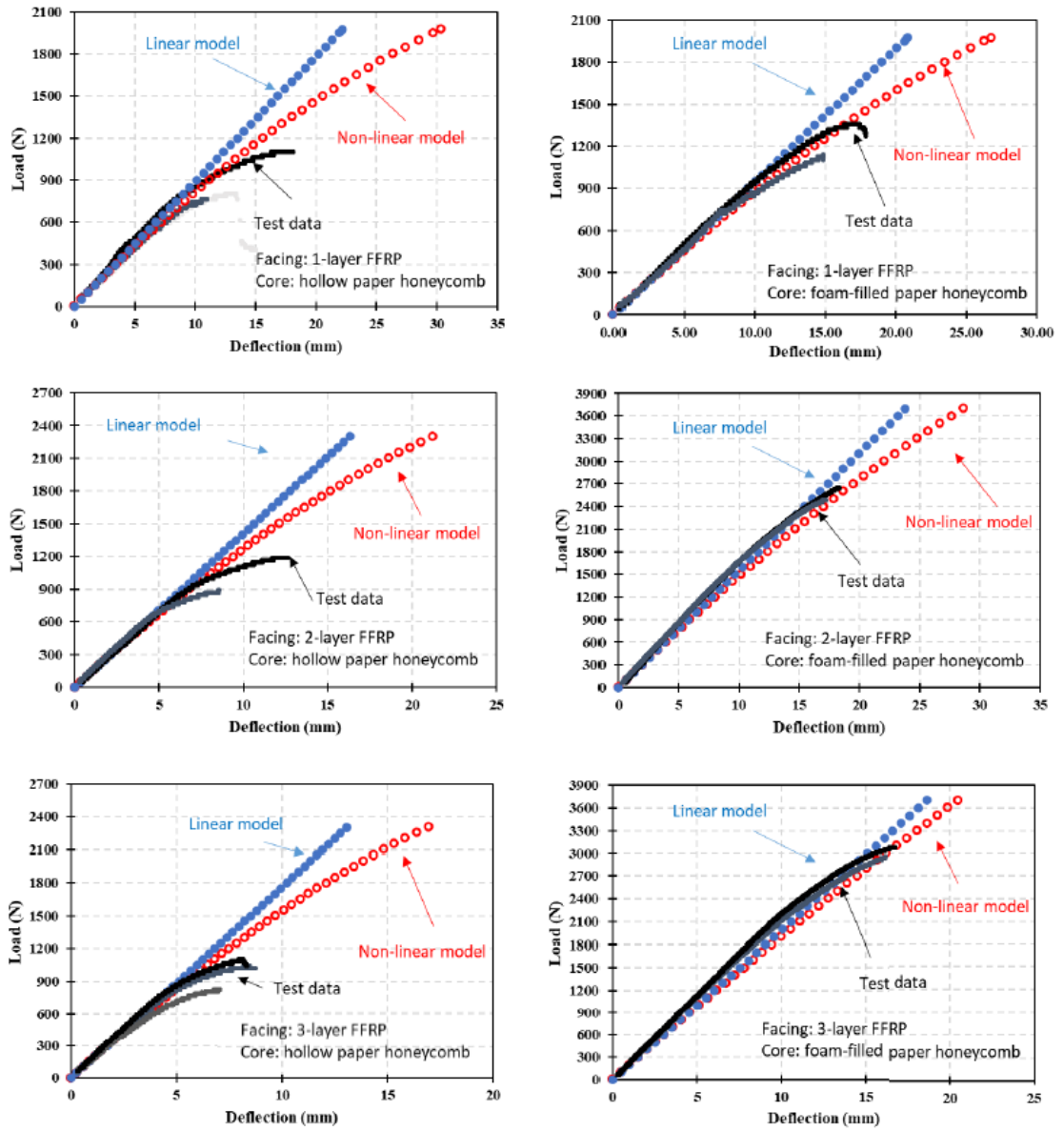


Figure 4-8 Load-deflection curve with predicted peak loads as terminal points: a) 1FL-H; b) 1FL-F; c) 2FL-H; d) 2FL-F; e) 3FL-H; f) 3FL-F.

Table 4-3 Data Comparison Test and Model

Case #	Specimen Group ID	Peak load (N)				Failure Modes			Deflection at Peak load				
		Test			Model	Test to Model ratio	Test	Model	Test			Model	Test to Model ratio
		AVG	SD	COV (%)					AVG	SD	COV (%)		
1	1FL-F	1039.6	413.5	39.8	1975.049	0.53	CS/Debonding	TR	12.45	4.6	36.9	26.8	0.46
2	1FL-H	898	178.2	19.8	1975.049	0.45	CS	TR	12.76	2.75	21.6	30.4	0.42
3	2FL-F	2392	472.3	19.7	3692.154	0.65	CS/Debonding	CS	16.74	1.09	6.5	28.7	0.58
4	2FL-H	926.3	246.2	26.6	2306.352	0.40	CS	CS	11.55	3.5	30.3	21.3	0.54
5	3FL-F	2377.9	1196.2	50.3	3692.181	0.64	CS/Debonding	CS	12.65	6.07	48.0	20.5	0.62
6	3FL-H	990.0	144.6	14.6	2306.363	0.43	CS	CS	7.33	0.75	10.2	17.0	0.43

As shown in the figure and table, the predicted peak loads are much larger than the peak loads that were found in the tests. Almost all the specimens were failed by core shear failure much earlier than the peak load from model prediction. There are two potential reasons to cause this problem. Firstly, it maybe caused by the errors of core material properties. As mentioned in section 3.3.2.2, the core specimens were overestimated in shear test. When the core specimens were being fabricated, the paper absorbed too much resin that went throughout the thickness of the core. Also, as mentioned in section 2.3.2.2, the thickness of core shear test specimens shall be equal to the thickness of the sandwich beam. However, because of the limitation of the testing instrumentations, the core shear test specimens were 20 mm thick, while the sandwich beam specimens were over 80 mm thick. The core shear test results were possibly influenced by different sizes of the specimens. Secondly, it maybe caused by the debonding failure modes that were not observed. For example, three specimens were observed that they failed by debonding. Debonding is a failure mode that leads specimens to premature failure. It is possible that other specimens were also failed by debonding and then followed by core shear in a sudden, so the debonding failure were not observed. Therefore, debonding failure mode was studied and will be present in Appendix A.

#### **4.5. PARAMETRIC STUDY**

A parametric study was conducted on sandwich beams made from FFRP facings and paper honeycomb cores. Only 6 groups of these sandwich beams were tested in this study, so, for the further analysis, the structural behaviors with respect to other changing variables were obtained by parametric study in this section. Four parameters were

considered in parametric study: thickness of core component,  $c$ , thickness of facing component,  $t$ , unsupported span length,  $L$ , and type of core (hollow and foam-filled).

Therefore, there were totally 3 cases were analyzed:

1)  $t = 3$  mm,  $L = 1$  m, and changing variables of  $c$  (75 mm, 100 mm, 125 mm, 150 mm).

2)  $c = 150$  mm,  $L = 1$  m, and changing variables of  $t$  (3 mm, 6 mm, 9 mm, 12 mm).

3)  $t = 3$  mm,  $c = 150$  mm, and changing variables of  $L$  (1 m, 2 m, 3 m, 4 m).

The outcomes for each case were: initial stiffness,  $K$ , ultimate stiffness,  $K_u$ , peak load,  $P_u$ , total deflection at peak load,  $\delta$ , facing strain at peak load,  $\varepsilon$ , and failure mode. The ultimate stiffness is the slope of the secant line that connects the original point and the endpoint of load-deflection curve, as shown in Figure 4-9. The peak load is the terminal point of all models, which was calculated by the failure mode concepts presented in section 4.4. The results are summarized in Table 4-4, 4-5, and 4-6.

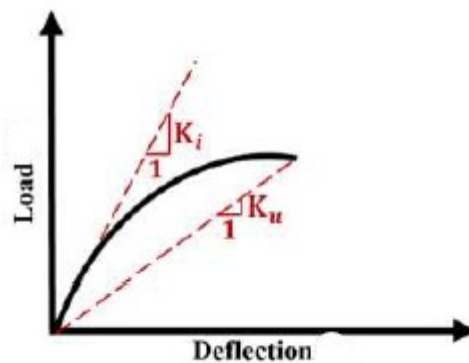


Figure 4-9 Initial stiffness and ultimate stiffness.

Table 4-4 Mechanical properties of sandwich beams with varying core thickness and core type (t = 3 mm, L = 1 m)

Core Thickness (mm)	Hollow Paper Honeycomb Core							Foam-Filled Paper Honeycomb Core						
	Initial Stiffness, K (N/mm)	Ultimate Stiffness, Ku (N/mm)	$\frac{K_u}{K}$	Peak Load, Pu (N)	Total Deflection @ Peak Load, $\delta$ (mm)	Facing Strain @ Peak Load, $\epsilon$ (mm/mm)	Failure mode	Initial Stiffness, K (N/mm)	Ultimate Stiffness, Ku (N/mm)	$\frac{K_u}{K}$	Peak Load, Pu (N)	Total Deflection @ Peak Load, $\delta$ (mm)	Facing Strain @ Peak Load, $\epsilon$ (mm/mm)	Failure mode
75	164.68	124.26	0.75	2246.5	18.08	0.003560	CS	183.12	157.22	0.86	3596.3	22.87	0.006358	CS
100	246.97	182.93	0.74	2995.4	16.37	0.003600	CS	278.86	241.99	0.87	4795.3	19.81	0.006443	CS
125	334.58	242.15	0.72	3744.2	15.46	0.003625	CS	382.24	334.71	0.88	5994.2	17.91	0.006495	CS
150	425.78	302.60	0.71	4493.1	14.85	0.003641	CS	490.94	433.16	0.88	7193.1	16.61	0.006530	CS

Table 4-5 Mechanical properties of sandwich beams with varying facing thickness and core type (c = 150 mm, L = 1 m)

Facing Thickness (mm)	Hollow Paper Honeycomb Core							Foam-Filled Paper Honeycomb Core						
	Initial Stiffness, K (N/mm)	Ultimate Stiffness, Ku (N/mm)	$\frac{K_u}{K}$	Peak Load, Pu (N)	Total Deflection @ Peak Load, $\delta$ (mm)	Facing Strain @ Peak Load, $\epsilon$ (mm/mm)	Failure mode	Initial Stiffness, K (N/mm)	Ultimate Stiffness, Ku (N/mm)	$\frac{K_u}{K}$	Peak Load, Pu (N)	Total Deflection @ Peak Load, $\delta$ (mm)	Facing Strain @ Peak Load, $\epsilon$ (mm/mm)	Failure mode
3	425.78	302.60	0.71	4493.1	14.85	0.003641	CS	490.94	433.16	0.88	7193.1	16.61	0.006530	CS
6	522.27	367.20	0.70	4493.1	12.24	0.001663	CS	621.51	586.79	0.94	7193.1	12.26	0.002769	CS
9	570.91	401.28	0.70	4493.1	11.20	0.001066	CS	688.88	657.09	0.95	7193.1	10.95	0.001747	CS
12	603.53	426.49	0.71	4493.1	10.53	0.000777	CS	733.94	702.47	0.96	7193.1	10.24	0.001265	CS

Table 4-6 Mechanical properties of sandwich beams with varying core thickness and core type (t = 3 mm, c = 150 mm)

Span Length (m)	Hollow Paper Honeycomb Core							Foam-Filled Paper Honeycomb Core						
	Initial Stiffness, K (N/mm)	Ultimate Stiffness, Ku (N/mm)	$\frac{K_u}{K}$	Peak Load, Pu (N)	Total Deflection @ Peak Load, $\delta$ (mm)	Facing Strain @ Peak Load, $\epsilon$ (mm/mm)	Failure mode	Initial Stiffness, K (N/mm)	Ultimate Stiffness, Ku (N/mm)	$\frac{K_u}{K}$	Peak Load, Pu (N)	Total Deflection @ Peak Load, $\delta$ (mm)	Facing Strain @ Peak Load, $\epsilon$ (mm/mm)	Failure mode
1	425.78	302.60	0.71	4493.1	14.85	0.003641	CS	490.94	433.16	0.88	7193.1	16.61	0.006530	CS
2	106.81	76.20	0.71	4234.4	55.57	0.008299	TR	114.43	89.87	0.79	4234.4	47.11	0.008299	TR
3	38.9	28.96	0.74	2822.9	97.44	0.008296	TR	40.37	30.62	0.76	2822.9	92.17	0.008296	TR
4	17.84	13.25	0.74	2117.2	159.80	0.008299	TR	18.25	13.62	0.75	2117.2	155.43	0.008299	TR

#### 4.5.1. Effect of Core Thickness (Hollow Paper Honeycomb Core and Foam-filled Paper Honeycomb Core)

In this case, core thickness was analysed at a range between 75 mm and 150 mm, while the facing thickness and unsupported span length were remaining constant. The changes of mechanical properties of sandwich beams with respect to varying core thickness and core type are shown in Table 4-4 and Figure 4-10. The load capacity and stiffness of the beams increased along with the thicker core applied. This is because that Table 4-4 shows all the beams are governed by core capacity. When the core component becomes stronger, the load capacity of the whole beam is increased. Also, comparing to the sandwich beam with hollow core, the sandwich beam with foam-filled core shows a higher load capacity, higher stiffness, and higher total deflection and facing strain at failure.

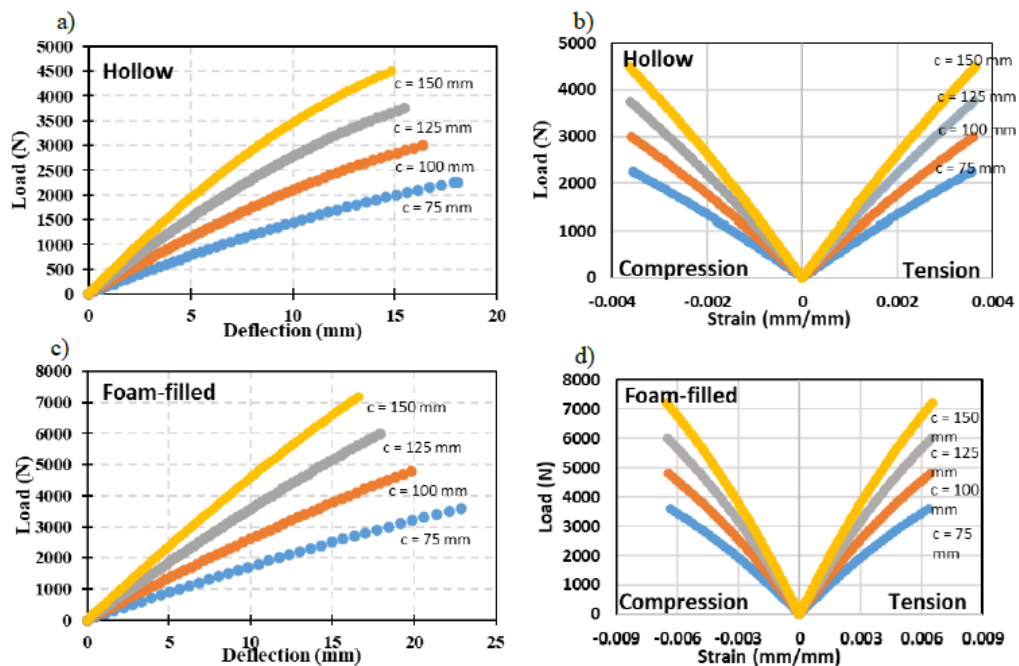


Figure 4-10 Load-deflection and load-strain curves for sandwich beams with varying core thickness and core type: a-b) hollow paper honeycomb core; c-d) foam-filled paper honeycomb core.

#### 4.5.2. Effect of Facing Thickness (Hollow Paper Honeycomb Core and Foam-filled Paper Honeycomb Core)

In this case, the facing thickness of sandwich beams was analysed at a range between 3 mm to 12 mm, while core thickness and unsupported span length were remaining constant. The changes of mechanical properties of sandwich beams with respect to varying facing thickness and core type are shown in Table 4-5 and Figure 4-11. By adding thicker facing component, the stiffness of the sandwich beam was increased. However, the load capacities of the beams were not improved because the core governed the failure. Also, along with the thicker facing component applied, the ratio of ultimate stiffness and initial stiffness was increased and closer to 1, especially for foam-filled core sandwich beams. This means the load-deflection curves become more linear. The reason of that is, as shown in Table 4-5, the facing strains at failure decreased with the thicker facing applied, so the stress-strain behavior of the facing component was infinitely close to a straight line with slope of its first elastic modulus.

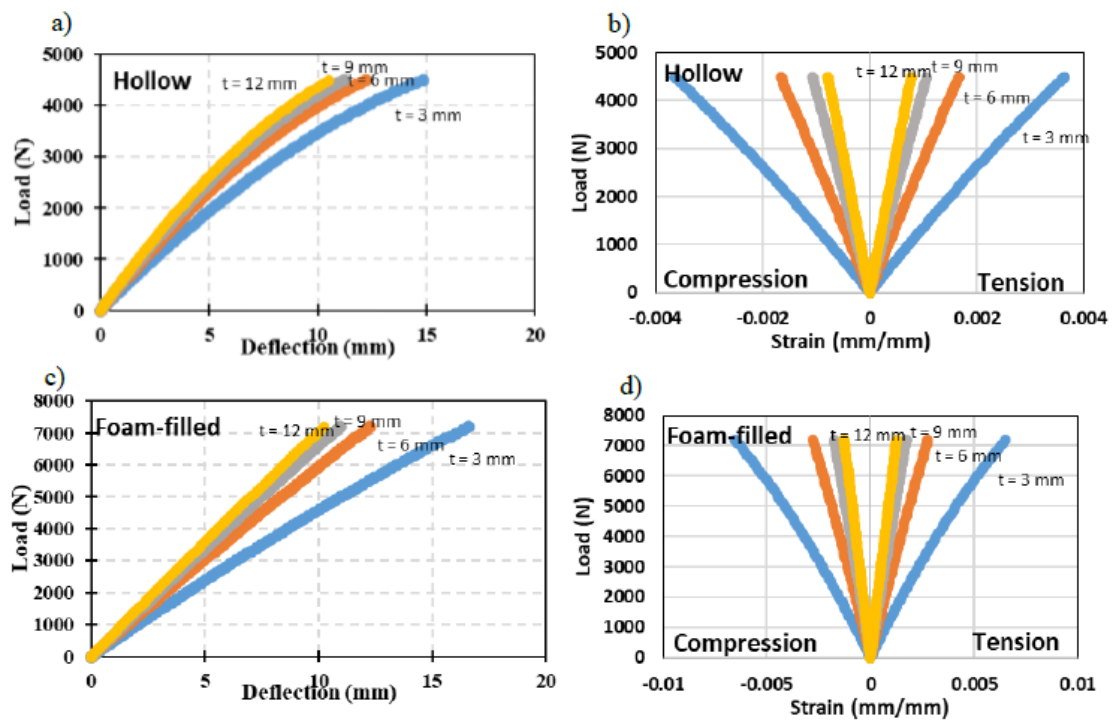


Figure 4-11 Load-deflection and load-strain curves for sandwich beams with varying facing thickness and core type: a-b) hollow paper honeycomb core; c-d) foam-filled paper honeycomb core.

#### 4.5.3. Effect of Span Length (Hollow Paper Honeycomb Core and Foam-filled Paper Honeycomb Core)

In this case, unsupported span length of sandwich beam was analysed at a range between 1 m to 4 m, while core thickness and facing thickness were remaining constant. The changes of mechanical properties of sandwich beams with respect to varying facing thickness and core type are shown in Table 4-6 and Figure 4-12. The load capacities and stiffness of the beams were sharply decreased. On the other hand, the deflections the beams were obviously increased at failure. Also, the failure mode turned to tension facing rupture from core shear when unsupported span length increased.

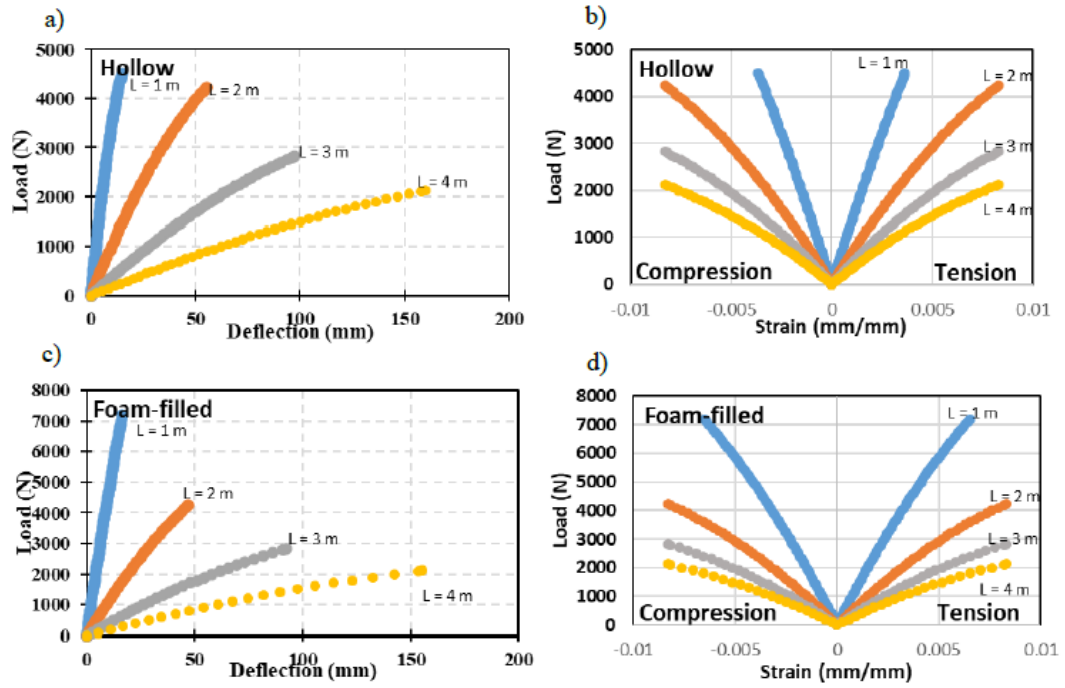


Figure 4-12 Load-deflection and load-strain curves for sandwich beams with varying unsupported span length and core type: a-b) hollow paper honeycomb core; c-d) foam-filled paper honeycomb core.

## CHAPTER 5 CONCLUSIONS AND RECOMMENDATIONS

### 5.1 CONCLUSIONS

In this study, sandwich beams were fabricated using bio-based materials, tested under three-point bending, and modeled based on analytical study. The motivations of this research are to investigate and understand the characteristics of structures made by bio-based materials and to show they have potential to replace conventional material for structural purposes. The environment would benefit with the use of high-efficient structural systems made of sustainable materials. A total of 18 sandwich beam specimens were fabricated by two configuration of paper honeycomb core (namely, hollow and foam-filled) and flax FRP facing. The test matrix included 6 sets of specimens, and 3 identical specimens were tested for each set. The main parameters of the specimens were type of the core and thickness of facing. Two types of cores were studied: hollow paper honeycomb core and foam-filled paper honeycomb core. Three different thicknesses of facing were studied experimentally: 1-layer, 2-layer, and 3-layer. Also, a non-linear stress-strain model was developed for flax FRP based on the model proposed by Betts (2018). The hollow paper honeycomb core and foam-filled paper honeycomb core specimens were fabricated and tested under shear, and a non-linear model was developed for each of them. Then, an analytical model was developed to describe the non-linear load-deflection behavior of bio-based sandwich beams. Based on the experimental testing results and analytical models of the core component, facing component, and sandwich beams, the following conclusions are made:

- Based on the test results, the stress-strain curves of flax FRP have non-linear

behaviors under both tension and compression loadings. The initial and second tension moduli were evaluated to be 7.51 GPa and 4.59 GPa, respectively.

- Two methods were used to model the stress-strain curve of flax FRP facing component: a bilinear model and a parabolic model. Results produced by the two models were compared against the test data. The parabolic model fits better to test data because, unlike other fibers (e.g. plastic fibers), the natural fibers do not show a bilinear stress-strain curve.

The density of hollow paper honeycomb was determined to be 19.12 kg/m<sup>3</sup>.

The density of the spray foam that used to fill the hollow core was measured to be 27.8 kg/m<sup>3</sup>. The hollow paper honeycombs were filled with foam, and the density of foam-filled paper honeycomb was evaluated as 43.78 kg/m<sup>3</sup>.

Both hollow and foam-filled core were tested under shear, and the initial shear moduli for hollow and foam-filled core were 10.236 MPa and 12.773 MPa, respectively. Also, the shear stress-strain curves showed non-linear behaviors. Therefore, the shear stress-strain curves were also modeled by parabolic equation.

- Based on the test results of sandwich beams, the parameter of honeycomb core configurations have relatively smaller effect on the initial stiffness and initial flexural rigidity, but the peak loads of 1-layer, 2-layer, and 3-layer specimens were increased by 51.2%, 158.2%, and 209.9%, respectively, by changing the hollow honeycomb core to foam-filled honeycomb core. The parameter of facing thickness has major impact on initial stiffness and initial flexural rigidity.

The initial stiffness and initial flexural rigidity were increased by 77% and 160%, respectively, by changing the number of layers from 1 to 2.

- Almost all the sandwich beams were failed by core shear failure mode, and two sandwich beams with foam-filled core were failed by premature debonding failure. The debonding failure was possibly caused by pre-existing crack between core and facing component. The pre-existing crack was impossible to be avoided because the foam was manually filled.
- The load-deflection behaviors of bio-based sandwich beams were modeled considering the non-linearity of facing and core components together.
- The shear deflection contribution was decreased by increasing the core density, and it was increased by applying thicker facing component. According to developed analytical model, by filling the core with foam, the shear contributions to total deflection were decreased by 7%, 10%, and 9%, respectively, for 1-layer, 2-layer, and 3-layer specimens. By applying thicker facing from 1 to 3 layers of flax FRP, the shear contribution to total deflection were increased by 27% and 29%, respectively, for foam-filled and hollow paper honeycomb cores.
- In analytical study, the failure modes predictions showed that almost all sets of specimens should be failed by core shear failure, which were constant to the testing results. However, the predicted peak loads were overestimated. This was caused by that the material properties of cores were overestimated in shear tests.

- According to parametric study on the sandwich beams made from FFRP facings and paper honeycomb core. The core materials always govern the load capacity of the beam when the unsupported span length is remaining 1 m long. Therefore, by increasing the core thickness, the load capacity and stiffness can be improved. However, the load capacity was not increased by adding thicker facings, but the stiffness was increased. Also, the stiffness and load capacity were sharply decreased by applying longer unsupported span length, and it has potential to shift the failure mode from core failure to facing failure.

## **5.2 RECOMMENDATIONS FOR FUTURE RESEARCH**

The recommendations for future research are concluded:

- Instead of manually filling the foam into honeycomb core, use the finished product from industry to improve the quality of sandwich beam specimen and to avoid premature failure.
- In-deep understanding of the debonding failure of sandwich panels.
- Follow the size guidance, that is included in Section 2.3.2.2, of core specimens in core shear test.
- Analyze the mechanical performance of sandwich beams under impact loads and post-impact residual strength.
- Study the sustained/long-term loads on sandwich beams to analyse fatigue and creep capacity.
- Analyze the mechanical performance of sandwich panels under two-way flexural loads.

## BIBLIOGRAPHY

- Álvarez-Chávez, C., Edwards, S., Moure-Eraso, R., & Geiser, K. (2012). Sustainability of bio-based plastics: General comparative analysis and recommendations for improvement. *Journal of Cleaner Production*, 23(1), 47-56.
- Adekunle, K., Cho, S., Ketzscher, R., & Skrifvars, M. (2012). Mechanical properties of natural fiber hybrid composites based on renewable thermoset resins derived from soybean oil, for use in technical applications. *Journal of Applied Polymer Science*, 124(6), 4530-4541.
- Aktay, L., Johnson, A., & Kröplin, B. (2008). Numerical modelling of honeycomb core crush behaviour. *Engineering Fracture Mechanics*, 75(9), 2616-2630.
- Asprone, D., Auricchio, F., Menna, C., Morganti, S., Prota, A., & Reali, A. (2013). Statistical finite element analysis of the buckling behavior of honeycomb structures. *Composite Structures*, 105, 240-255.
- Allen, H. G. (1969). *Analysis and Design of Structural Sandwich Panels* (1st ed.). Oxford: Pergamon.
- Betts, D., Sadeghian, P., & Fam, A. (2018). Experimental Behavior and Design-Oriented Analysis of Sandwich Beams with Bio-Based Composite Facings and Foam Cores. *Journal of Composites for Construction*, 22(4), 4018020.
- Betts, D., Sadeghian, P., & Fam, A. (2020). Structural behavior of sandwich beams with flax fiber-reinforced polymer faces and cardboard cores under monotonic and impact loads. *Journal of Architectural Engineering*.
- Betts, D., Sadeghian, P., & Fam, A. (2021). Experiments and nonlinear analysis of the impact behaviour of sandwich panels constructed with flax fibre-reinforced polymer faces and foam cores. *Journal of Sandwich Structures & Materials*, 23(7), 3139-3163.
- Betts, D., Sadeghian, P., & Fam, A. (2021). Post-impact residual strength and resilience of sandwich panels with natural fiber composite faces. *Journal of Building Engineering*, 38, 102184.
- Babu, R., O'Connor, K., & Seeram, R. (2013). Current progress on bio-based polymers and their future trends. *Progress in Biomaterials*, 2(1), 1-16.
- Carlsson, L. A., & Kardomateas, G. A. (2011). *Structural and failure mechanics of sandwich composites* (Vol. 121). Springer Science & Business Media.
- CoDyre, L., Mak, K., & Fam, A. (2018). Flexural and axial behaviour of sandwich

- panels with bio-based flax fibre-reinforced polymer skins and various foam core densities. *Journal of Sandwich Structures & Materials*, 20(5), 595-616.
- Fu, Y., & Sadeghian, P. (2020). Flexural and shear characteristics of bio-based sandwich beams made of hollow and foam-filled paper honeycomb cores and flax fiber composite skins. *Thin-walled Structures*, 153, 106834.
- Faruk, O., Bledzki, A., Fink, H., & Sain, M. (2012). Biocomposites reinforced with natural fibers: 2000–2010. *Progress in Polymer Science*, 37(11), 1552-1596.
- Florence, A., Jaswin, M., Arul Prakash, M., & Jayaram, R. (2020). Effect of energy-absorbing materials on the mechanical behaviour of hybrid FRP honeycomb core sandwich composites. *Materials Research Innovations*, 24(4), 244-255.
- Hosseini, N., Webster, D., & Ulven, C. (2016). Advanced biocomposite from highly functional methacrylated epoxidized sucrose soyate (MAESS) resin derived from vegetable oil and fiberglass fabric for composite applications. *European Polymer Journal*, 79, 63-71.
- Hristozov, D., Wroblewski, L. & Sadeghian, P. (2016). Long-term tensile properties of natural fibre-reinforced polymer composites: comparison of flax and glass fibre. *Composites Part B: Engineering* 95, 82-95.
- Herrmann, A. S., Zahlen, P. C., & Zuardy, I. (2005). Sandwich structures technology in commercial aviation. In *Sandwich structures 7: Advancing with sandwich structures and materials* (pp. 13-26). Springer, Dordrecht.
- ISIS Canada. (2006). An introduction to FRP Composites for Construction. ISIS Educational Module 2. Structural Innovation and Monitoring Technologies Resource Centre.
- Johansson, C., Bras, J., Mondragon, I., Nechita, P., Plackett, D., Šimon, P., . . . Aucejo, S. (2012). RENEWABLE FIBERS AND BIO-BASED MATERIALS FOR PACKAGING APPLICATIONS – A REVIEW OF RECENT DEVELOPMENTS. *Bioresources*, 7(2), 2506-2552.
- Kabasci, S. (2014). *Bio-based plastics: Materials and applications* (Wiley series in renewable resources). Chichester, West Sussex, United Kingdom: John Wiley & Sons.
- MacDonnell, L., & Sadeghian, P. (2020). Experimental and analytical behaviour of sandwich composites with glass fiber-reinforced polymer facings and layered fiber mat cores. *Journal of Composite Materials*, 54(30), 4875-4887.

- McCracken, A., & Sadeghian, P. (2018). Corrugated cardboard core sandwich beams with bio-based flax fiber composite skins. *Journal of Building Engineering*, 20, 114-122.
- Monti, A., El Mahi, A., Jendli, Z., & Guillaumat, L. (2017). Experimental and finite elements analysis of the vibration behaviour of a bio-based composite sandwich beam. *Composites Part B: Engineering*, 110, 466-475.
- Omonov, T., & Curtis, J. (2014). Biobased epoxy resin from canola oil. *Journal of Applied Polymer Science*, 131(8), N/a.
- Ramesh, M., Palanikumar, K., & Reddy, K. (2017). Plant fibre based bio-composites: Sustainable and renewable green materials. *Renewable & Sustainable Energy Reviews*, 79, 558-584.
- Rajesh, M., Pitchaimani, J., & Rajini, N. (2016). Free Vibration Characteristics of Banana/Sisal Natural Fibers Reinforced Hybrid Polymer Composite Beam. *Procedia Engineering*, 144, 1055-1059.
- Statista. (2018). 13,000 Buildings Per day. Learn why the construction industry needs to build an average of 13,000 buildings every day through 2050.
- Sparnins, E. (2009). Mechanical properties of flax fibers and their composites. University of Technology, Department of Engineering Sciences and Mathematics, Material Science.
- Sadeghian, P., Hristozov, D., & Wroblewski, L. (2018). Experimental and analytical behavior of sandwich composite beams: Comparison of natural and synthetic materials. *The Journal of Sandwich Structures & Materials*, 20(3), 287-307.
- Sharma, S., Sharma, S., & Mudhoo, A. (2011). A handbook of applied biopolymer technology (Vol. 12, RSC green chemistry). Cambridge: NBN International.
- Soltani, S. A., Keshavanarayana, S., Krishnamaraja, M. T., & Bhasin, A. (2014). STUDY OF HONEYCOMB CORE SHEAR-COMPRESSION PROPERTIES DURING AUTOCLAVE PROCESSING.
- Samaan, M., Mirmiran, A., & Shahawy, M. (1998). Model of concrete confined by fiber composites. *Journal of structural engineering*, 124(9), 1025-1031.
- Su, W., Liu, S. (2021). A couple-stress model to predict the wrinkling stress of sandwich panels with foam cores, *Composite Structures*
- Triantafillou, T. C., and Gibson, L. J. (1987). "Failure Mode Maps for Foam-Core Sandwich Beams." *Materials Science and Engineering*, 95, 37–53.

- URBANE. (2019). Blog: The advantages of using natural building materials. Urbane Eco: Sustainable Building Solutions.
- Vinson, J. R. (2005). Sandwich structures: past, present, and future. In *Sandwich structures 7: advancing with sandwich structures and materials* (pp. 3-12). Springer, Dordrecht.
- Väisänen, T., Das, O., & Tomppo, L. (2017). A review on new bio-based constituents for natural fiber-polymer composites. *Journal of Cleaner Production*, 149, 582-596.
- Wool, R., & Sun, Xiuzhi Susan. (2005). *Bio-based polymers and composites*. Amsterdam: Elsevier Academic Press. Chapter 5.
- Wang, Z. (2019). Recent advances in novel metallic honeycomb structure. *Composites. Part B, Engineering*, 166, 731-741.
- Yadav, M., & Agarwal, M. (2021). Biobased building materials for sustainable future: An overview. *Materials Today : Proceedings*, 43, 2895-2902.
- Yusuff, S. (1955). Theory of wrinkling in sandwich construction. *The Aeronautical Journal*, 59(529), 30-36.
- Zhu, X., Kim, B., Wang, Q., & Wu, Q. (2013). Recent Advances in the Sound Insulation Properties of Bio-based Materials. *Bioresources*, 9(1), 1764-1786.
- Zenkert, D. (1997). *The Handbook of Sandwich Construction*. Cradley Heath: Engineering Materials Advisory Services Ltd.

## APPENDIX A Debonding Failure Mode

### A1 Overview

Debonding is another important failure mode in sandwich structure, and it happens between the core and facing component. Comparing to other failure modes, such as facing rupture, core shearing, and top face wrinkling, debonding happens only if there is a relatively large crack at the interface of the core and the facing before the load applied; otherwise, it is preceded by another mode of failure (Triantafillou et al., 1989). In other words, debonding is a premature failure, and the load for debonding failure mode is relatively highly depends on the quality of fabrication of specimen. If the core and the facing are perfectly bonded, it would be possible to avoid the debonding failure. When debonding happens, the capacity of sandwich beam decreases sharply, and the beam fails in a sudden.

### A2 Analysis of Debonding Failure Mode

Nowadays, debonding failure modes are analyzed by using Finite Element Model (FEM) to describe the interface crack propagation (Saeid et al., 2016; Bragagnolo et al., 2020). Triantafillou et al (1989) also provide equations to predict the load for debonding failure load, shown in Equation A-1 to A-3 and Figure A-1.

If the half crack length,  $a$ , is larger than the core thickness,  $c$ , as shown in Figure A1a), the failure load of debonding is calculated as:

$$P_d = \sqrt{(4b^2cG_cG_{IIc})} \quad \text{Eq. A-1}$$

If the half crack length is smaller than the core thickness, as shown in Figure A1b), the

failure load of debonding is calculated as:

$$P_d = \sqrt{\frac{8b^2c^2G_cG_{IIc}}{\pi a}} \quad \text{Eq. A-2}$$

Where  $G_{IIc}$  is the strain energy release rate, and it can be calculated by:

$$G_{IIc} = \frac{F_d^2 c}{4G_c b^2 (L - 2a)^2} \quad \text{Eq. A-3}$$

Where  $F_d$  is the load for delamination, and it can be measured by shear test as shown in Figure A-1 c).

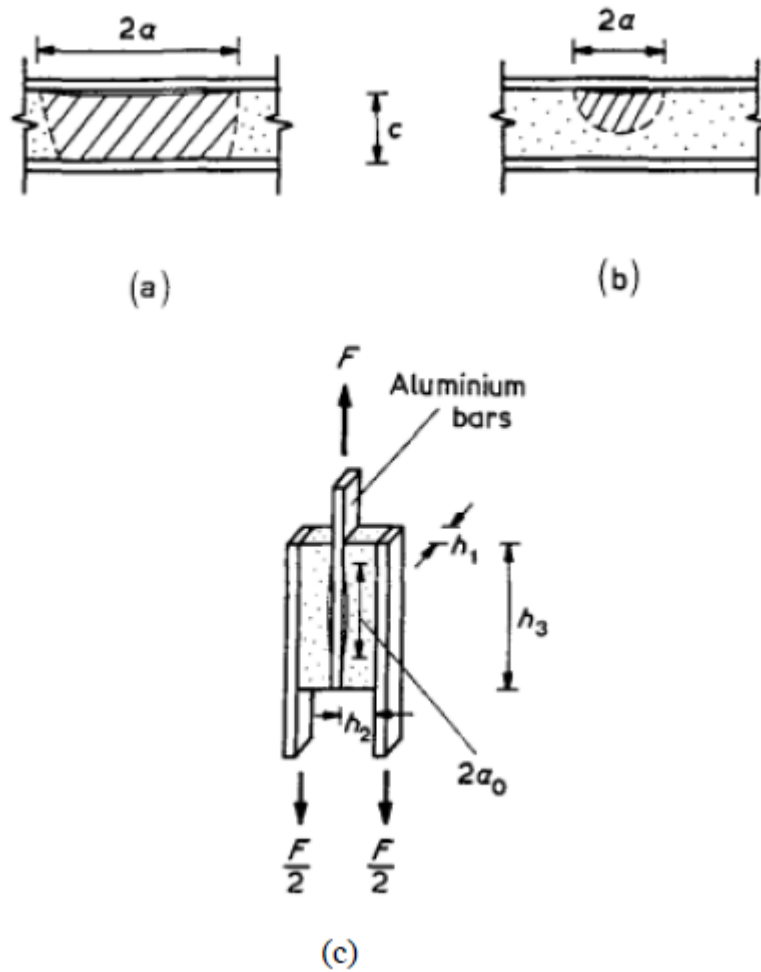


Figure A-1 a) Crack length greater than the depth of the core; b) Crack length less than the depth of the core; c) Double shear test setup (Triantafyllou et al., 1989)

To predict the debonding failure of the specimens in this study, the crack length was assumed to be equal to the size of the honeycomb cell (16 mm). The half crack length is smaller than core thickness, so the Eq A-2 was used. The results were shown in Table A-1.

Table A-1 Calculation Results of Debonding Failure

Specimen Group ID	Peak load (N)						Test to Model ratio
	Test	Debonding	Tensile Rupture	Core Shear	Wrinkling	Failure Mode	
1FL-F	1039.6	1308.8	1975.05	3692.12	3200.05	DB	0.79
1FL-H	898	777.9	1975.05	2306.33	2761.38	DB	1.15
2FL-F	2392	1308.8	4025.577	3692.15	6522.4	DB	1.83
2FL-H	926.3	777.9	4025.577	2306.35	5628.29	DB	1.19
3FL-F	2377.9	1308.8	6151.58	3692.18	9967.04	DB	1.82
3FL-H	990.0	777.9	6151.58	2306.36	8600.72	DB	1.27

Looking at the results from the table, all the specimens were predicted to be failed by debonding, and almost all debonding failure load were underpredicted. The reason of that the debonding equation was for foam cores having an initial crack with the width as same as the testing specimens. Therefore, to get more accurate calculation results of debonding failure, more research is needed in the future.

## **Appendix B Bilinear Model of Sandwich Beam**

### **B1 Overview**

Bilinear model of tested specimens was also established. Comparing to parabolic model, bilinear model is not suitable for flax FRP in this study. However, it works great with the materials that have bilinear stress-strain behavior, such as plastic FRP. Hence, this section presents the steps of developing the bilinear model, and diagrams are shown in Figure below.

### **B2 Bilinear Model**

As mentioned in section 3.3.1.2 in Chapter 3, the stress-strain curve of flax FRP was modeled by bilinear curve by using Richard and Abbott equation shown in Eq. 3-1. Then, to model the deflection due to bending, the same method that is shown in Figure 4-2 was used. Instead, the parabolic model equation of flax FRP was replaced by Eq. 3-1. To model the deflection due to shear, the exact same method that is presented in section 4.2.2.2 was used. After adding deflection due bending and deflection due to shear together, the diagrams are shown below.

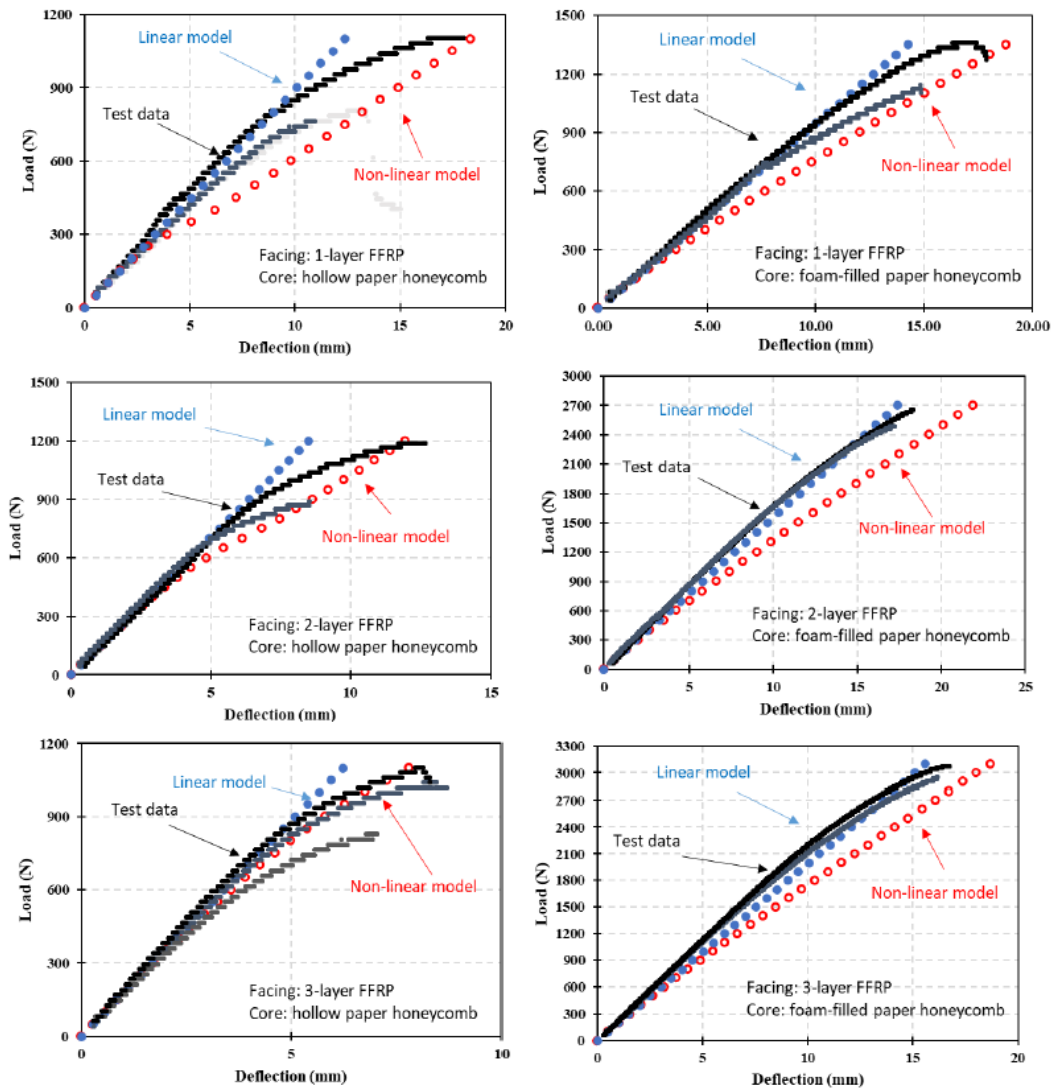


Figure B-1 Load-deflection curve comparison between linear model, Bilinear model, and test data: a) 1FL-H; b) 1FL-F; c) 2FL-H; d) 2FL-F; e) 3FL-H; f) 3FL-F.